
Politecnico di Milano
School of Industrial and Information Engineering
Department of Energy
Master of Science in Nuclear Engineering

# Development of the EUROfusion pedestal database for ELMy H-Mode for the TCV tokamak

*Advisor:*
Prof. Matteo Passoni

*Co-Advisor:*
Dr. Labit Benoit

*Graduation thesis of:*
Edoardo Rovere
854892

Academic year 2018-2019

**Abstract**

When, in a tokamak, external power is supplied above a threshold level, the plasma undergoes an abrupt transition which leads to the creation of an edge transport barrier, thus improving the confinement capabilities of the plasma itself. This regime is called High-confinement Mode, or H-Mode; its features are several: the increasing of the temperature, density and pressure profiles, leading to the formation of a region of steep gradients at the plasma edge, called pedestal; the generation of an edge current called bootstrap current; and, most importantly, the improvement of the energy confinement time, which approximately doubles in value with respect to the confinement regime preceding the H-Mode, the so-called L-Mode. For these reasons, the H-Mode confinement regime is one of the primary operational scenarios at ITER, the future international project regarding nuclear fusion feasibility at ignition conditions.
However, one of the consequences when operating in H-Mode is the arising of instabilities called Edge Localized Modes (or ELMs), which are ejections of plasma from the region where the plasma itself is confined; ELMs are triggered after the confined plasma reaches an MHD instability limit, and even though they have ameliorating effects on some negative aspects of the H-Mode, such as expelling impurities from the highly confined plasma, the plasma ejections correspond to a loss of confinement and pulsed heat loads against key components like the divertor, thus significantly reducing their operating life.
Depending on a wide range of conditions, such as power input, impurity and fuel injections, geometric and magnetic configuration parameters and much more, the ELMs that will generate will be different. As such, one would like to understand which are the most significant conditions that will influence the generation of a type of ELM with respect to another, in order to predict which ELMs will generate inside the considered machine. Since there is an extensive bibliography about this topic, but ELMs study is still an open research field, the theory concerning this phenomenon is majorly empyrical. As such, the need scaling laws and behaviors that repeats themselves in different tokamaks is imperative, and this means that gathering data from different experiments and from different machines can be a good starting point to reach that goal. For this reason, EUROFusion is promoting the creation of a database concerning ELMy H-Mode plasmas from tokamaks all over the world, focusing in particular in the region of the pedestal, since there is a correlation between this region and the ELMs generation, with the objective to understand and predict the ELMs behavior and appearance in ITER.
This thesis work aims to build a first version of what the pedestal database will be for the machine operating at the Swiss Plasma Center, the *Tokamak à Configuration Variable*, or *TCV*; in order to do so, data from the Thomson Scattering System have been gathered, then getting fitted profiles from them and by calculating the plasma at equilibrium by using the CHEASE iterative code, thus using the extrapolated quantities to build the database itself; finally, some considerations over the quantities of the newly built database, such as common behaviors and basic trends, have been made.

**Sommario**

Quando, in un tokamak, viene fornita potenza al di sopra di un livello di soglia, il plasma subisce una brusca transizione che porta alla creazione di una barriera di trasporto ai bordi, migliorando così le capacità di confinamento del plasma stesso. Questo regime è chiamato High-confinement Mode, o H-Mode, le cui caratteristiche principali sono: l'aumento dei profili di temperatura, densità e pressione, che porta alla formazione di una regione di elevato gradiente al bordo del plasma, chiamata pedestal; il sorgere di una corrente di bordo chiamata bootstrap current; e, soprattutto, il miglioramento dell'energy confinement time, che raddoppia approssimativamente di valore rispetto al regime di confinamento che precede l'H-Mode, il cosiddetto L-Mode. Per queste ragioni, il regime di confinamento in modalità H è uno dei principali scenari operativi di ITER, il futuro progetto internazionale sulla possibilità e la convenienza di effettuare reazioni di fusione nucleare. Tuttavia, una delle conseguenze quando si opera in H-Mode è l'insorgere di instabilità chiamate Edge Localized Modes (o ELMs), che sono espulsioni di plasma dalla regione in cui il plasma stesso è confinato; Gli ELMs sono attivati dopo che il plasma confinato raggiunge un limite di instabilità MHD, e anche se hanno effetti migliorativi su alcuni aspetti negativi della modalità H-Mode, come l'espulsione di impurità dal plasma altamente confinato, tali espulsioni di plasma corrispondono ad una perdita di confinamento e carichi termici pulsati contro componenti chiave come il divertore, riducendo così significativamente la loro vita operativa.
A seconda di un ampio intervallo di parametri, come la potenza assorbita, le iniezioni di impurità e di combustibile, fattori geometrici e configurazione magnetica del plasma e molto altro ancora, gli ELM che verranno generati saranno diversi. Come tale, vorremmo capire quali sono le condizioni più significative che influenzeranno la generazione di un tipo di ELM rispetto ad un altro, al fine di prevedere quali ELM si genereranno all'interno della macchina considerata. Poiché, nonostante esista un'ampia bibliografia su questo argomento, lo studio dei ELM sia ancora un campo di ricerca aperto, la teoria relativa a questo fenomeno è prevalentemente empirica. Come tale, abbiamo bisogno di profili e comportamenti che si ripetono anche in tokamak diversi, e questo significa che raccogliere dati da esperimenti e macchine diverse può essere un buon punto di partenza per raggiungere tale obiettivo. Per questo motivo, EUROFusion sta promuovendo la creazione di un database riguardante i plasmi H-Mode con generazione di ELM da parte di tokamak in tutto il mondo, concentrandosi in particolare nella regione del pedestal, in quanto esiste una correlazione tra questa regione e la generazione di ELMs, con l'obiettivo di comprendere e prevedere il comportamento e l'aspetto degli ELMs in ITER. Questo lavoro di tesi mira a costruire una prima versione di quello che sarà il database del pedestal in ELMy H-mode per la macchina operante presso lo Swiss Plasma Center, il *Tokamak à Configuration Variable*, o *TCV*; per fare ciò, sono stati raccolti i dati dal Thomson Scattering System in servizio nella macchina, ricavando dei fit dai dati e calcolando il plasma in equilibrio utilizzando il codice iterativo CHEASE, utilizzando così le quantità estrapolate per costruire il database stesso; infine, sono state fatte alcune considerazioni sulle quantità del nuovo database costruito, come profili che si ripetono in altre macchine.

# Contents

# List of Figures

# List of Tables

# Estratto

In questa tesi è stato realizzato un progetto di costruzione di un database degli esperimenti svolti a TCV (*Tokamak* á *Configuration Variable*) all'É*cole Polytechnique Fédérale de Lausanne*, Svizzera. In particolare, in questo lavoro di tesi viene trattato il processo di costruzione del database, il prelevamento dei dati di interesse da un sistema installato a TCV, il *Thomson Scattering System*, la manipolazione dei dati di interesse per ricavare i fit dei dati, al fine di utilizzare tali fit per estrapolare dati di interesse, e di quantità legate all'equilibrio, tramite il codice CHEASE; l'inserimento di quantità operative (come la potenza iniettata nel plasma) ed il calcolo di ulteriori quantità adimensionali (come il parametro di confinamento magnetico $\beta$); infine, l'utilizzo dei dati ricavati nel database per fare delle discussioni qualitative sul comportamento delle quantità trovate. Questo database si concentra su una regione periferica del plasma, caratterizzato da alti gradienti, chiamato *pedestal*; quest'ultimo si forma quando il plasma è in un particolare regime di confinamento, detto *H-Mode*, in cui si può osservare la generazione di instabilità denominate *Edge Localized Modes* (ELMs).
Nel capitolo 1 si è discusso dei concetti introduttivi della fusione nucleare, del riscaldamento del plasma e del suo confinamento, e infine si è fatta una panoramica dello stabilimento di ricerca dove si è svolto questo lavoro di tesi, e dei macchinari e delle diagnostiche da cui si sono ricavati i dati con cui tesi è stata svolta. In particolare, una reazione di fusione nucleare si ottiene quando si cerca di fondere due nuclei leggeri per ottenerne uno più pesante. Questo libera una grande quantità di energia, dell'ordine dei MeV o delle decine di MeV, comparabile a quella di un reattore a fissione, rendendo questo fenomeno molto interessante per la produzione di energia in impianti industriali. Tuttavia, occorre fare in modo che i due nuclei abbiano abbastanza energia da superare la barriera di potenziale coulombiana che ciascuna delle due cariche possiede; per questo motivo, le particelle coinvolte devono necessariamente essere abbastanza leggere; i nuclei più usati sono quindi l'idrogeno (nella forma di deuterio D e trizio T) e l'elio (sia elio-3 che elio-4); in particolare, il trizio, elemento molto raro sulla Terra, è ricavabile dalla reazione (n,$\alpha$) del $^6$Li. Poichè la quantità di $^6Li$ sulla Terra è tale che, se usato solo per fusione, potrebbe durare per $10^6$ anni, e che il deuterio è abbastanza comune sul pianeta e facile da estrarre, la fusione nucleare potrebbe essere un metodo di produzione di energia a lungo termine [9].
Per dare abbastanza energia alle particelle, occorre scaldarle al punto da raggiungere il valore ottimale di probabilità di reazioni di fusione o, in altri termini, fare in modo che raggiungano il massimo valore della sezione d'urto di fusione; tale valore si raggiunge attorno ai 10 keV che, per la relazione

di Boltzmann $E = k_B T$ ($k_B = 8.6 \times 10^{-5}\ eVK^{-1}$), si raggiunge quando le particelle cariche hanno una temperatura di circa 100 milioni di Kelvin. A tali valori di temperatura, le particelle cariche non presentano alcun tipo di aggregazione in atomi, ma rimangono un gas di particelle cariche, non legate le une alle altre, chiamato plasma; questo è quindi un gas di particelle cariche, ma che risulta essere globalmente neutro (se non si crea un disequilibrio tra cariche negative e positive). Poichè le particelle in un plasma sono cariche, esse obbediranno alle leggi di Maxwell.
Dopo che le particelle acquisiscono abbastanza energia, occorre assicurarsi che rimangano a tale livello di energia nella regione dove le reazioni di fusione nucleare avvengono, e che ci rimangano per un tempo sufficiente a reagire anch'esse; questo tempo è chiamato *energy confinement time*, $\tau_e$, ed è una delle quantità più importanti nello studio della fusione nucleare.
L'obiettivo principale delle ricerche sulla fusione è il raggiungimento della condizione di *ignizione*, una situazione in cui l'energia liberata dal plasma sia sufficientemente elevata da autosostenere l'intero processo, senza ulteriore riscaldamneto da parte di sorgenti esterne. Le condizioni per raggiungere l'ignizione sono espresse dalla formula empirica [9]:

$$\hat{n}\tau_e\hat{T} > 5 * 10^{21} m^{-3} keV s \tag{1}$$

dove $\hat{n}$ e $\hat{T}$ sono rispettivamente la densità e la temperatura degli ioni nel plasma, e $\tau_e$ è l'energy confinement time descritto sopra.
Data la temperatua del plasma, occorrerà confinarlo in qualche modo in una regione circoscritta. Un metodo è utilizzare il confinamento inerziale (metodo usato alla *National Ignition Facility* (NIF) a Livermore, USA), ma il più diffuso è quello a confinamento magnetico, su cui si basa questa tesi; in particolare, il miglior modo di confinare il plasma è di usare una combinazione di campi magnetici per circoscriverlo in una regione di spazio toroidale; questa configurazione magnetica è utilizzata da macchine chiamate *tokamaks*, un acronimo russo per "macchine toroidali con solenoidi magnetici" (**TO**roidalnaya **KA**mera **MA**gnitnaya **K**atushka). In queste macchine, il plasma viene confinato per interazione delle particelle cariche con campi magnetici, generati dalla macchina, tramite la forza di Lorentz $\vec{F} = q\vec{v} \times \vec{B}$. Si può dimostrare che le derive causate dalla forza di Lorentz implicano che le particelle non saranno confinate qualora si dovesse usare solo un campo magnetico le cui linee di campo sono solo nella direzione toroidale; di conseguenza è richiesta una ulteriore componente nella direzione poloidale del campo magnetico, essenziale per un tokamak, che farà in modo di compensare le derive e confinare il plasma. Questa componente può essere generata inducendo una corrente toroidale nel plasma, utilizzando il principio del trasformatore, dove il primario sarà un solenoide centrale attorno alla struttura del tokamak, e il secondario sarà il plasma stesso. Questo però implica che, per la legge di Faraday, occorra variare il campo magnetico in continuazione, permettendo alla macchina di lavorare solo in modalità pulsata, e non in maniera continua; questa è una delle sfide che la ricerca sulla fusione nucleare deve affrontare.
Per quanto riguarda il tokamak in cui questo lavoro di tesi ha avuto luogo,

il tokamak sperimentale TCV, dall'inizio della sua vita nel 1992, ha avuto come obiettivo principale lo studiare gli effetti del confinamento e della stabilità del plasma; per fare ciò, la caratteristica che distingue TCV dagli altri tokamaks, è la capacità di cambiare la forma della sezione di campo magnetico poloidale secondo i requisiti specificati dall'operatore; in questa tesi in particolare, la configurazione usata è denominata Single Null (SN) inferiore, ed è una delle più comuni configurazioni utilizzate, prevista anche a ITER.
TCV presenta una serie di sistemi di alimentazione esterna, che permettono di raggiungere le condizioni di H-Mode per il plasma. In particolare, i due sistemi di alimentazione sono l'ECRH (acronimo di *Electron Cyclotron Resonance Heating*), che, grazie ad una serie di girotroni, possono iniettare onde elettromagnetiche a frequenze corrispondenti alla seconda armonica della frequenza di ciclotrone degli elettroni [9] (sei girotroni, detti X2, a 82.7 GHz l'uno) ed alla terza armonica (tre girotroni, detti X3, a 118 GHz l'uno), e l'NBH (acronimo di *Neutral Beam Heating*), un sistema di alimentazione esterno che riscalda il plasma iniettando in esso un fascio di particelle neutre (principalmente deuterio), che trasferisce l'energia cinetica delle particelle iniettate al plasma per collisione. In questa tesi i due sistemi utlizzati nei dato sono stati i 3 girotroni X3 dell'ECRH, e l'NBH.
Oltre a ciò, TCV ha una serie di diagnostiche per misurare caratteristiche fondamentali del plasma; in particolare, in questa tesi la dignostica utilizzata è stata quella di Scattering Thomson, che attraverso l'iniezione di un fascio laser all'interno del vessel e del plasma, è in grado di ricavare quantità come la temperatura e la densità elettroniche mediante la luce riflessa per scattering Thomson [3].
Nel capitolo 2 ci si è invece concentrati sulla presentazione di concetti teorici introduttivi sulla fisica dei plasmi, oltre alla modalità di confinamento del plasma di interesse per questo lavoro di tesi, e le conseguenze di questo regime.
Si comincia con la considerazione che il plasma è composto da particelle cariche che genereranno un campo elettromagnetico a causa del loro movimento; questo influenzerà il moto delle cariche circostanti, che a loro volta emetteranno un campo elettromagnetico; quest'ultimo influenzerà la prima carica considerata; un problema di questo tipo, dove un'entità è influenzata come conseguenza di qualcosa che produce, è chiamato *problema auto-consistente*, ed è un problema tipico per la fisica dei plasmi.
Esso può essere descritto come problemi di singole particelle che interagiscono l'un l'altra tramite la forza di Lorentz, ma si tratta di un problema a molti corpi dove il numero di corpi è dell'ordine (nel caso di TCV) di $10^{19}$; per questo motivo, il sistema non è risolvibile. La procedura che si adotta è quindi quella di ottenere delle quantità medie che permettano di valutare quantità misurabili del plasma, per riuscire a risolvere il problema; questo tuttavia fa sì che i comportamenti delle singole particelle si perdano nel comportamento medio del plasma. In questo modo si può arrivare alle due descrizioni derivate maggiormente utilizzate sono la *descrizioni a fluidi multipli*, che tratta il plasma come un aggregato di fluidi composti ciascuno da un'unica specie, come ioni ed elettroni, e la *descrizione magneto-idrodinamica* (MHD),

che descrive il plasma come un unico fluido globalmente neutro; entrambe queste descrizioni devono essere "chiuse" in qualche modo, dato che in un'equazione per un momento, comparirà sempre un termine di ordine superiore in una gerarchia infinita di equazioni.
Per risolvere il problema autoconsistente, nel modello MHD occorrerà usare le equazioni della teoria MHD per arrivare ad ottenere l'*equazione di Grad-Shafranov*, che permette di risolvere il problema autoconsistente, trovando la configurazione di equilibrio della corrente di plasma e del campo magnetico toroidale; il fatto che questo problema abbia bisogno di $\psi$ per essere risolta, che è contenuta nelle quantità $J$ e $B$ a loro volta, rende il problema impossibile da risolvere analiticamente. Una soluzione è risolvere il problema in maniera iterativa, usando un primo profilo come ipotesi e, dopo aver risolto il problema, mettere la nuova soluzione trovata nel problema, per trovare una soluzione sempre più accurata; un programma utilizzato per questa tesi, di nome CHEASE, adotta questa procedura per risolvere il problema autoconsistente.
La tesi prosegue descrivendo le modalità di confinamento del plasma, e le conseguenze del regime di confinamento H-Mode. Nonostante la teoria per un plasma neoclassico sia ben conosciuta [9], essa è applicabile per colonne di plasma, e se dovesse essere applicata alla geometria toroidale, i valori che ci si aspettano per quantità come l'energy confinement time $\tau_e$ sarebbero molto diversi da quelli trovati sperimentalmente. In base alle condizioni in cui un plasma si trova, ci possono essere diversi regimi di confinamento, a cui corrispondono diverse leggi di scala per quanto riguarda l'energy confinement time $\tau_e$. Il primo regime che si incontra è l'*ohmic confinement mode*, dove la temperatura del plasma aumenta per effetto Joule; tuttavia, dato che un plasma si comporta da conduttore perfetto, esso diminuisce la sua resistività a potenze elevate, il che risulterà in una minore potenza assorbita. Se si comincia a fornire potenza tramite sorgenti esterne, il plasma passa alla *L-Mode of confinement*. Lo svantaggio maggiore di questa modalità è che il tempo di confinamento in L-Mode decresce con l'aumentare della potenza, il che rende impraticabile usare un regime L-Mode per plasmi ad alta potenza.
Se viene fornita ulteriore potenza, eventualmente superando un certo valore di soglia, si passa nel *H-Mode of confinement*. Le caratteristiche principali di questa modalità di confinamento sono il sorgere di una barriera di trasporto, che si forma per un profilo di rotazione di taglio causato da un campo elettrico radiale [1], e in particolare dal contributo dato da $\vec{E}_r \times \vec{B}$; questo comportamento sopprime le turbolenze a lungo raggio nel plasma; il profilo rotazionale è chiamato *$E_r$ well*. Questa modalità di confinamento ha il vantaggio di avere un valore più elevato dell'energy confinement time $\tau_e$, che risulta essere circa il doppio di quello in L-Mode. Inoltre, il plasma in H-Mode, a causa della barriera di trasporto, vede un aumento dei profili di temperatura, densità e pressione, che culminano in una brusca discesa a valori prossimi allo zero verso il bordo; questa regione ad alti gradienti è chiamata *pedestal*.
Un'altra caratteristica dell'H-Mode è il sorgere di una corrente, detta *bootstrap current*, che è collegata alle collisioni tra particelle libere di ruotare attorno

al plasma e quelle che invece, a causa della configurazione magnetica, rimangono "intrappolate" in una regione di spazio; questa frizione trasferisce momento, risultando in una corrente netta che dipende dal gradiente di pressione nella regione al bordo del plasma, nella regione del pedestal; questa corrente gioca un ruolo importante, dato che è una componente aggiuntiva nella generazione del campo magnetico poloidale, che quindi confina ulteriormente il plasma.
Per queste caratteristiche, la modalità H-Mode sarà lo scenario operativo principale di ITER.
Tuttavia, in un plasma H-Mode si formano instabilità; un possibile meccanismo secondo cui queste instabilità si formano è ipotizzato dal modello EPED1, dove il gradiente del pedestal cresce fino ad un certo limite di stabilità imposto da un modo di instabilità chiamato *Kinetic Balloning Mode* (KBM), per poi innalzarsi ed allargarsi (mantenendo quindi il gradiente costante) fino a quando non si raggiunge un secondo limite di stabilità, per un secondo tipo di instabilità chiamato *Peeling Ballooning Mode* (PB); quando entrambi i limiti vengono raggiunti, si ha la culminazione in un processo di rilassamento chiamato *Edge Localized Mode* (ELM), la cui conseguenza è l'espulsione di plasma dalla regione in cui il plasma è confinato; questo fa sì che i componenti presenti all'interno del vessel siano sottoposto a carichi termici in maniera pulsata, che possono generare sforzi termici considerevoli, riducendo la vita del componente; uno dei componenti più a rischio è il divertore, un elemento essenziale di un tokamak, in quanto è la regione in cui le linee di campo magnetico si chiudono sul vessel.
Ci sono diversi tipi di ELMs, ma le più note sono le *ELM di tipo III*, caratterizzate da emissioni di plasma meno intense, ma più frequenti, la cui frequenza diminuisce con la potenza iniettata nel plasma, e le *ELM di tipo I*, meno frequenti, ma la cui energia emessa è molto elevata, al punto che queste ELMs sono considerate le più pericolose per l'elevato carico termico pulsato; esse aumentano in frequenza all'aumentare dell'energia iniettata [10].
Per questi motivi, occorre studiare le ELMs per prevederne il comportamento in future macchine, come ITER. L'idea è quindi di raccogliere dati dai vari tokamak, per poi avere tutti i dati per ricavare andamenti per le quantità secondo i vari tokamak in diverse condizioni, con il fine ultimo di estrapolare i valori dei tokamak futuri facendo considerazioni su dove tali punti si troverebbero sul grafico considerato, e l'andamento dei punti ricavati con gli altri tokamaks.
Nel capitolo 3 si è descritto il processo di costruzione del database, i fit dei dati ed il calcolo di quantità legate all'equilibrio del plasma. Il database in questo lavoro di tesi è stato costruito avendo come obiettivo l'accesso rapido ai dati di interesse, per poi fare ulteriori considerazioni su di essi; il programma che costruisce il database, scritto in Matlab, è stato pensato per non fermarsi mai durante l'esecuzione del programma, attraverso l'utilizzo delle funzioni Matlab *try()* e *catch()*; oltre a ciò, il programma permette la manipolazione dei dati già salvati in sessioni precedenti.
La prima fase della costruzione del database è stata di scegliere una serie di scariche di plasma, prese da una serie di 6 tabelle composte da esperimenti effettuati negli anni 2017-2018, sotto la condizione di stazionarietà di quan-

tità come la potenza fornita al plasma dall'NBH e dall'ECRH, la densità e la corrente di plasma; sono stati scelti in questo modo $\sim 280$ scariche. Sotto queste condizioni, vengono prelevati i dati dalla diagnostica di Scattering Thomson sulla temperatura e densità del plasma, che poi sono stati sottoposti ad un processo di fitting: in particolare, due fitting, lineare e a tangente iperbolica modificata (mtanh), sono stati utilizzati; in questo modo è stato possibile ricavare quantità rilevanti sul pedestal. Oltre a ciò, si è utilizzato il codice CHEASE per risolvere iterativamente il problema autoconsistente, e quindi l'equazione di Grad-Shafranov, in modo tale da ricavare quantità come la corrente di bootstrap e il campo magnetico nel vessel. Infine, quantità riguardanti direttamente le ELM e quantità operative come la potenza dell'NBH o dell'ECRH, o geometriche come la triangolarità e l'eccentricità del plasma, prese dal codice LIUQE (inverso di EQUIL) sono state salvate nel database. I dati sono stati presi dall diagnostica di Scattering Thomson tramite la funzione *plot_ts_ELM.m*.
Dopo aver estratto i dati dalla diagnostica, il programma ha cominciato il fit dei dati. Per quanto riguarda il fitting lineare dei dati, si è utilizzata una funzione formata da tre rette, composte tra loro in modo da realizzare la forma del pedestal attraverso la funzione di Heaviside, ottenendo così, dopo aver applicato le opportune condizioni al contorno:

$$\begin{aligned} linfit([b_1, b_2, b_3, b_4, b_5], \psi) = (b_1\psi + b_2) \times H(b_3 - \psi) \\ + (b_4\psi + b_{01}) \times H(\psi - b_3) \times H(b_5 - \psi) \end{aligned} \tag{2}$$

I valori salvati nel database sono composizioni di quelli calcolati: la posizione del pedestal, ($p_{ped} = (b_5 + b_3)/2$), la sua altezza ($h_{ped} = b_1 b_3 + b_2$) e ampiezza ($w_{ped} = b_5 - b_3$), la pendenza della regione di core prima del pedestal ($coreslope = b_1$) e l'offset della coda del pedestal ($h_{offset} = b_4 b_5 + b_3(b_1 - b_4) + b_2$). Per il fit mtanh, si è usata la funzione:

$$mtanh(x) = \frac{e^{ax} - e^{-bx}}{e^{cx} + e^{-dx}} \tag{3}$$

dove:

$$w_{ped} = 4w \qquad core\ slope = \frac{h^{ped} - h^{offset}}{4w} s \tag{4}$$

I fit dei profili di temperatura e densità sono stati poi selezionati in base al loro coefficiente di bontà del fit $R^2$. In particolare, tale test è stato condotto per tutti e quattro i profili, e se uno solo di essi non ha presentato un valore di $R^2$ superiore a 0.91, il valore di soglia scelto come criterio per avere un buon fit, la scarica di plasma è stata scartata completamente. Inoltre, per uniformare i dati rispetto alle fluttuazioni dei dati acquisiti dal sistema di Scattering Thomson, una convenzione usata è di traslare rigidamente il profilo di temperatura in modo tale da avere, a $\psi = 1$, cioè alla *Last Closed Flux Surface* (LCFS), un valore di temperatura di 50 eV.
I profili di temperatura e pressione sono stati quindi inseriti come prima iterazione per risolvere il problema autoconsistente, tramite il codice CHEASE. In questo modo quantità legate alla configurazione in equilibrio del problema sono state derivate, come la bootstrap current [5], ma anche quantità

come il *normalized pressure gradient*, $\alpha$, definito come:

$$\alpha = -\frac{2}{(2\pi)^2}\frac{\partial V_{tot,mtanh}}{\partial \psi}\left(\frac{V_{tot,mtanh}}{2\pi^2 R}\right)^{1/2}\mu_0\frac{\partial p_e}{\partial \psi} \tag{5}$$

in particolare, quest'ultima quantità è importante nello studio della stabilità del plasma. Il resto delle quantità del database sono state ottenute dalla derivazione dai fit o da CHEASE, oppure è stato ricavato dal codice LIUQE. In particolare, nel database sono contenute quantità riguardanti informazioni sul pedestal, come la sua posizione e ampiezza, o il massimo valore del gradiente del profilo considerato, e del tipo di fit considerato. Successivamente è stato considerato il calcolo di quantità come il volume del plasma fino al punto più alto del pedestal, o il volume totale del plasma, che è stato calcolato fino alla posizione corrispondente alla fine del pedestal, e la temperatura degli ioni, ottenuta ipotizzando $T_i = 0.7T_e$, e $n_i = n_e$. Successivamente, sono state calcolate quantità adimensionali come il confinamento magnetico $\beta$ e la collisionalità $\nu^*$. Una sezione del database è dedicata a quantità relative solamente alle ELMs, come la loro frequenza e la durata media (in ms) di una singola ELM nella scarica, mentre un'altra sezione riporta le quantità operative per la singola scarica, quali la potenza fornita tramite l'NBH o l'ECRH, la potenza irraggiata, e anche i flussi di particelle iniettati nel plasma durante la scarica, sia di fuel che di impurità, effettuate dato che c'è una correlazione tra le caratteristiche del pedestal e le condizioni di *fueling* e *impurity seeding* della scarica di plasma [8]. Infine, si ha nel database una sezione per le quantità operative collegate alla geometria del plasma, come la triangolarità e l'elongazione del plasma, le coordinate delle linee di campo magnetico sul vessel, e quantità legate all'equilibrio derivate da CHEASE, come $p'$ e $FF'$, e la corrente di bootstrap.
Dai dati ricavati nel database, si è quindi cercato di fare delle considerazioni di tipo qualitativo sugli andamenti e comportamenti dei dati, cercando di relazionarli anche con altri lavori, sia interni che esterni a TCV; questo lavoro è descritto nel capitolo 4. In particolare, si sono fatte ulteriori restrizioni ai dati racavati nel database; si è imposto un intervallo di tempo di almeno 0.15 s, in modo da avere un intervallo di tempo almeno superiore a 5 volte il valore dell'energy confinement time $\tau_e$, e si sono eliminate altre scariche per motivi come l'assenza di dati in certe situazioni. Il database finale comprende circa 95 scariche.
Dopo aver elencato alcune delle quantità nel database e le loro variazioni, si è cercato di investigare le conseguenze della potenza iniettata nel sistema sulla generazione di ELM nel plasma. In particolare, si è notata nel database la presenza tra ELM di tipo I e di tipo III, in base alle caratteristiche che distinguono questi due tipi di ELMs [10]. Si è inoltre notato che quantità come la potenza, la temperatura e la collisionalità sono correttamente correlate tra loro, con la collisionalità che decresce al crescere della temperatura e della potenza applicata.
Si è guardato inoltre alla perdita di energia per ELM per entrambi i tipi di ELMs, sia di tipo I che di tipo III, notando che le prime emettono più energia, ma sono meno frequenti delle ELM di tipo III, che invece emettono

meno energia.
Tuttavia, se si guarda alla frazione di potenza persa da tutte ELM nella scarica, definita come $\Delta W_{ELM} f_{ELM}/P_{net}$, si vede come le ELM di tipo III perdano molta più potenza delle ELM di tipo I; infatti le ELM di tipo III, benchè emettano di meno singolarmente, complessivamente fanno in modo che il plasma perda più potenza, il che risulta in una perdita di plasma (e di confinamento) maggiore.
Dopo aver fatto queste considerazioni sugli effetti della potenza iniettata sulle ELM, si sono fatte delle osservazioni qualitative riguardo alle quantità trovate facendo i fitting dei dati del pedestal; queste sono solo considerazioni qualitative, dato che, per fare delle considerazioni più avanzate, si dovrebbe tenere in conto di tutte le condizioni in cui la scarica si è trovata, di tipo geometrico (triangolarità), di potenza di alimentazione (NBH, ECRH o entrambi accesi), di fueling e seeding e così via.
I valori usati sono quelli derivati dai fit mtanh, perchè non c'è una grande variabilità tra i valori dati da questo fit e quello lineare. Per quanto riguarda la temperatura, l'ampiezza del pedestal sembra incrementare all'aumentare dell'altezza del pedestal, mentre ci sono quattro punti ad altezze elevate che sembrano decrescere in ampiezza, ma non ci sono dati sufficienti per fare delle considerazioni a riguardo. Invece, per quanto riguarda il valore massimo del gradiente del pedestal (trovato circa a metà del pedestal stesso), questo incrementa nettamente con l'aumentare dell'altezza del pedestal, e lo stesso si può dire del gradiente normalizzato $\nabla T_{e,max}/T_{e,ped}$; questo significa che il pedestal diventa più ripido man mano che la sua altezza sale. Sono state inoltre visualizzate le condizioni di fueling e seeding delle varie scariche.
Per quanto riguarda la densità, i dati non hanno portato ad alcun tipo di comportamento conclusivo con solo questa analisi qualitativa, ad eccezione del gradiente di densità, che aumenta anch'esso all'aumentare del pedestal.
Per concludere, si sono fatte delle prime considerazioni sulla possibilità di estrapolare delle leggi di scala dai dati contenuti nel database. Il database è stato testato ad una legge di scala sulla durata media delle ELM $\tau_{ELM}$, che però non si è rivelata accurata. A questo proposito si è proposta una seconda legge di scala, basata sul confinamento $\beta$ e la temperatura del pedestal, sia degli ioni che degli elettroni, assumendo $T_{i,ped} = 0.7 T_{e,ped}$, e la frequenza delle ELM; in questo caso, i dati sembrano seguire in maniera più accurata la legge di scala.
Infine, in questo lavoro di tesi si è fatta una prova riguardo alla legge di scala proposta dal modello EPED1 sull'ampiezza del pedestal:

$$w_{ped} = D\sqrt{\beta_\theta^{Ped}} \tag{6}$$

dove D è un parametro diverso per ogni tokamak; si sono quindi confrontati i dati con un lavoro esterno per il tokamak JET-ILW, ottenendo così che i dati sono in accordo tra loro, ma entrambi non seguono le leggi di scala proposte.
Si è infine guardato al lavoro svolto in [8], per testare se le scariche del database si comportassero nello stesso modo, dato che sono state prese nella

stessa tabella di esperimenti, e alcune sono le stesse scariche. Mettendosi nelle stesse condizioni di [8], si è ottenuto che i dati del database, a parte alcuni punti, sono in buon accordo tra loro. Infine, nel capitolo 5, relativo alle conclusioni, si sono fatte delle considerazioni finali sul database; esso ha raggiunto i requisiti di essere affidabile (non fermandosi mai nell'esecuzione) e ben definito (tutte le quantità sono facilmente accessibili), rimanendo relativamente flessibile nella formulazione (i dati possono essere manipolati e modificati fino ad un certo livello); tuttavia, ci sono alcuni miglioramenti da fare, come il raffinare il criterio di selezione dei profili di fit, e il risolvere problemi legati alla ricostruzione del profilo di CHEASE. In futuro, questo database potrebbe essere utilizzato come punto di partenza per la realizzazione di un database per TCV che, messo assieme ai database degli altri tokamaks nel mondo, costituirà la fonte di informazioni principali nello studio delle ELM nell'ottica della progettazione di ITER.
Questo lavoro di tesi è stato sviluppato in un periodo di quasi sei mesi allo Swiss Plasma Center (SPC), all'É*cole Polytechnique Fédérale de Lausanne*, Svizzera, sul tokamak sperimentale TCV (*Tokamak* á *Configuration Variable*).

# Chapter 1

# Introduction

In the Modern era, nuclear physicists started to describe the atomic world and, by going even deeper, the phenomena that happen inside the atom itself; because of that, nuclear reactions, akin to the more conventional chemical ones, started to be discussed by brilliant scientist like Henri Becquerel, Marie and Pierre Curie and Ernest Rutherford.
In particular, two specific reactions began being; in 1932, the first artificial nuclear reaction had been achieved by Rutherford's assistants, the irish Ernest Walton and the british John Cockcroft, by splitting in two $\alpha$ particles a $^7Li$ atom, and, in the same year, the australian physicist Mark Oliphant realized the first nuclear fusion of heavy hydrogen isotopes.
However, nuclear fission research proceeded in a more prominent way than nuclear fusion for quite some time; in 1934, a group of Italian physicists, lead by Enrico Fermi (the so called *ragazzi di via Palisperna*), realized the first fission of $^{235}U$, but they thought they were creating other transuranics; in 1938, german nuclear chemists Otto Hahn and Fritz Strassman were the first ones that managed to demonstrate that a nucleus of $^{235}U$ can undergo fission if successfully struck by a thermal neutron.
During the events of the Second World War, there was already some solid knowledge about the possibility to produce electrical power from nuclear fission; the very first fission reactor, *Chicago Pile-1*, had been built in 1942 and, under the supervision of Enrico Fermi, it operated for the first time for 28 minutes.
However, the possibility of the fission reaction to release tremendous amount of energy in an explosive way also led to the creation of the Manhattan project, in order to develop nuclear based weapons; the first one had been made explode the $16^{th}$ July, 1945 and, in August, the dramatic drops of "Little Boy" on Hiroshima and "Fat Man" on Nagasaki occurred in a timelapse of three days (the $6^{th}$ and $9^{th}$ August 1945, respectively).
One year after these dramatic events, in a scientific meeting at Los Alamos in 1946, ungarian physicist Edward Teller supported the possibility to build a bomb that employed nuclear fusion reactions, instead of fission ones. Since the U.R.S.S., after seeing such a powerful military asset America had, started developing nuclear weapons as well, the research of a fusion reaction-based bomb intensified from both sides. The first H-bomb exploded the $1^{st}$ December, 1952, and it was of russian origin. These were the years of the so called Cold War.
In the 50s, serious studies about energy production via fusion reactions began as well,

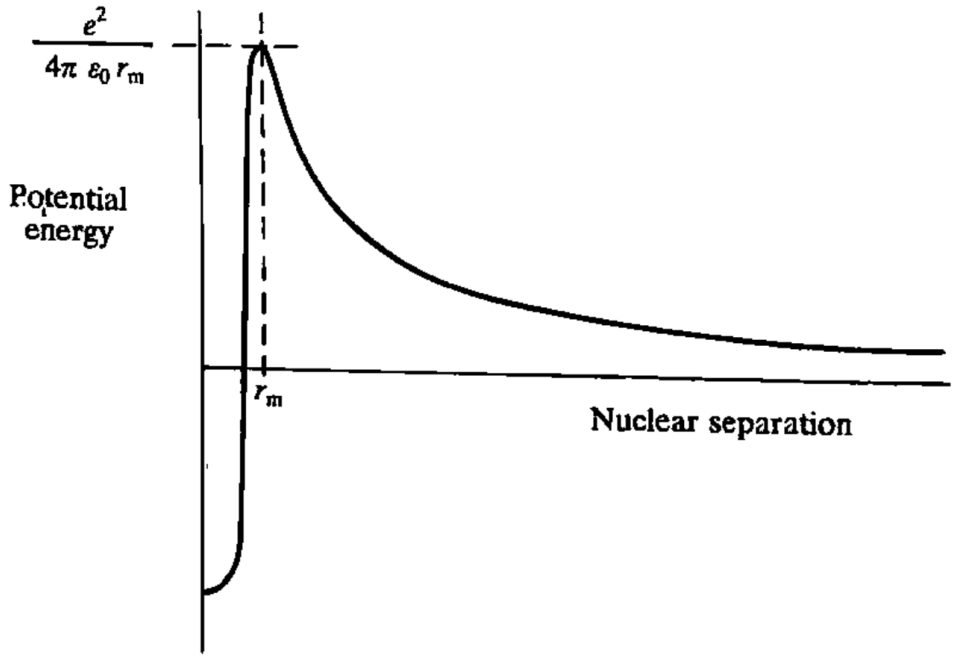


Figure 1.1: Coulomb repulsion energy as a function of the distance between nuclei

and, almost 70 years later, the research in this field is still going on, and the construction of the *International Tokamak Experimental Reactor*, *ITER*, is its most recent and most important effort to demonstrate the feasibility of producing electrical power by exploiting nuclear fusion reactions.

## 1.1 Basics of nuclear fusion reactions

A nuclear fusion reaction is obtained by making two lighter nuclei merge; the result would be an heavier nucleus, in addition to several other particles, such as charged particles, neutrons and neutrinos; however, after the reaction occurred, it can be seen that the mass of the reaction products will be lower than the sum of the separate nuclear reagents; this missing quantity of mass is called *mass deficit* and, according to Einstein's mass-energy equivalence $E = mc^2$, is equivalent to the energy liberated when the two lighter atoms fuse together, which is translated into kinetic energy for the fusion reaction products.
The attractive force that makes nuclear fusion reactions possible is the strong nuclear force which, at very short distances, is able to overcome the Coulomb repulsion force. This is accomplished by supplying enough energy to the system, making the nucleons overcome the Coulomb repulsion energy barrier. However, according to quantum physics considerations, there is a finite probability by which the nucleons can pass through the Coulomb energy barrier even though they don't have enough energy to overcome it, which decreases exponentially with the energy barrier length; this phenomenon, called *quantum tunneling*, reduces the overall probability of nuclear fusion reactions, thus lowering the value of the reaction cross section. A depiction of the Coulomb energy barrier is shown at figure 1.1. Lighter elements are more likely to undergo fusion reactions, since

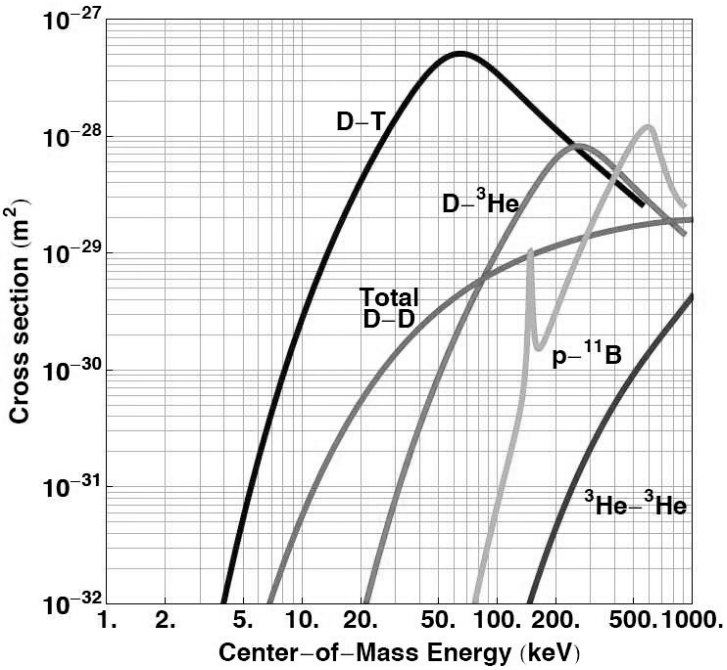


Figure 1.2: Cross sections for D-T, D-D, D-$^3He$ reactions. Other less common fusion reactions are shown as well [9].

the heaviest particles would have to overcome a huge Coulomb energy barrier caused by the higher number of protons in the nucleus. In particular, the lightest nuclei (hydrogen, both in deuterium (D) and tritium (T) form, and helium) are the most used elements as far as fusion reactions for the production of energy are concerned:

$$ {}^2_1\mathrm{D} + {}^3_1\mathrm{T} \longrightarrow {}^4_2\mathrm{He}\,(3.5\,\mathrm{MeV}) + {}^1_0\mathrm{n}\,(14.1\,\mathrm{MeV}) \tag{1.1} $$

$$ {}^2_1\mathrm{D} + {}^2_1\mathrm{D} \longrightarrow {}^3_2\mathrm{He} + {}^1_0\mathrm{n} + (3.27\,\mathrm{MeV}) \tag{1.2} $$

$$ {}^2_1\mathrm{D} + {}^3_2\mathrm{He} \longrightarrow {}^4_2\mathrm{He} + {}^1_1\mathrm{H} + (18.3\,\mathrm{MeV}) \tag{1.3} $$

However, several more reactions have been proposed, even though less known (fig. 1.2). The D-T nuclear reaction is the most favorable one because it reaches the highest cross-section at just over 100keV, while the others have lower cross sections at higher energy levels.

In the D-T reaction, both the reagents are a variant of hydrogen; D is present in H for one part in 6700, which makes it naturally abundant (the oceans contain a quantity of D to satisfy the current energy needs for approximately $10^{11}$ years [9]), while T, because of its short half-life time of 12.3 years, is almost not existant on our planet; however, it can be produced by exploiting the (n,$\alpha$) nuclear reactions of $^6Li$:

$$ {}^6_3\mathrm{Li} + {}^1_0\mathrm{n} \longrightarrow {}^4_2\mathrm{He}\,(2.05\,\mathrm{MeV}) + {}^3_1\mathrm{T}\,(2.75\,\mathrm{MeV}) \tag{1.4} $$

Other reactions for the production of Tritium are with endothermic reactions using $^7Li$, or by using $^{10}B$ and high energy neutrons:

$$ {}^7_3\mathrm{Li} + {}^1_0\mathrm{n} \longrightarrow {}^4_2\mathrm{He} + {}^3_1\mathrm{T} + {}^1_0\mathrm{n} \tag{1.5} $$

$$^{10}_{5}\mathrm{B} + ^{1}_{0}\mathrm{n} \longrightarrow 2\,^{4}_{2}\mathrm{He} + ^{3}_{1}\mathrm{T} \tag{1.6}$$

Since the quantity of $^6Li$ on Earth is such that, if used for nuclear fusion, had been estimated to meet the global energy consumption for $10^4$ years for lithium on land and $10^6$ years for lithium in the oceans [9], and since deuterium has a natural abundance on oceans of about one atom in 6420 of hydrogen, which could meet the global energy consumption for $10^{11}$ years and it is easily separable, nuclear fusion can become a long lasting source of energy.

## 1.2 Conditions for a plasma

In order to achieve fusion reactions, the most promising method would be to make the particles reach a temperature corresponding to the cross section peak. In order to estimate the temperature, one should look at the Boltzmann equation $E = k_B T$, where $k_B = 8.6 \times 10^{-5}\ eVK^{-1}$ is the Boltzmann constant. So, if the maximum fusion cross section is achieved at 100 $keV$ for the D-T reaction, a temperature of the order of roughly $10^9 K$ is required to achieve maximum probability of fusion for a single particle. However, since the reactions at the maximum energy occur in the high energy tail of the Maxwellian distribution of the particles, making the particles escape the system sooner, in order to achieve a significant number of reactions with good probability the optimal energy is around 10 $keV$, at the order of 100 million of $K$ [9].
At such temperature, ions and electrons behave as free charged particles, not organized in atoms. This is recognized as a different state of matter, called *plasma*, which can be described as a fully ionized, globally neutral gas. Since it is composed of charged particles, such state of matter is subjected to the influence of electromagnetic fields, both internal to the plasma and applied from outer sources, due to the Maxell's equations, which in their most general form read:

$$\begin{cases} \nabla \cdot E = 4\pi k_1 q \\ \nabla \cdot B = 0 \\ \nabla \times E = -k_3 \frac{\partial \vec{B}}{\partial t} \\ \nabla \times B = \frac{1}{c^2 k_3} \frac{\partial \vec{E}}{\partial t} + 4\pi \frac{k_2}{k_3} \vec{J} \end{cases} \tag{1.7}$$

Where, in SI notation, $k_1 = \frac{1}{4\pi\epsilon_0}$, $k_2 = \frac{\mu_0}{4\pi}$ and $k_3 = 1$, and in Gaussian notation $k_1 = 1$, $k_2 = \frac{1}{c^2}$ and $k_3 = \frac{1}{c}$. Both forms will be used in this thesis.
The extreme temperature conditions a plasma has means there should be a machine designed to confine such a material, which will be further discussed in the following chapter. After such energy is provided, the particles must retain it and stay in the region where fusion reactions occur for a period of time long enough to let them undergo fusion reactions themselves; firing beams of particles against a solid target or against another beam are ineffective methods to achieve fusion, because in the first case the particles lose their energy too rapidly, while in the second case the density achieved by each of the beams is too low.
The main goal of nuclear fusion research is to achieve *ignition* conditions, in which the

energy released by the fusion reactions heats the plasma high enough to render the whole process self-sustaining, without further heating input from outer sources. The condition to achieve ignition can approximately be expressed by:

$$\hat{n}\tau_e\hat{T} > 5 * 10^{21} m^{-3} keV s \tag{1.8}$$

where $\hat{n}$ and $\hat{T}$ are respectively the peak ion density and temperature in the plasma and $\tau_e$ is the energy confinement time.

## 1.3 Magnetic confinement: Tokamak

Due to the very high temperature, a plasma must be confined in some way; nowadays, two methods are used, from which two very different types of machine have been built: one relies on what is called *inertial confinement* ; a solid fuel pellet made of D and T at cryogenic temperature is irradiated by a set of lasers pulsed all at the same time and over all directions of the pellet; the thermal shock causes a very rapid ablation of the pellet external layer, causing in turn, according to the action-reaction law, a violent contraction of the pellet itself; this compression is so violent that the temperature in the gaseous core is able to rise high enough to trigger fusion reactions in the pellet; a machine that uses such concept is located at the *National Ignition Facility* (NIF) at Livermore, USA.
The other method of confinement is to use electromagnetic fields, by employing as fuel gaseous D and T, which will become the plasma. If the magnetic field configuration is arranged in straight field lines, the plasma column that generates must be contained by compressing the extremities of the magnetic field, thus reflecting the particles at the extremities back by so called *mirror effect* [9]. However, the best way to contain particles with high velocities is to reconnect the plasma column by arranging it in a toroidal fashion. This magnetic field configuration is used in machines that are called *tokamaks*, a russian acronym for *toroidal chamber with magnetic coils* (**TO**roidalnaya **KA**mera **MA**gnitnaya **K**atushka).
Inside a tokamak, since the particles in a plasma are charged, they will be affected by the Lorentz force $\vec{F} = q\vec{v} \times \vec{B}$, thus drifting in the perpendicular direction of the magnetic field lines; these drifts can be caused by [9] :

- the presence of an electric field $\vec{E}$ perpendicular to the toroidal direction, which generates an $\vec{E} \times \vec{B}$ drift.
- because a gradient of the magnetic field $\vec{B}$ in its perpendicular direction exists.
- because the magnetic field lines are curved.

These drifts imply that the particles in the plasma cannot be confined with only a magnetic field in the toroidal direction, but require an additional field operating perpendicularly to it, a so-called poloidal component of the magnetic field; this component is such that the magnetic field lines follow an helical path along the toroidal direction, and the

charged particles orbit around such lines; this quite complex motion is capable of confining the particles inside the torus, compensating the drifts; such poloidal field is then essential in confining the plasma [9].
In a tokamak, by inducing a movement of the plasma in the toroidal direction, a toroidal current $I_{tor}$ can be generated, and as a consequence, the poloidal field as well; moreover, being a plasma a gas composed by charged particles, it is characterized by a pressure which makes the plasma itself expand; this expansion is prevented by applying a vertical magnetic field $\vec{B}_v$, which balances, thanks to the Lorentz force, the pressure gradient, $\nabla p$, that arises inside the tokamak.
In order to induce a toroidal current, the transformer principle is employed, where the central solenoid acts as the primary winding, while the plasma itself acts as the secondary. However, even though there is the advantage to keep the toroidal symmetry, this configuration cannot operate in stationary conditions; because one of the Maxwell's equations, the *Faraday-Newmann-Lenz's law* :

$$\nabla \times E = -\frac{\partial B}{\partial t} \tag{1.9}$$

the only way to induce a current inside the tokamak is to keep varying the magnetic field in time, allowing only pulsed operation conditions; thus, one of the major research fields in nuclear fusion is to think about other methods to drive the plasma current in a continous way.
The magnetic structure in a tokamak consists into an infinite set of toroidal surfaces nested one inside each other, and they not only represent iso-surfaces of magnetic field and current, but also of pressure. The ratio of the difference in toroidal angle $\Delta\phi$ with respect to a complete toroidal revolution is called safety factor q, alternatively written (by assuming tokamaks with large aspect ratio and circular plasma cross section) as:

$$q = \frac{\Delta\phi}{2\pi} = \frac{rB_\phi}{RB_\theta} \tag{1.10}$$

where $r$ and $R$ are respectively the minor and major radius of the torus, and $B_\phi$ and $B_\theta$ the toroidal and poloidal magnetic field. Since the stability of the plasma is mainly tied to the behaviour of $B_\theta$ and the current density $\vec{j}$, which depends on the toroidal field, the safety factor q is an essential parameter in determining the MHD (Magneto-Hydro Dynamic) stability of the plasma inside the tokamak, with higher values generally determining greater stability. For rational values of q, the field line closes after a number of revolutions, thus allowing the generation of MHD instabilities in the plasma, which can cause damage to the tokamak's plasma facing components.

## 1.4 TCV

The *Tokamak* á *Configuration Variable*, or TCV, is an experimental tokamak located at the Swiss Plasma Center (SPC), inside the É*cole Polytechnique Fédérale de Lausanne* (EPFL) campus, Lausanne, Switzerland. This thesis work has been carried out at this facility.

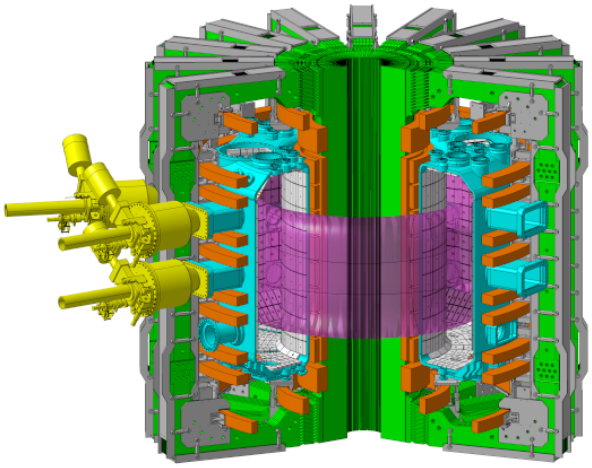

(a)

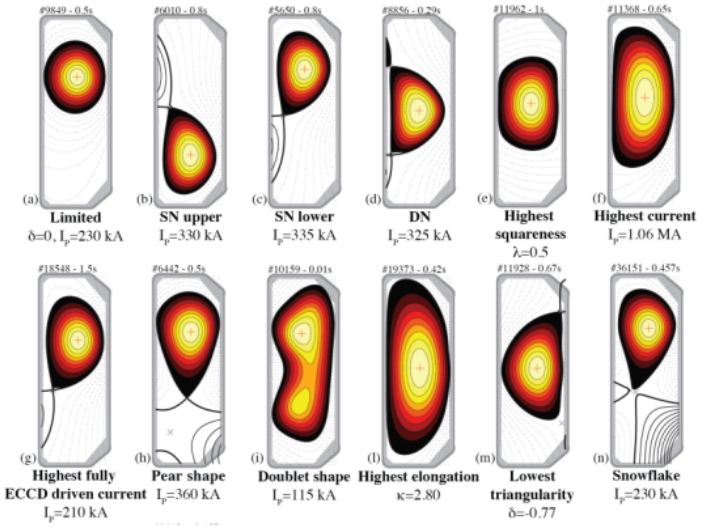


(b)

Figure 1.3: (a) TCV section and key components overview; plasma shaping poloidal field coils (orange); vessel (light blue); plasma (purple); poloidal coils (green); main support structure (grey); external power supplies ports (yellow). (b) TCV plasma cross section configurations.

The main objective of TCV since 1992 has been to study the effects of plasma confinement and stability; because of this, its distinctive feature from all the other existing machines is that it allows to change the shape of the poloidal section to the desired configuration. The principal shape used in this thesis is the *Single Null* (SN) lower configuration (see fig. 1.3(b)).

In order to accomplish such feature, a total of 16 independently controlled poloidal field coils, mounted at the side of the plasma vessel (fig. 1.3(a)), are used. Thanks to them, the tokamak is able to operate at high plasma elongation, $\kappa \leq 2.8$ and triangularity $\delta$ between -0.6 and 0.8. The main TCV quantities are listed in table 1.1 The tokamak is equipped with several ports that allow the connection of diagnostics and multiple heating power supply systems; moreover, the data collected from the diagnostics are sent to a computer cluster after each plasma experiment, or *shot*, where several codes are able to calculate relevant parameters, and then stored.

Table 1.1: TCV main parameters

| | |
|---|---|
| Major radius R | 0.88 m |
| Minor radius a | 0.25 m |
| Max. Magnetic field $B_{tot}$ | 1.54 T |
| Max. Plasma current $I_P$ | 1.0 MA |
| Max. elongation $\kappa$ | 2.8 |
| Triangularity $\delta$ | -0.6÷0.8 |
| Ohmic heating $P_\Omega$ | 0.2÷1.0 MW |
| Neutral Beam Heating $P_{NBH}$ | 1MW |
| Electron-Cyclotron Heating $P_{ECRH}$ | 0.5÷3.0 MW (X2)<br>0.45÷1.2MW (X3) |
| Toroidal field coils | 16 |
| Poloidal field coils | 16 external+2 internal |
| Time pulse s | typ. 2 s, max. 4s |
| Main species | H, D, He |
| Electron density $m^{-3}$ | $1 \div 20 \times 10^{19}$ $m^{-3}$ |
| Electron temperature keV | up to 15 keV |
| Ion temperature keV | up to 2.5 keV |

### 1.4.1 Heating power supplies

At TCV, two external power supplies are employed, apart the energy caused by ohmic effect; the first one is the *Electron Cyclotron Resonance Heating* (ECRH or ECH) system, while the other, more recent one is the *Neutral Beam Heating* (or *Injection*) system, or NBH (or NBI).
The ECH is composed by six gyrotrons working at the frequency of 82.7 $GHz$, for heating at the second harmonic of the electron cyclotron resonance frequency (X2), and three of them that work at 118 $GHz$, at the third harmonic (X3) [6]. The polarization of the beam is modifiable; the extraordinary mode of propagation is the one usually used.
The X2 system is installed as separate launchers both in equatorial and upper positions in the tokamak; they are able to heat the plasma up to the cut-off density of the second harmonic of the electron cyclotron frequency, set at $n_{e,cut-off,X2} = 4.25 \times 10^{19}\ m^{-3}$, and the nominal power each gyrotron can reach is of 465 $kW$ [6].
With respect to X2, the X3 system combines its respective three launchers in a single port at the top of the vessel, and they can heat the plasma up to the cut-off density of the third harmonic propagation, higher than the second one: $n_{e,cut-off,X3} = 11.5 \times 10^{19}\ m^{-3}$. In order to maximize the absorption, the launcher is almost tangential to the resonant plasma surface; the nominal power of the gyrotrons is 480 $kW$ each. If power modulation of 50% duty cycle is used on one gyrotron, it can be used to attain half power [6].
The NBH working principle is different from the ECH; instead of injecting electromagnetic waves in the plasma, it injects a beam of neutral particles, which should be the same as the ones that compose the fuel; this way, energy is transferred from the beam's

particles, which will ionize and become part of the plasma itself, thanks to collision phenomena. The maximum power reachable by the NBH is 1.2 $MW$.
In this thesis, the power supplied in all experiments is due to the X3 ECH, the NBH, or a combination of both, while the X2 gyrotrons are never used , since it imposes a too severe limitation on the cut off density.

### 1.4.2 Diagnostic: Thomson Scattering System

There are several diagnostic systems at TCV, such as magnetic probes and a Far InfraRed (FIR) interferometer; the most used one in this thesis is the *Thomson Scattering System*, a diagnostic system that gathers data on the electron temperature and density profiles inside the plasma, by gathering the light emitted by the electrons in the plasma by Thomson scattering (see Appendix A).
In order for this scattering to occur, plasma electrons are irradiated by three pulsed Nd-YAG lasers of beam energy 1.5 $J$ and pulse duration of 10-15 $ns$. The laser has a wavelength of 1064 $\mu m$, in the infrared spectrum, with a frequency of 20 $Hz$ per pulse. The beam diameter is $\sim 10$ $mm$, and its beam divergence of about 1 $mrad$.
The lasers are located in a separate room from TCV, and they are grouped on an optical table; they are then guided towards a box underneath TCV as a bundle through five steering mirrors, and then two mirrors for each beam align them for their passage through the vessel. The linearly polarized beams, which have their electric field parallel to the toroidal magnetic field of the plasma, travel from the bottom to the top of the vessel [6]. When the beam passes through the plasma, the scattering takes place, and the light is collected by three wide-camera lenses installed on the side of the vessel, their optical axes aligned with the toroidal field. The scattered light is then collected by 89 fiber channels, organized in bundles and connected to polychromators which send the signal to the diagnostic system. The data are then converted into density and temperature data.

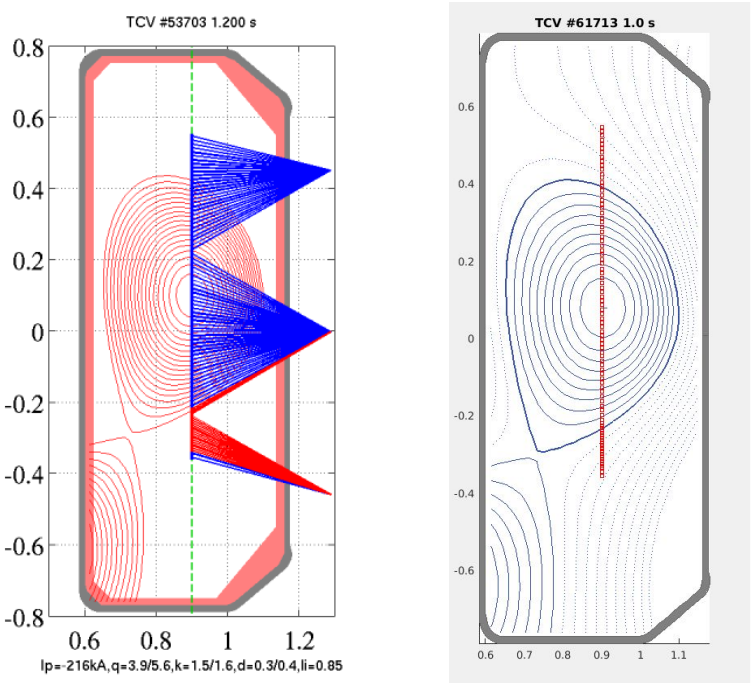


(a) (b)

Figure 1.4: (a)Thomson scattering laser system. The laser (green line) is emitted from below. The emitted light from scattering is then collected by the fiber bundles, located at three different main positions; in particular, the red lines refer to a lower temperature, while the blue lines refer to an higher one. (b)Thomson scattering system for the shot #61713, 0.88-1.12s, characterized an ELMy H-Mode plasma; the red squares are the positions where the scattered light is emitted.

## 1.5 Purpose and structure of this thesis

The H-Mode plasma is the most promising operational scenario for future tokamaks, in particular of *ITER*, an acronym for **I**nternational **T**hermonuclear **E**xperimental **R**eactor, the project that will demonstrate the feasibility of nuclear fusion as a source of energy. When a plasma is in H-mode, a region of high gradients at the edge of the plasma itself, the so-called pedestal, is created.
Furthermore, the H-mode plasma is subjected to periodic relaxation processes of MHD (Magneto Hydro Dynamic) origin, called ELMs. These ELMs are responsible of loss of plasma confinement and of energy, which gets discharged towards the vessel inner walls, posing a significant threat to plasma facing components, shortening their life; in particular, the divertor, the component to which the outward plasma deposits, is the component most exposed in this process.
It seems there is a correlation between ELMs and the pedestal dynamics. As such, the study of the pedestal is essential for understanding the ELMs behavior, and possibly for trying to extrapolate how they will behave in bigger machines, such as ITER.
Thus, data gathering from different machines has been promoted by EUROFusion, in order to construct an international database from which such derivation of ELMs behavior and extrapolation for ITER's ELMs prediction can be carried out.
This thesis aimed to build a first version of what will be the database for TCV. It is structured as follows:

1. A brief introduction on nuclear fusion reactions and the story of their discovery, as well as the reason a plasma is needed to achieve them; moreover, a couple of ways to confine the plasma are described; finally, a short summary of the main features of TCV and the primary systems used in this thesis is presented.

2. Some basics of MHD theory, and a description of ohmic, L and H-mode plasmas; finally, an introduction to the relaxation processes known as ELMs.

3. What has been done in this thesis work. The steps taken in the construction of the database, the fits used for the data profiles, the use of the code CHEASE for calculating equilibrium related quantities.

4. The analysis of trends common to previous work on TCV and other machines as well; an introductory look at the EPED1 model.

5. Finally some conclusions about the results achieved and the future for this research topic.

# Chapter 2

# Theoretical background and motivations

In this chapter, an introduction about the physics of magneto-hydro-dynamic (MHD) plasmas is presented. In addition to that, another section will talk about the behavior of the plasma when subjected to different confinement regimes, with particular regards with the case of interest for this thesis, the H-mode. After that, there will be a brief description of the ELMs, regarding what they are, the consequences of their existence and their categorization.

## 2.1 Results in plasma physics: plasmas and MHD descriptions

As described in chapter 1.2, the plasma can be considered as a gas composed by charged particles. As such, the particles generate an electro-magnetic field that, by influencing the surrounding particles which emit an electro-magnetic field as well, will influence the considered particles as well; this kind of problem is called self-consistent, and requires the simultaneous solution of the plasma dynamics and the electro-magnetic field. However, such a problem is, in the majority of cases, not solvable analytically. One solution is to introduce approximations in the description, which allows to average the quantities in order to simplify and, ultimately, to render the problem solvable. This averaging procedure implies though a loss of informations to a certain extent, since the ability to describe the behavior of every single element of the description is lost, and only average behaviors can be derived.
In this section the different descriptions that can be adopted for a plasma are discussed. From the single particle description, easier to understand but impossible to calculate on a practical level, the problem will then be modified by using the averaging procedure mentioned above, in order to obtain, hopefully, a description whose quantities can be measured and, ultimately, a problem that can be solved, which will result in the *Multiple Fluids* and the *Magneto-Hydro-Dynamic (MHD) descriptions*, both widely used in plasma fusion research.

### 2.1.1 Equations of motion for single particles

The description of all the particle motion, coupled with the electromagnetic field they generate, can be written as a function of the position x, the velocity v and the electromagnetic field ($\vec{E}$ and $\vec{B}$):

$$\begin{cases} \frac{dx_{i,a}}{dt} = \vec{v}_{i,a} \\ m_a \frac{d\vec{v}_{i,a}}{dt} = q_a[\vec{E}_{micr}(\vec{x}_{i,a},t) + \frac{\vec{v}_{i,a}}{c} \times \vec{B}_{micr}(\vec{x}_{i,a},t)] = \vec{F}_{micr}(\vec{x}_{i,a},\vec{v}_{i,a},t) \end{cases} \tag{2.1}$$

where the subscript a=1→N is the population at which the considered particle belongs to, and the subscript i=1→$N_a$ is the particle considered in the population "a". The first equation describes the particle motion, while the second one is the Newton's law, where the force $\vec{F}$ is the Lorentz force. This system holds true in the case of a non-relativistic, non-quantum plasma description. In addition to these equations, in the description the Maxwell's equations, as well as the equation for the charges and currents:

$$\begin{aligned} &\nabla \cdot \vec{E}_{micr}(\vec{x}_{i,a},t) = 4\pi\rho^{tot}_{micr}(\vec{x}_{i,a},t) \qquad \nabla \times \vec{B}_{micr}(\vec{x}_{i,a},t) = \frac{4\pi}{c}\vec{J}^{tot}_{micr}(\vec{x}_{i,a},t) + \frac{1}{c}\frac{\partial \vec{E}_{micr}(\vec{x}_{i,a},t)}{\partial t} \\ &\rho^{tot}_{micr}(\vec{x}_{i,a},t) = \rho_{ext} + \sum_a \rho_{micr,a} = \rho_{ext} + \sum_a q_a \sum_i \delta(\vec{x} - \vec{x}_{i,a}(t)) \\ &\vec{J}^{tot}_{micr}(\vec{x}_{i,a},t) = \vec{J}_{ext} + \sum_a \vec{J}_{micr,a} = \vec{J}_{ext} + \sum_a q_a \sum_i \vec{v}_{i,a}(t)\delta(\vec{x} - \vec{x}_{i,a}(t)) \end{aligned} \tag{2.2}$$

must be included. Equations 2.2 are expressed in Gaussian notation, as well as all the other equations in this section.
The whole description is a set of (2N+3) coupled equations, all coupled together; it is then impossible to solve them analytically.
However, an interesting aspect of this problem is that the Newton's law is connecting two entities that behave in a very different way: particles (which are described by trajectories and, then by a so-called *Lagrangian* approach) and fields (which are described by an *Eulerian* approach). In particular, in the *Eulerian* approach one would be able to introduce an averaging procedure in order to describe an average field of the considered quantity; this means that, if the Newton's law can be converted into an equation that uses a completely *Eulerian* description, approximations and simplifications of said equations by averaging the quantities can take place. This is possible by introducing the concept of *phase space*, in which a microscopic distribution function, $f_{micr,a}(\vec{x}_{i,a},\vec{v}_{i,a},t)$, lives in; this quantity gives informations about the position and velocity of each particle in an instant of time t:

$$f_{micr,a}(\vec{x}_{i,a},\vec{v}_{i,a},t) = \sum_i \delta(\vec{x} - \vec{x}_{i,a})\delta(\vec{v} - \vec{v}_{i,a}) \tag{2.3}$$

By using this equation, it can be seen that the density $\rho_{micr,a}$ and the current $\vec{J}_{micr,a}$ can be expressed as a function of $f$:

$$\rho_{micr,a} = q_a \int f_{micr,a} d^3\vec{v}$$
$$\vec{J}_{micr,a} = q_a \int \vec{v} f_{micr,a} d^3\vec{v} \tag{2.4}$$

Moreover, a balance equation for $f_{micr,a}$ is found, by utilizing the Newton's law; the result is called Klimontovich equation:

$$\left[\frac{\partial}{\partial t} + \vec{v}\cdot\frac{\partial}{\partial \vec{x}} + \frac{q_a}{m_a}(\vec{E}_{micr} + \vec{v}\times\vec{B}_{micr})\frac{\partial}{\partial \vec{v}}\right] f_{micr,a} = \hat{L}_{a,micr} f_{micr,a} = 0 \tag{2.5}$$

The operator $\hat{L}_{a,micr}$ is called *Klimontovich operator*. This equation, coupled with eq. 2.2 and 2.4, gives the kinetic description of a plasma.

### 2.1.2 Basics of the kinetic description

After the conversion of the problem into a complete Eulerian description, the kinetic description has been derived. As such, the average procedure can be carried out. The average distribution function per unit volume, whose integral is the average number of particles in a phisically infinitesimal volume, is introduced:

$$f_a = \langle f_{micr,a}\rangle = f_{micr,a} - \widetilde{f}_{micr,a} \tag{2.6}$$

where $\widetilde{f}_{micr,a}$ are the fluctuations in the distribution function. The method would then be decomposing the quantities of the Klimontovich equation into the average and the fluctuation ones, and then averaging; as such, the average of the fluctuations is zero, aside from the composition between fluctuations. We therefore obtain:

$$\hat{L}_a f_a = -\frac{q_a}{m_a}\Big\langle\Big(\vec{E} + \frac{\vec{v}}{c}\times\vec{B}\Big)\cdot\frac{\partial \widetilde{f}_a}{\partial \vec{v}}\Big\rangle = C_a \tag{2.7}$$

Where the last term cannot be considered 0 since it is a product between fluctuations. This equation,coupled with the Maxwell's equations (which will be subjected to the same average), is called *Boltzmann equation*, and it is the equation used for a kinetic description of the plasma.
In order to close the system, the term $C_a$ must be determined. In the case $C_a$=0, we obtain the *Vlasov equation*:

$$\hat{L}_a f_a = 0 \tag{2.8}$$

and, in the case $C_a = -\frac{f_a - f_{0,a}}{t_R}$, where $t_R$ is the relaxation time of Coulomb collisions, we obtain the Boltzmann equation in the *relaxation time approximation*:

$$\hat{L}_a f_a = -\frac{f_a - f_{0,a}}{t_R} \tag{2.9}$$

where $f_{0,a}$ is the distribution function at the equilibrium.
In order to fully understand the term $C_a$ though, one should derive equations for the fluctuations. However, this leads to higher order terms that have to be described by using

another equation; this leads to an infinite hierarchy of equations that must be closed by making some simplifying assumption, this truncating the product of fluctuations.

### 2.1.3 Basics of the multiple fluid description

After the kinetic description, there could be the possibility of describing the plasma as a fluid, which means describing it in terms of densities, velocity and temperature fields, stess tensors, etc.; note that such a fluid will interact with an electromagnetic field, and it will be coupled with the Maxwell's equations. A possible description of the plasma would be to describe the charged particles populations (e.g. electrons, ions, etc.) as different fluids that are moving in the same region of space, thus constituting the plasma. This is obtained by averaging the mean value of the distribution function over the velocities:

$$\begin{aligned} \rho_a &= q_a \int f_a d^3v = q_a n_a, \qquad n_a = \int f_a d^3v \\ \vec{J}_a &= q_a \int \vec{v} f_a d^3v = q_a n_a \vec{u}_a, \qquad \vec{u}_a = \frac{\int \vec{v} f_a d^3v}{n_a} \end{aligned} \tag{2.10}$$

What can be seen as far as $n_a$ and $\vec{u}_a$ are concerned, is that these two quantities can be derived by a more general form:

$$\langle \psi(\vec{v}) \rangle_a = \frac{\int \vec{\psi} f_a d^3v}{n_a} \tag{2.11}$$

This means that it could be possible to write evolution equations for $\psi_a$, where this quantity can be whatever quantity is decided. In order to do so, the kinetic equation is taken, it is multiplied by $\psi_a$, then averaged over $d^3v$. In this way, average quantities $\langle \psi(\vec{v}) \rangle_a$ should appear. The resulting equation after applying this method is:

$$\frac{\partial (n_a \langle \psi \rangle_a)}{\partial t} + \frac{\partial}{\partial \vec{x}} \cdot (n_a \langle \vec{v} \psi \rangle_a) - \frac{q_a}{m_a} n_a \Big\langle \left( \vec{E} + \frac{\vec{v}}{c} \times \vec{B} \right) \cdot \frac{\partial \psi}{\partial \vec{v}} \Big\rangle_a = \int C_a d^3v \tag{2.12}$$

According to the value of $\psi$ chosen, the evolution equation will be different:

$$\begin{aligned} &\psi = 1: \qquad \frac{\partial n_a}{\partial t} + \frac{\partial}{\partial \vec{x}} \cdot (n_a \vec{u}_a) = \int C_a d^3v \\ &\psi = m_a \vec{v}: \qquad \frac{\partial}{\partial t}(m_a n_a \vec{u}_a) + \nabla \cdot (n_a m_a \langle \vec{u}_a \vec{u}_a \rangle_a) + \nabla \cdot \underline{\underline{P_a}} = q_a n_a \left( \vec{E} + \frac{\vec{u}_a}{c} \times \vec{B} \right) + R_a \\ &\quad \text{where } R_a = \int C_a m_a \vec{v} d^3v, \quad \text{and } P_a \text{ is the stress tensor } \underline{\underline{P_a}} = P_a \underline{\underline{I}} + \underline{\underline{\Pi_a}} \\ &\psi = \frac{1}{2} m_a \psi^2: \quad \frac{1}{2} m_a n_a \frac{du_a^2}{dt} + \frac{3}{2} n_a \frac{dT_a}{dt} = -\nabla \cdot \vec{Q}_a - \nabla \cdot (\underline{\underline{P_a}} \cdot \vec{u}_a) + \vec{J}_a \cdot \vec{E} + \int \frac{1}{2} m_a v^2 C_a d^3v \end{aligned} \tag{2.13}$$

With the remark that the system must be closed in some way, for example, by using the Fourier equation, which can become a *polytropic law* in the case of an adiabatic system:

$$p_a n_a^{-\gamma} = const. \tag{2.14}$$

### 2.1.4 MHD description

The last description is the Magneto-Hydro-Dynamic (MHD) one; it is based upon the fact that the plasma can be approximated as a locally charged, but globally neutral fluid; as such, in the MHD description the distinction between population of charged particles (the core concept of the multiple fluid description) is not made anymore ($n_e = n_i = n$). This means that the plasma can be described by fluid quantities, like the average density and velocity field, which are derived by averaging over all the particle populations:

$$\begin{aligned} \text{Mass density:} \quad & \rho(\vec{x},t)_m = \sum_a m_a n_a \\ \text{Charge density:} \quad & \rho(\vec{x},t) = \sum_a q_a n_a \\ \text{Velocity field:} \quad & \vec{u}(\vec{x},t) = \frac{\sum_a m_a n_a \vec{u}_a}{\rho_m} \end{aligned} \tag{2.15}$$

Since they are derived from the multiple fluid equations, they will present with an infinite hierarchy of equations as well, and it will be necessary to close the system by truncating the hierarchy in some way. The assumption of globally neutral fluid has some implications; the phase velocity of electromagnetic waves inside the plasma is well below the speed of light ($v_{phase} \ll c$), and the average thermal velocity of the particles can be well considered in the non-relativistic domain. By averaging the equations of the multiple fluid description in this way the MHD equations can be derived; if the continuity equation in the multiple fluid description is averaged:

$$\begin{aligned} &\frac{\partial \rho_m}{\partial t} + \nabla \cdot (\rho_m \vec{u}) = 0 \\ &\frac{\partial \rho}{\partial t} + \nabla \cdot \vec{J} = 0 \end{aligned} \tag{2.16}$$

As well as the momentum equation for the plasma, by making the assumption of neglecting the ion motion because significantly slower than electrons, and the fact that in the equation the divergence of the stress tensor appears, but the anisotropic part can be considered negligible ($\nabla \cdot \underline{\underline{P}} = \nabla p + \nabla \cdot \underline{\underline{\Pi}} \simeq \nabla p$) in the case of the *ideal MHD model*, where plasma is assumed being dominated by collisions, and the plasma resistivity is not taken into account:

$$\rho_m \frac{d\vec{u}}{dt} = -\nabla p + \frac{\vec{J}}{c} \times \vec{B} \tag{2.17}$$

The system is closed by assuming adiabatic behavior, and thus again by applying a polytropic law:

$$\frac{\partial p}{\partial t} + \vec{v} \cdot \nabla p = -\gamma p \nabla \cdot \vec{v} \tag{2.18}$$

Where $\gamma$ is called *adiabatic coefficient*. In the case the resistivity is considered, the model becomes known as *resistive MHD model*; the difference is in writing the generalized Ohm's law:

$$\vec{E} + \frac{\vec{u}}{c} \times \vec{B} = \begin{cases} 0 & \text{Ideal MHD model} \\ \eta \vec{J} & \text{Resistive MHD model} \end{cases} \tag{2.19}$$

The assumptions used in order to derive these equations in an ideal MHD model implies some consequences, which define the *validity range of the ideal MHD model* [6]:

- High plasma collisionality, which is not satisfied in tokamaks and fusion plasmas in general, due to relatively low plasma density and high temperatures.
- Macroscopic scale length of the plasma much larger of the ion Larmor radius, which, in the case of ELMs, with a narrow mode structure, is not valid as well.
- Large plasma size, which makes resistive diffusion negligible; it has been proved valid in tokamak plasmas.

Even though there are issues in the validity of some of these assumptions, the plasma stability and equilibrium calculations in several years of fusion research do almost completely neglect the phenomena the assumptions describe.

## 2.2 MHD equilibrium and stability

In this chapter it is briefly introduced the topic of plasma equilibrium in the MHD description; in particular, the Grad-Shafranov equation will be explained as the equation from which quantities directly related to equilibrium, such as pressure and current, are calculated [9].

### 2.2.1 Grad-Shafranov equation

The equilibrium configuration in the MHD model is derived by imposing time independence in the MHD equations, coupled with the Maxwell's equations as well. The problem will then give the pressure profile and the behavior of the plasma current; the equations used are:

$$\begin{cases} \nabla p = \frac{1}{c} \vec{J} \times \vec{B} \\ \nabla \cdot \vec{B} = 0 \\ \nabla \times \vec{B} = \frac{4\pi}{c} \vec{J} \end{cases} \tag{2.20}$$

This problem is subjected to toroidal symmetry, which means that the considered quantities are independent from the toroidal angle $\phi$, $\frac{\partial f}{\partial \phi} = 0$, thus depending only on the poloidal components $r$ and $z$.
As such, by representing the equations in toroidal symmetry, and by introducing the scalar potentials $\psi$ and $I$:

$$\begin{aligned} B_r &= -\frac{1}{r}\frac{\partial \psi}{\partial z} & B_z &= \frac{1}{r}\frac{\partial \psi}{\partial r} \\ J_r &= -\frac{1}{2\pi r}\frac{\partial I}{\partial z} & J_z &= \frac{1}{2\pi r}\frac{\partial I}{\partial r} \end{aligned} \tag{2.21}$$

It can be proven that the scalar potential $I$ is the current flowing in the toroidal direction, which will be the one that will generate a poloidal magnetic field inside the tokamak, and that it is a function of $\psi$. Moreover, it can be proven that the plasma pressure $p$ can be expressed as a function of the scalar potential $\psi$ as well. A more detailed calculation can be found in [9]. The end result of these calculations is the *Grad-Shafranov equation* :

$$\begin{aligned} &\Delta^*\psi = -4\pi r^2 p' - FF', \qquad \text{where } F = \frac{2I}{c} \\ &\Delta^* = r\frac{\partial}{\partial r}\left(\frac{1}{r}\frac{\partial}{\partial r}\right) + \frac{\partial^2}{\partial z^2} \end{aligned} \tag{2.22}$$

From this equation, if the quantity $\psi$ is found, the equilibrium configuration can be found, thus finding the pressure and current profiles inside the toroidal problem. The function $\psi$ can be demonstrated to be flux quantities, since they are proportional to the flux associated with the poloidal magnetic field $B_p$:

$$\psi = \int_{A_{tor}} \vec{B} \cdot d\vec{S} \tag{2.23}$$

Where $A_{tor}$ is an arbitrary cross section of a flux surface.
The main issue with this equation is that $\psi$ must be found by knowing the profiles of $p$ and $J$, but these are functions of $\psi$ itself, thus rendering the problem non-linear. This means that an analytical solution cannot be found, and the only way to solve the problem is by an iterative procedure. It will be seen in the next chapter that it will be the case when computing equilibrium related quantities, where it will be described the necessity of using a code (CHEASE) that takes the density and temperature profiles (which will give the pressure profile) obtained by fitting the data as a first guess, as well as the flux, thus resolving the Grad-Shafranov equation iteratively.

### 2.2.2 Basics of plasma MHD stability

Plasma instabilities in their simplest form are described by the MHD description, and they can arise from [9]:

- Current gradients.
- Pressure gradients combined with adverse magnetic field curvature.

Moreover, different instabilities can arise according to the adopted MHD description, Ideal or Resistive.
The parameter describing stability is the *safety factor q*, already introduced in chapter 1.3; generally, an higher value of q means greater stability; in addition to that, this parameter seems to be connected with transport theory as well [9]; as already introduced in eq. 1.10, and reported in this chapter for convenience, the expression of q reads:

$$q = \frac{\Delta\phi}{2\pi} \tag{2.24}$$

In the axisymmetric equilibrium each magnetic field line has a value of q; the value $\Delta\phi$ is the displacement in toroidal angle of a magnetic field line after a toroidal revolution has taken place. Rational values of $q$ play an important role in stability; in particular, if $q$ is a rational number, $q$=$m/n$, and the plasma becomes unstable; $m$ and $n$ are integers, meaning that the field line closes after $m$ toroidal and n poloidal rotations around the torus. By using the equation of the field line:

$$R\frac{d\phi}{ds} = \frac{B_\phi}{B_p} \tag{2.25}$$

Where $B_\phi$ and $B_p$ are respectively the toroidal and poloidal magnetic field. The value of the safety factor $q$ can then be calculated as:

$$q = \frac{1}{2\pi}\oint \frac{1}{2\pi}\frac{B_\phi}{B_p}ds \tag{2.26}$$

Thus obtaining, for high aspect ratio and circular cross section machines:

$$q = \frac{rB_\phi}{R_0 B_p} \tag{2.27}$$

Where $r$ is the minor radius and $R_0$ is the major radius of the tokamak.
Instabilities, both ideal and resistive ones, have an infinite spectrum of modes, each one being characterized by the form $exp[i(m\theta - n\phi)]$ in the case of large aspect ratio machines, where $m$ and $n$ are respectively the poloidal and the toroidal mode number; these two values are the same numbers that appear when the safety factor $q$ is a rational number, as described before [9].
In the case of generation of *Edge Localized Modes (ELMs)*, the plasma relaxation phenomena further discussed in chapter 2.4 and main topic of this thesis, the instability processes that seem to be related to them are the *Kinetic Ballooning Mode* (KBM) and the *Peeling Ballooning Mode* (PB); for a more detailed description of these MHD plasma stability, see [9]. It has been seen that these modes limit the range of conditions in which the plasma can be stable, and thus does not collapse into an ELM. These two instability modes depends on the toroidal mode number $n$ [1]; in particular, the higher $n$, the bigger is the region in which the plasma is stable; for values of $n \leq 20$, KBM instabilities start to arise significantly, while PB start to close the stability region for $n \leq 8$. It is seen that, for $n \sim 5$, the two instability modes couple and they completely close the region in which the plasma can be stable, as seen in fig. 2.1.
The mechanism for which the ELM generate as a relaxation process for these instabilities is not yet completely determined, but several models have been proposed. For a specific type of ELMs, the so called *type I ELMs*, the most used model is the EPED1 model, and a qualitative explanation of it is given in chapter 2.4.2.

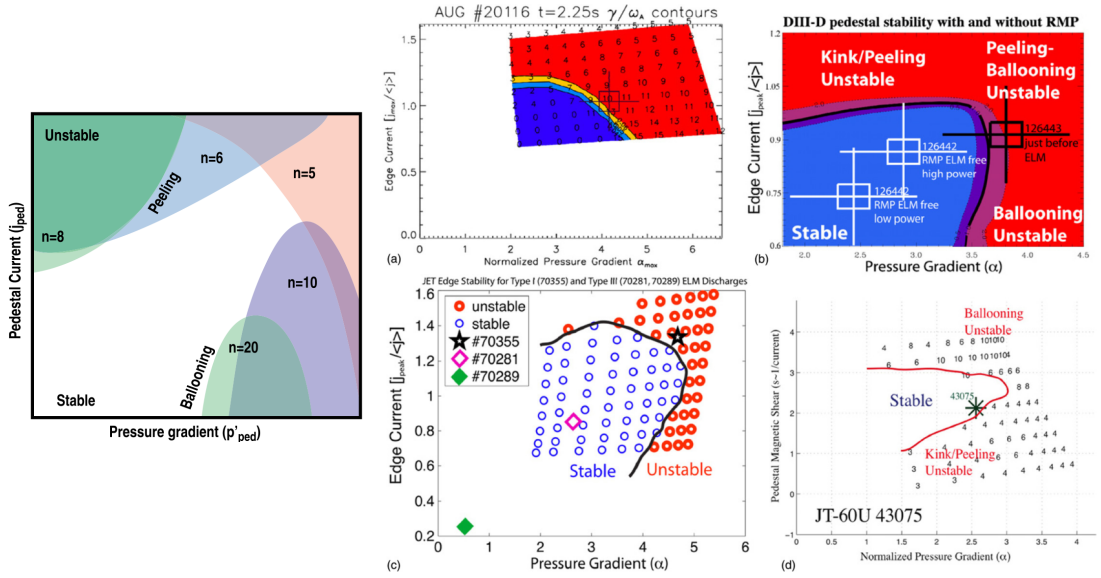


(a) (b)

Figure 2.1: Stability region as a function of the current density at the pedestal and the pedestal pressure gradient (a). At the left (b), stability region diagrams for (a) AUG, (b) DIII-D, (c) JET and (d) JT-60U [1].

## 2.3 Plasma heating and modes of confinement

### 2.3.1 Plasma heating

As said in chapter 1.3, the toroidal field along which the plasma moves is generated by transformer effect; however, the charged particles that compose the plasma will move singularly according to their own equation of motion, causing collisions with each other; these collisions will generate an average electrical resistance; such a plasma is called an *ohmic plasma*. Since there is a non zero value of the electrical resistivity $\eta$, the plasma will be able to heat up because of resistive effects:

$$P_\Omega = \eta j \tag{2.28}$$

However, since the collision times increase following $T^{\frac{3}{2}}$, the plasma behaves more like a perfect conductor the higher the temperature becomes, which means plasma losses by collisions will be reduced, but at the same time the plasma will be heated less by ohmic effect. This means that the only other way to further heat up the plasma is to supply energy from external sources.

A solution would be to use *radio frequency* (RF) cavities to induce electro-magnetic waves of the same frequency as the resonance frequencies of the particles inside the plasma, according to their dispersion relation. In TCV, the ECRH works adopting this principle, generating third harmonics of the electron cyclotron frequency, from which its name is derived (Electron Cyclotron Resonance Heating).

Another solution would be to inject neutral particles inside the plasma at higher energy, the particles being made of hydrogen and deuterium, heating the plasma by collision, which will propagate the received energy in the whole plasma by further collisions. The

NBI (Neutral Beam Injection) machine is an example of this technique being employed at TCV (see chapter 1.4.1).

### 2.3.2 Ohmic and L-mode plasma confinement

Confinement of the plasma in a tokamak is not yet fully understood. Indeed, even though the neoclassical theory for a plasma (see [9] for a more detailed discussion) predicts a way to find the value of the energy confinement time, plasmas in a tokamak do not follow such theory, resulting in experimental values of $\tau_e$ much shorter than the ones predicted. As a result, resort to empirical formulation of the confinement time, by the use of scaling laws, is required. However, it is found that there are several regimes of operation, according to the power supplied to the system, in which the confinement behavior changes drastically. One of such regimes of operation is when plasmas are *ohmically heated*, because of collisions between particles inside the plasma itself. At low density, it was found that the energy confinement time scaled as [9]:

$$\tau_e = 0.07(\frac{n}{10^{20}})aR^2q \quad s \tag{2.29}$$

where $n$ is the average electron density, $a$ and $R$ are respectively the minor and major radii, and $q$ is the cylindrical equivalent edge safety factor. While in neoclassical theory it was predicted that the confinement should worsen if the density increases, in eq. 2.29 there is a linear correlation between $n$ and $\tau_e$.
With the increase of $n$, the linear correlation is lost, by reaching an asymptote for the value of $\tau_e$:

$$n_{sat} = 0.06 * 10^{20} IRA^{0.5}\kappa^{-1}a^{-2.5} \quad m^{-3} \tag{2.30}$$

where $I$ is the plasma current, $A$ is the atomic mass of the ions and $\kappa$ is the elongation of the plasma.
As said before, ohmic confinement becomes worse for higher temperatures, so in order to go further with the heating regime, external power must be supplied, reaching the so called *L-mode* of confinement. Different scaling laws have been proposed for this confinement regime; the scaling law found by Goldston from the experiments of several tokamaks reads [9]:

$$\tau_G = 0.037\frac{IR^{1.75}\kappa^{0.5}}{P^{0.5}a^{0.37}} \quad s \tag{2.31}$$

Another more precise scaling law for $\tau_e$ derived in order to have better predictive capablities for ITER, called *ITER89-P* [9], is:

$$\tau_e^{ITER89-P} = 0.048\frac{I^{0.85}R^{1.2}a^{0.3}\kappa^{0.5}(\frac{n}{10^{20}})^{0.1}B^{0.2}A0.5}{P^{0.5}} \quad s \tag{2.32}$$

where $B$ is the toroidal magnetic field.
The biggest disadvantage that can be seen is that in L-mode the confinement time always decreases with increasing heating power $P$, which makes this regime of confinement unsuitable for higher-power scenarios.

### 2.3.3 H-mode plasma confinement

If further power is applied, after a certain power threshold, the plasma undergoes a transition in which abrupt changes emerge; when this happens, the plasma has entered the *H-mode* confinement regime; various empirical scaling laws have been found by studies on several machines [2]:

$$P_{thr} = 1.42(\frac{n_{e.l.a.}}{10^{20}})^{0.58} B_{\phi}^{0.82} R^{1.00} a^{0.81} \quad MW \tag{2.33}$$

where $n_{e.l.a.}$ is the line averaged electron density (expressed in $10^{19} m^{-3}$), $B_{\phi}$ is the toroidal magnetic field in Tesla and $a$ and $R$ are respectively the minor and major radii of the machine (in meters).
The main feature of H-mode is the arising of an edge transport barrier, as well as a growth in the pressure, density and temperature profiles. In the region at the edge of the plasma, close to the *last closed flux surface* (LCFS), said profiles decrease to zero very rapidly; such region of high profile gradients is called *pedestal*.
The edge transport barrier in an H-mode plasma is formed because of a sheared perpendicular rotation profile, caused by a radial electric field $\vec{E}_r$, in particular by the $\vec{E}_r \times \vec{B}$ contribution in the plasma edge; this suppresses the long-wave turbulence of L-mode. Due to its characteristic shape, the rotational profile is also called $E_r$ *well*. Such rotational profile leads to steeper gradients in the density, temperature and pressure profiles in the LCFS, defining the aforementioned pedestal; this region is more pronounced for electrons, while ions are characterized by less steep gradients.
A characteristic feature of H-mode is the fall in the $D_{\alpha}$ signal from the edge of the plasma; the $D_{\alpha}$ emission is originated by the $K_{\alpha}$ emission of neutral deuterium, and it is a signature of recycling of hydrogen between plasma and the tokamak's surrounding surfaces; so, a fall in this emission indicates that this recycling process has worsened, and thus the plasma confinement has improved (see fig. 2.3).

As far as scaling laws for the energy confinement time are concerned, the behavior that was obtained for $\tau_e$ for many tokamaks is an analogue of the ITER89-P scaling law used in L-mode (eq. 2.32), and is called *ITER93-P*:

$$\tau_{th}^{ITER93-P} = 0.053 \frac{I^{1.06} R^{1.9} a^{0.11} k^{0.66} (\frac{n}{10^{20}})^{0.17} B^{0.32} A^{0.41}}{P^{0.67}} \tag{2.34}$$

where *th* refers to the confinement time for the thermal plasma [9]. The confinement times in both H and L mode can be compared by a parameter $H$ so that:

$$H = \frac{\tau_e^H}{\tau_e^L} \tag{2.35}$$

Usually, the value of $H$ is around 2, thus meaning that H-mode has better confinement capabilities than L-mode.
The improved confinement, alongside an increase in the temperature, density and pressure

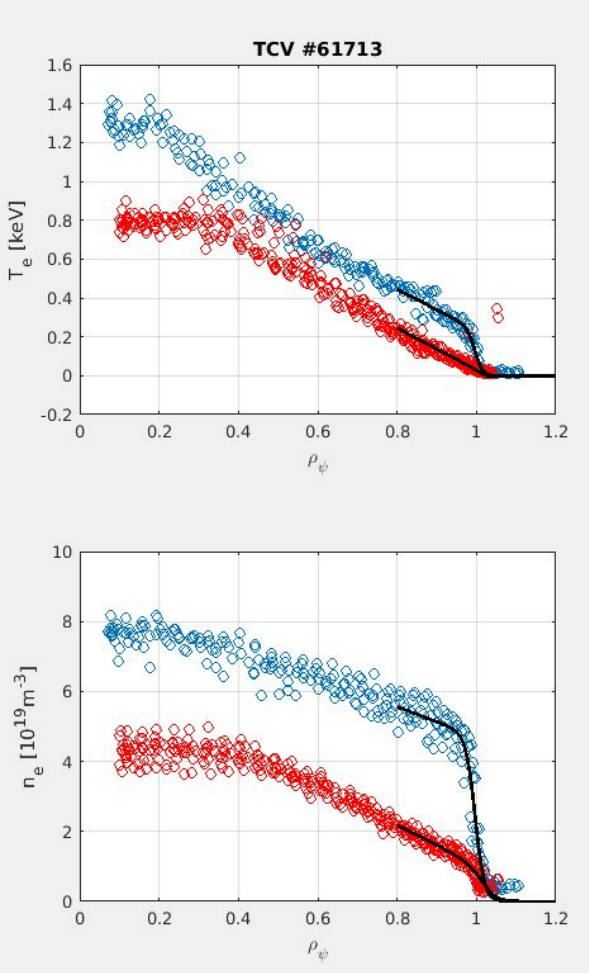


(a)

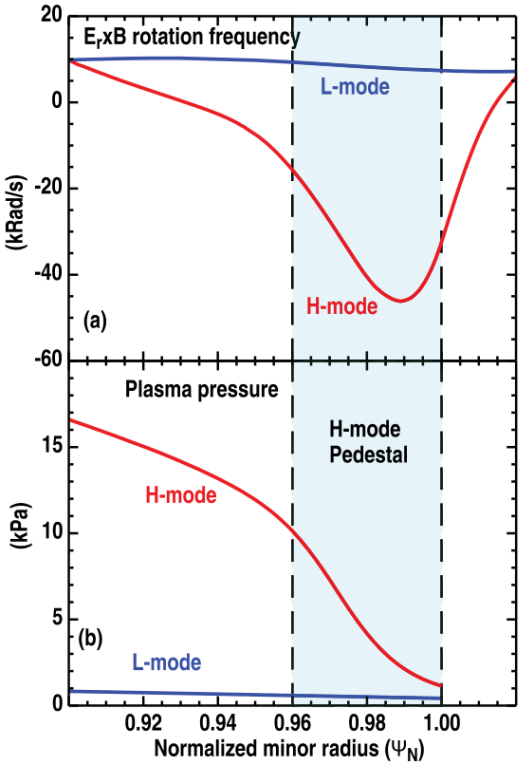


(b)

Figure 2.2: (a) Comparison between electron temperature (top) and density (bottom) profiles both in L (red points) and H-mode (blue points) for TCV shot #61713, with fitted profiles as well (black lines). (b) $E_r$ well representation [1].

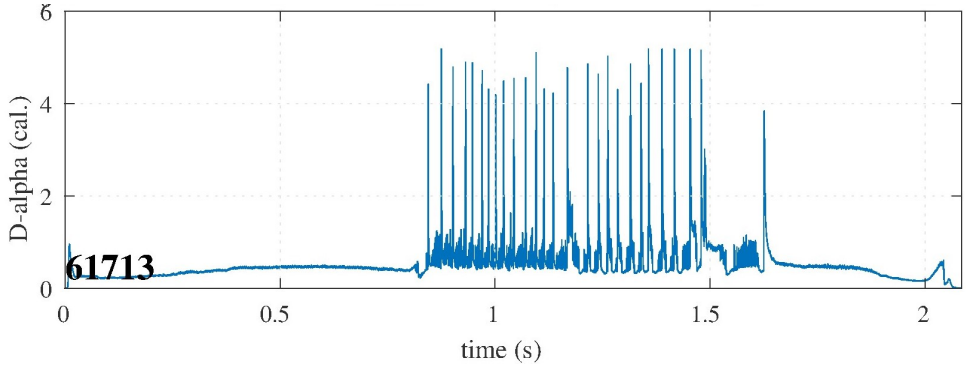


Figure 2.3: $D_\alpha$ signal of plasma shot 61713

profiles, as well as the generation of the bootstrap current, are the main causes for which ITER is envisioned to work in H-mode confinement regime.

### 2.3.4 Bootstrap current

In a plasma, a phenomenon that occurs because of collisions is that the generation of a toroidal current related to the trapped particles in banana orbits because of the magnetic configuration, the so called *bootstrap current* [9]; this current is generated from the collision between passing and trapped particles, which transfers momentum between them as a result, and a net current, which depends on the pressure gradient at the edge of the plasma region. The bootstrap current is that, since it develops in the toroidal direction, it will develop a poloidal magnetic field; as it also depends on the profile pressure gradient, this current will be stronger at the plasma edge in H-mode plasmas compared to the plasma current at the edge of other modes of confinement, because of the presence of the pedestal; this means that this current can contribute in generating the poloidal magnetic field necessary to confine the plasma itself; this is another motivation of the H-Mode being selected as the primary regime of confinement at ITER. The bootstrap current profile is roughly estimated as:

$$J_b \sim -\epsilon^{\frac{1}{2}} \frac{1}{B_p} \frac{dp}{dr} \tag{2.36}$$

Where $\epsilon$ is the inverse of the aspect ratio, $B_p$ is the poloidal magnetic field and p is the plasma pressure profile.
This current profile will be given by the solution of the Grad-Shafranov equation (see chapter 2.2.1) in an iterative way, by using the code CHEASE [5]. The difference between the current density profile of L and H-mode, as well as the behavior of the bootstrap current in H-mode for the test shot 61713 can be seen in fig. 2.4.

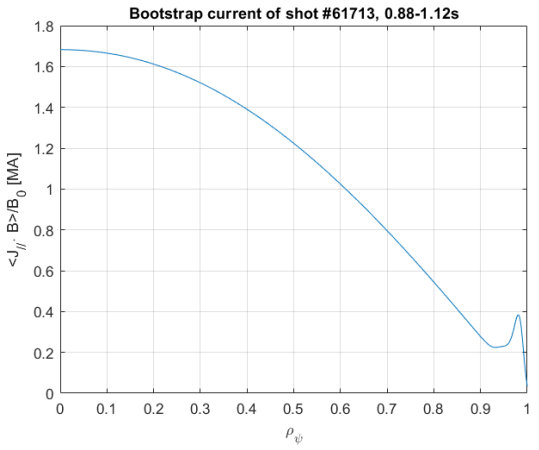


(a)

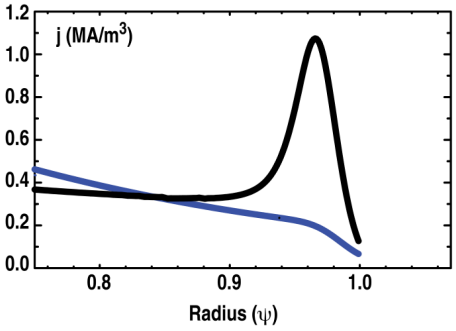


(b)

Figure 2.4: (a) Bootstrap current profile for the considered shot and (b) the difference between L mode (blue) and H mode (black) bootsrap current density profiles. The peak at the plasma edge (towards $\psi \sim 1$) present in both figured is caused by the presence of the pedestal.

## 2.4 Edge Localized Modes

When a plasma is in H-mode confinement, instabilities of MHD nature arise. These instabilities are called *Edge Localized Modes* (ELMs), and are relaxation processes that periodically happen inside a plasma; each ELM is associated with a burst of plasma outwards the region where the plasma itself is confined, which causes a reduction of temperature and density inside the plasma; moreover, when a burst occurs, the $D_\alpha$ emission has peaks in the profile, meaning that the confinement is worsened during the ELM, which improves the recycling of neutral hydrogen; as a consequence, the $D_\alpha$ spectrum is an indicator of the presence of ELMs, and which type is present as well.
The scaling laws of the energy confinement time are different when in presence of ELMs; a well known one is the *IPB98(y,2)* [9]:

$$\tau_E^{IPB98(y,2)} = 0.145 \frac{I^{0.93} R^{1.39} a^{0.58} \kappa^{0.78} (\frac{n}{10^{20}})^{0.41} B^{0.15} A^{0.19}}{P^{0.69}} \quad s \tag{2.37}$$

Where $I$ is in MA and $P$ in MW.
The consequences of ELMs are ejections of matter and pulsed heat loads towards key components that are facing the plasma inside the tokamak chamber, in particular, the divertor, the component located in the region where the edge of the plasma, also called *Scrape Off Layer* (SOL), collides with the vessel; this causes the considered component to be subjected to periodic thermal shocks that, in time, can severely damage it, shortening its operational life.
As such, the mechanism of ELM generation must be understood in order to predict their behavior in different machines.

### 2.4.1 Types of ELMs

Numerous experiments on H-mode plasmas and the rich bibliography related to them managed to provide a classification of the ELMs into several categories according the the machines' operational regimes:

- **Type I ELMs:** They are ELMs characterized by a low frequency of emission, but an high $H_\alpha$ signal; as such, they are the most dangerous ELMs for plasma facing components, since even though few in number, they discharge more energy per burst. They seem to appear when an H-mode plasma has an high enough power injected, and their frequency seems to increase with increasing power: $\frac{df_{ELM}}{dP_{sep}} > 0$, where:
$$P_{sep} = P_{tot} - \frac{dW}{dt} - P_{rad,core} \tag{2.38}$$
is the power through the plasma separatrix [10].

- **Type III ELMs:** They are ELMs with a lower $D_\alpha$ signal than type I ELMs, but at higher frequency; as a consequence, confinement is worse than when type I ELMs appear. They usually arise at low heating power, and, as the opposite of type I

ELMs, their frequency seem to decrease with increasing heating power: $\frac{df_{ELM}}{dPsep}<0$ [10].

These are the most common types of ELMs, the type I ones being the most concerning for future machines such as ITER. However, there exist other types of ELMs [9] [1]:

- **Type II ELMs:** also called *grassy* ELMs, these ELMs appear for highly shaped, close to double null configuration and high-collisionality plasmas.
- **Type IV ELMs:** they appear at low power, close to the power threshold between the L-H transition of low collisionality plasmas.
- **Type V ELMs:** ELMs that have been observed in the *National Spherical Torus Experiment* (NTSX) tokamak.

As said before, type I ELMs are the most concerning for the design of future tokamaks, and as such predictive models have been developed for these ELMs in particular; one of the most known is the EPED1 model.

### 2.4.2 Qualitative description of the ELM generation according to the EPED1 model

The EPED1 is a model whose objective is to make predictions over the pedestal width and height behavior, by assuming an ELM generation mechanism.
The model focuses on the description of type I ELMs only, and it predicts the stability of the pedestal top pressure (and, thus, the plasma) through the kinetic ballooning mode (KBM) and the peeling ballooning mode (PB) instabilities limits [8], [9].
The ELM generation mechanism assumed by the EPED1 model states that, after the pedestal is formed and the plasma is in H-Mode confinement regime, its gradient keeps increasing until reaching a limit value, dictated by transport. The KBM model is what determines this value. However, the height of the pedestal can still increase, while keeping the gradient constant, by increasing the pedestal width w. Since the pedestal width keeps growing, the pedestal height grows as well, up to the limit for which the PB mode (which is set by ideal MHD) is reached. When this happens, the plasma is at the intersection between KBM and PB limits, and the pedestal at the plasma edge relaxes itself, collapsing and ejecting matter in the process; this collapse is the Edge Localized Mode of type I. After this collapse has happened, the cycle begins anew [8].
The pedestal width, according to the EPED1 model, should increase as:

$$w = D\sqrt{\beta_\theta^{Ped}} \tag{2.39}$$

where w is the aforementioned pedestal width, $\beta_\theta^{Ped}$ is the ratio $p_{Ped}/(B_\theta^2/2\mu_0)$ ($p_{Ped}$ is the pedestal pressure, $B_\theta$ is the poloidal magnetic field and $\mu_0$ is the vacuum diamagnetic constant), and D is a parameter related to the pedestal gradient; the value of D in the EPED1 model is 0.076, inferred from low collisionality from DIII-D data with ITER like plasma parameters. However, other values of D have been found in other machines, such as 0.11 for AUG and 0.84 for JET [8].

# Chapter 3

# Database construction

In this chapter the procedure used to build the database will be explained. The database has been built by considering several shots as suitable, then skimming them by imposing additional conditions, such as goodness-of-fit parameters reaching a certain threshold value, and because of errors in the data acquisition process by the diagnostics. Moreover, two codes built at TCV were used, LIUQE and CHEASE. LIUQE is the code that calculates, independently or with the help of other codes, all the nodes specified in the SPC computer cluster, immediately after a shot has taken place in TCV; it can perform data gathering from all the diagnostics installed at TCV (such as the Thomson Scattering System) and a basic equilibrium reconstruction. CHEASE is a code dedicated to the iterative solution of the Grad-Shafranov equation at a deeper level than the solution that LIUQE gives; as such, it requires more computational time. After that, the database entries have been filled with the required data, which are derived from the profile data and the equilibrium related parameters previously calculated.

## 3.1 Database goals and features

The database was built with the purpose to have quick access to the required data, with a structure similar to the one proposed at JET. The input is a text file containing a list of all the desired shots' number and the time interval of interest. The program, written in Matlab, reads the entries, retrieves the data, and builds the database by means of a *for* cycle which executes all the parts of the program. If there is no database available, the program creates it, otherwise the new entries are added to the existing database. There is the option to update existing shots as well, provided the shot number and the time interval coincide with an existing entry.
Since the program is supposed to work after a shot at TCV has taken place, one of its goals is that it cannot stop mid-computation due to errors. As such, a *try and catch* procedure is implemented in the program, both in the main *for* cycle, and in the insertion of singular entries, which consist in encasing the code that can generate an error inside the Matlab *try*() function, and store the supposed error, and eventually correct it as well if possible by using the Matlab *catch*() function. In the case the error could not be cor-

rected, the program stores it into a Matlab structure, with all the information concerning its location and nature. In this way, the program ran over $\simeq 200$ shots without stopping once during the construction of the test database used in this thesis. The full database is visualized in table 3.1.
The database is composed by of several sections:

- The first section, containing the entries that will be given by the operator in the text file, such as the shot number, the initial, final and mid times, as well as the machine used (in the optic of making this database part of an international database).
- A section containing the parameters coming directly from the fitted profiles, such as pedestal position, height and slope for each profile, temperature, density and pressure, and for both the fits suggested to build the database, a linear fit and a mtanh fit (described in more detail in section 3.3).
- A section with other useful pedestal parameters, such as ion temperature, effective charge number Z, and pedestal velocity; this section had been left blank since the ion data were not known.
- A section containing derived parameters, from the fits and the CHEASE code, like the plasma volume, the pedestal electron energy and the normalized pressure gradient.
- A section which collects dimensionless parameters and parameters used in their definition, like the poloidal electron confinement parameter at the pedestal $\beta_{e,pol,ped.}$, which can be at the HFS (**H**igh **F**ield **S**ide) at the LFS (**L**ow **F**ield **S**ide), the borders of the plasma that are respectively the closest (resulting in an higher value of the magnetic field) and the farthest (with a lower value of the magnetic field) from the toroidal axis, or their average value. Moreover, in this section there are parameters such as the pedestal collisionality $\nu^*_{e,ped.}$, the normalized Larmor radius $\rho^*_{ped}$, the safety factors $q_{95}$ and the inverse of the aspect ratio $\epsilon$; moreover, the data related to the poloidal and toroidal magnetic fields, found by using the CHEASE code, were stored here. Since some parameters refer to the profiles, there are two values, one for the linear fit and one for the mtanh one.
- A section containing ELM-related data, such as ELM type, frequency and energy loss, and the characteristic time length for an ELM to collapse.
- A section where operational parameters are saved, such as the plasma current, the power injected both by NBH and ECRH, the MHD energy, the energy confinement time and the fueling and impurity rates.
- Finally, a section where profiles concerning equilibrium are stored, like the parameters related to the Grad-Shafranov equation as well as other operational parameters such as upper and lower triangularity, elongation and strike point coordinates (a strike point is where the poloidal magnetic field lines connect to the vessel), as well as the magnetic axis and the geometrical axis coordinates.

Table 3.1: Database entries. The "e" subscript refers to electron related quantities, while "i" refers to ions; the subscripts "mtanh" and "lin." refers to the mtanh and linearly fitted profiles; "pol." and "tor" refer respectively to poloidal and toroidal components; "HFS" and "LFS" respectively mean "High and Low Field Side". The symbol "/" indicates that multiple entries per argument are present in the database.

| | | |
|---|---|---|
| **General data** | | |
| Machine | TCV | string |
| Shot | Shot number | |
| $t_{start/end/med.}$ | Initial, final and medium time interval extremes | s |
| **Parameters directly related to the fits** | | |
| $T_{e,sep.}$ | Temperature at the separatrix | eV |
| $n_{e,sep.,mtanh/lin.}$ | Separatrix density | $m^{-3}$ |
| $p_{e,sep.,mtanh/lin.}$ | Separatrix pressure | Pa |
| $T/n/p_{e,ped.,mtanh/lin.}$ | Pedestal temperature, density and pressure | $eV/m^{-3}/Pa$ |
| $w^{e,ped.,mtanh,lin.}_{T,n,p}$ | Pedestal width (temperature, density and pressure) | $\psi$ (adim.) |
| $p^{e,ped.,mtanh,lin.}_{T,n,p}$ | Pedestal position (temperature, density and pressure) | $\psi$ (adim.) |
| $T/n/p_{e,offset,mtanh/lin.}$ | Pedestal offset in the temperature, density and pressure profiles in the Scrape-Off Layer | $eV/m^{-3}/Pa$ |
| Core slope $T/n/p_{e,mtanh/lin.}$ | Temperature, density and pressure core slope | $eV/\psi$, $m^{-3}/\psi$, $Pa/\psi$ |
| Max Grad $T/n/p_{e,mtanh/lin.}$ | Temperature, density and pressure pedestal maximum gradient | $eV/\psi$, $m^{-3}/\psi$, $Pa/\psi$ |
| Pos Max Grad $T/n/p_{e,mtanh}$ | Temperature, density and pressure pedestal max. gradient position | $eV/\psi$, $m^{-3}/\psi$, $Pa/\psi$ |
| mtanh/lin parameters | Parameters related to the construction of the fit | |
| **Other pedestal parameters** | | |
| $T_i, ped$ | Pedestal ion temperature | eV |
| $Z_{eff,ped}$ | Effective charge number at the pedestal | |
| $v_{pol,ped}$ | Pedestal poloidal velocity | m/s |
| $v_{tor,ped}$ | Pedestal toroidal velocity | m/s |
| **Derived parameters** | | |
| $W^{e/i,ped,mtanh/lin.}_{th}$ | Pedestal stored energy (for electrons and ions) | J |
| $V_{ped,mtanh/lin.}$ | Plasma volume at the pedestal top | $m^3$ |
| $V_{tot,mtanh/lin.}$ | Plasma total volume | $m^3$ |
| $\alpha_{max,e}$ | Max value of the normalized electron pressure gradient (in mtanh fit only) | |
| pos $\alpha_{max,e}$ | Position of $\alpha_{max,e}$ in $\psi$ space | $\psi$ |
| $p_{neutral}$ | pressure of the neutrals | Pa |
| **Dimensionless parameters** | | |
| $\beta_{pol,e,ped,avg,CHEASE}$ | Poloidal confinement parameter averaged over the flux surface derived from CHEASE | |
| $\beta_{pol,e,ped,avg/HFS/LFS,lin}$<br>$\beta_{pol,e,ped,avg/HFS/LFS,mtanh}$ | Poloidal confinement parameter of the pedestal at the HFS, the LFS and as an average over the flux surface value between both | |
| $\nu*_{ped,e,mtanh/lin.}$ | Pedestal normalized collisionality | |
| $\rho*_{ped,LFS/HFS/axis,e,mtanh/lin.}$ | Normalized Larmor radius of the pedestal at the HFS, the LFS and at the magnetic axis | |
| $B_{pol,avg,mtanh/lin.}$ | Poloidal magnetic field at the pedestal top averaged over the flux surface | T |
| $B_{pol/tor/tot,HFS/LFS,mtanh/lin.}$ | Poloidal, toroidal and total magnetic field at the HFS, LFS at the pedestal top | T |
| $\log(\Lambda_{mtanh/lin})$ | Small angle collision contribution | |
| $\epsilon$ | Inverse aspect ratio | |
| $q_{95}$ | Safety factor at $psi$=0.95 | |
| R | Major radius | |
| $B_{axis}$ | Magnetic field value at the magnetic axis | |
| **ELMs** | | |

| | | |
|---|---|---|
| $f_{ELM}$ | ELM frequency | Hz |
| ELM type | ELM type | string |
| $W_{ELM}$ | ELM energy loss | J |
| $\tau_{ELM}$ | Time length for the ELM to collapse | s |
| | **Global parameters to store** | |
| $I_p$ | Plasma current | A |
| $B_t$ | Average toroidal field | T |
| $P_{NBI}$ | NBI power | W |
| $P_{ICRH}$ | Ion Cyclotron Resonance Heating (not available at TCV) | W |
| $P_{ECRH}$ | Electron Cyclotron Resonance Heating | W |
| $P_\Omega$ | Ohmic power | W |
| $P_{tot}$ | (Total power)-(NBI shine through(complex to calculate)) - (dW/dt) | W |
| $P_{rad}$ | Radiative power | W |
| $W_{MHD}$ | MHD plasma energy | J |
| $W_{dia}$ | Diamagnetic plasma energy | J |
| $\beta_{N/p,global,MHD/dia}$ | Global confinement parameter both normal (N) and poloidal (p) from MHD or diamagnetic calculations | |
| $L_{i,MHD/dia}$ | Internal inductance form MHD or diamagnetic calculations | H |
| $\tau_e$ | Energy confinement time | s |
| ngw | Greenwald density | $m^{-3}$ |
| $n_{e.l.a}$ | Line averaged electron density | $m^{-3}$ |
| $H_{98}$ | H factor for the IPB98(y,2) scaling law | |
| $\tau_e e, IPB98(y,2)$ | Energy confinement time from the scaling law IPB98(y,2) | s |
| Main ion | Main ion (H,D,T,He,H-D,D-T) in the plasma | string |
| $M_{eff}$ | effective mass | |
| $H_{rate}$ | Hydrogen puff rate | e/s |
| $D2_{rate}$ | Deuterium puff rate | e/s |
| $He_{rate}$ | Helium puff rate | e/s |
| $T_{rate}$ | Tritium puff rate | e/s |
| $Imp_{seeding1}$ | Seeded specie 1 | string |
| $Imp_{seeding2}$ | Seeded specie 2 | string |
| $Imp_{seeding1}$ rate | Specie 1 puff rate | e/s |
| $Imp_{seeding2}$ rate | Specie 2 puff rate | e/s |
| $Z_{eff,line}$ | Line integrated $Z_{eff}$ | |
| $W_{th,tot}$ | Total thermal store energy | J |
| $W_{fast}$ | Fast particle energy | J |
| $\beta_{N,th}$ | total thermal $\beta_N$ | |
| | **Equilibrium** | |
| $\psi_{pol,norm,r}$ | Normalized flux coordinate $\psi$ vs radius at z=$Z_{mag}$ | |
| $r_{zmag}$ | radial basis for $\psi_{pol,norm,r}$ | |
| $r_{mid,profile}$ | Midplane radius vs normalized $\psi_{pol}$ | |
| $V_{profile}$ | Volume vs normalized $\psi_{pol}$ | |
| FF'$_{profile}$ | FF' vs normalized $\psi_{pol}$ | |
| p'$_{profile}$ | p' vs normalized $\psi_{pol}$ | |
| $q_{profile}$ | q vs normalized $\psi_{pol}$ | |
| shear profile | shear profile | |
| $q_{min}$ | min value of the safety factor | |
| $\psi_{axis}$ | $\psi_{pol}$ value at the axis | |
| $\psi_{sep}$ | $\psi_{pol}$ value at the separatrix | |
| $\delta_{upper}$ | Upper triangularity | |
| $\delta_{lower}$ | Lower triangularity | |
| $\kappa$ | Elongation | |
| Divertor Geometry | Divertor geometry (In this thesis, LSN) | string |
| Strike point | Position of the strike point | string |
| $r_{outer}$ | r coordinate of the outer strike point | m |
| $z_{outer}$ | z coordinate of the outer strike point | m |
| $r_{inner}$ | r coordinate of the inner strike point | m |
| $z_{inner}$ | z coordinate of the inner strike point | m |
| $R_{mag}$ | r coordinate of the magnetic axis | m |

| | | |
|---|---|---|
| $Z_{mag}$ | z coordinate of the magnetic axis | m |
| $R_{geo}$ | r coordinate of the geometric axis | m |
| $Z_{geo}$ | z coordinate of the geometric axis | m |
| a | Minor radius | m |
| $\psi_{grid}$ | Matrix for the $\psi$ grid | m×m (grid) |
| $r_{\psi,grid}$ | r for the $\psi$ grid | m |
| $z_{\psi,grid}$ | z for the $\psi$ grid | m |
| $J_{par,max}$ | max value of the bootstrap parallel current component | $A/m^2$ |
| $J_{par,mean}$ | mean value of the bootstrap parallel current component | $A/m^2$ |

## 3.2 Primary Shot selection criteria

The shots have been selected from several experiments taken from the CRPP (Swiss Plasma Center) intranet wiki, in particular from five tables comprising shots that occurred in the years 2017-2018; since the NBI system had been installed in early 2017, the ECRH, the NBH and a combination of both have been used in the shots (with respect to [6], where only the ECRH was operative). A total of $\sim 280$ shots have been selected.
Since the Thomson Scattering System did not register profiles related to the ions, but only for the electrons, in this thesis only the electron related parameters have been calculated, with few exceptions; in these exceptions, the temperature values for the ions have been assumed as 70% of the temperature values fro the electrons, while the density is assumed equal for both; all the other parameters have been derived from these assumptions. The conditions for choosing the shots had to be manually selected by using the tool jScope, a Java-based UI that allows visualization of several data and profiles, according to the selected overview.
The primary condition to select the shots was to consider the intervals of time where the power, the density and the current were at the same level; this means that the plasma regime could have been considered stationary and, as a consequence, the ELM generation would have been stationary as well.
After that, another condition used to choose the shots had been whether or not the fueling of deuterium or the seeding of impurities in the plasma is stationary as well (see fig. 3.1, 'flux' quantity); this because the pedestal profiles are influenced by the introduction of additional fuel and/or impurities, which changes its pedestal position and height (fig. 3.2) [8].
From these conditions, the operator had to manually specify the time interval for that particular shot.

## 3.3 Thomson data and profile fitting

### 3.3.1 Thomson data

After the shots have been selected, the data of each one of them have been extracted from the TCV database; in particular, the retrieved data were the electron temperature, density and pressure from the Thomson diagnostic. As a first task, the program is asked

to identify, inside such time interval, the instants at which the plasma is about to burst into an ELM; the condition for the functions that carries out this task is to look for the times in which the Thomson diagnostics was on, and to select the measurements that occurred in between [75%÷99%] of the ELM cycle (fig. 3.3(a) and 3.3(b)), 0% being immediately after an ELM, and 100% being when the ELM occurs. The selected data are then extracted into a structure, containing all the data related to temperature, density and pressure, as well as how many ELMs that matched the criteria have been found and at which times. Since the diagnostic collected data from 89 channels, all the profile data are multiples of 89; moreover, the data start from the end of the pedestal profile, then go towards the core value and they end back at the end of the profile; this is caused by the laser passing through the plasma from below, traversing the core and then exiting from the upper side of the vessel.

### 3.3.2 Profile fitting: x axis definition and linear fit

After obtaining the raw data from the Thomson diagnostics (figure 3.4), the fits of the temperature, density and pressure profiles have been extrapolated.

The profiles are all shown not as a function of the radial coordinate, but as a function of a normalized one, called normalized flux coordinate; this quantity goes from 0 to 1 by definition, where 0 indicates the position at the magnetic axis, while 1 indicates the Least Closed Flux Surface (LCFS), the edge of the plasma:

$$\psi = \frac{\phi(r) - \phi_{axis}}{\phi_{edge} - \phi_{axis}} \tag{3.1}$$

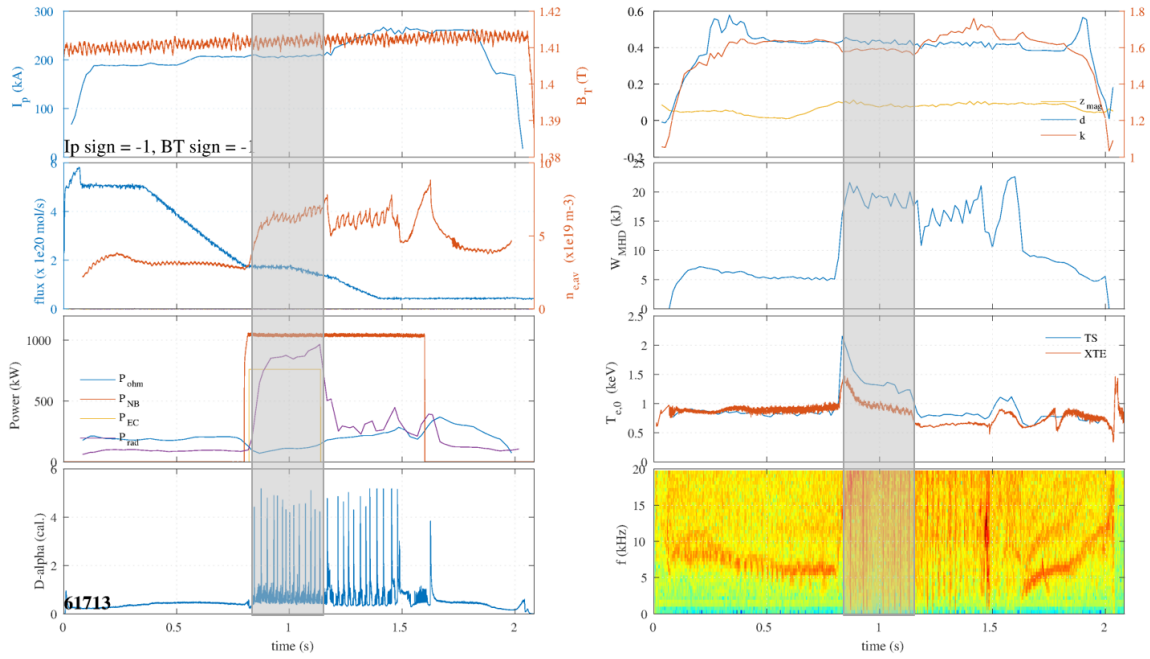


Figure 3.1: Example of data gathered for shot 61713; the grey box is the time interval assumed in stationary conditions, 0.88÷1.12 s7

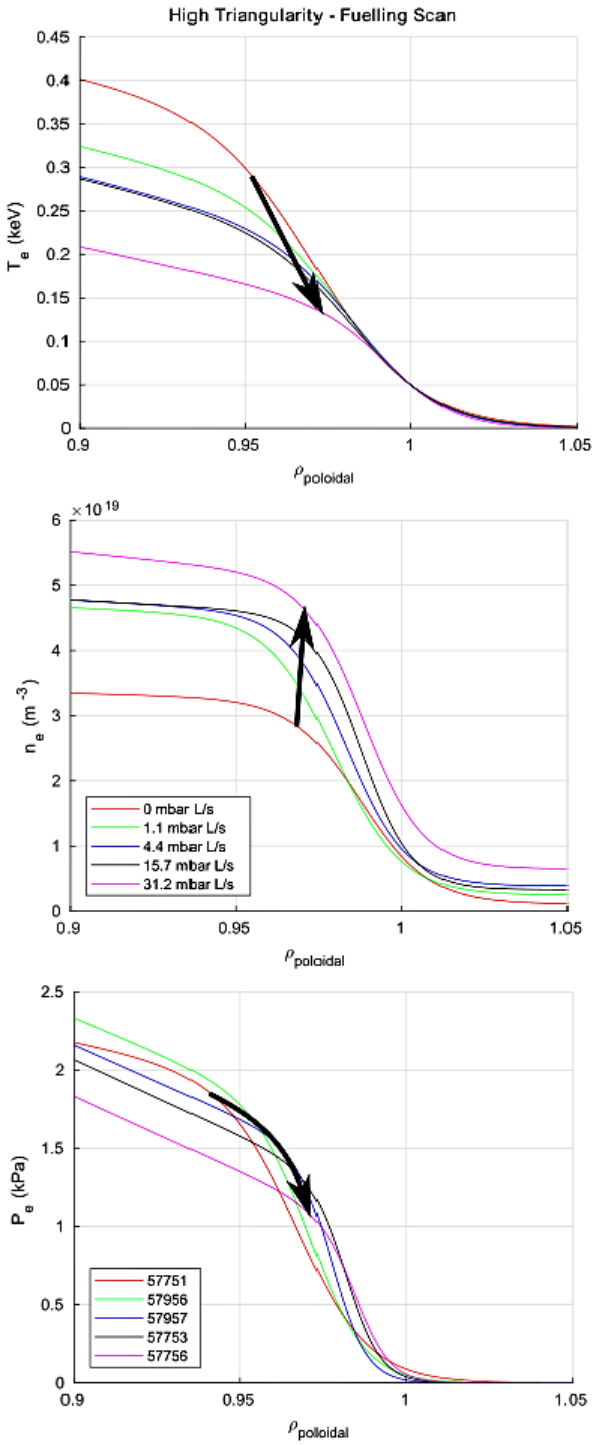


Figure 3.2: $T_e$, $n_e$ and $p_e$ pedestal behavior changes in different fueling conditions [8]

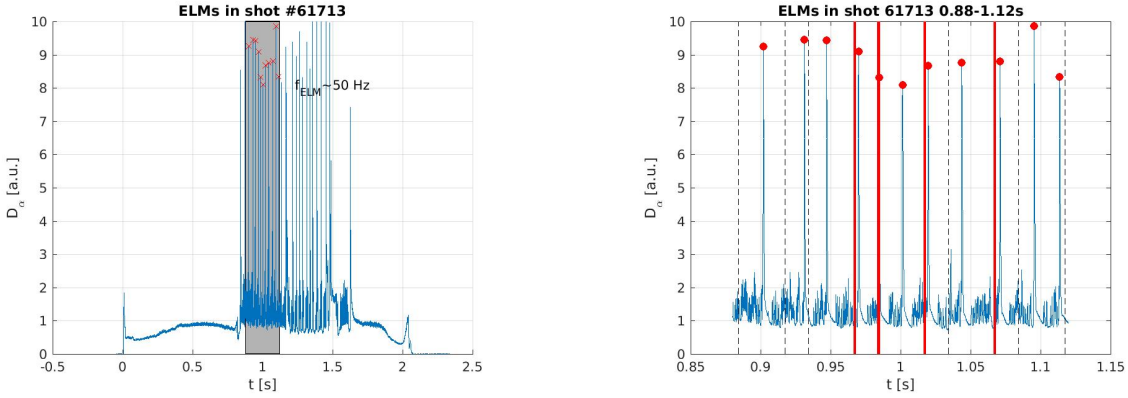


(a) (b)

Figure 3.3: (a) $D_\alpha$ signal. The grey box indicates the time interval selected. (b) $D_\alpha$ signal in the selected time interval. The segmented lines are the times at which the measurement from the Thomson scattering took place; the red lines indicate the measurement between $[75\% \div 99\%]$ of the ELM cycle

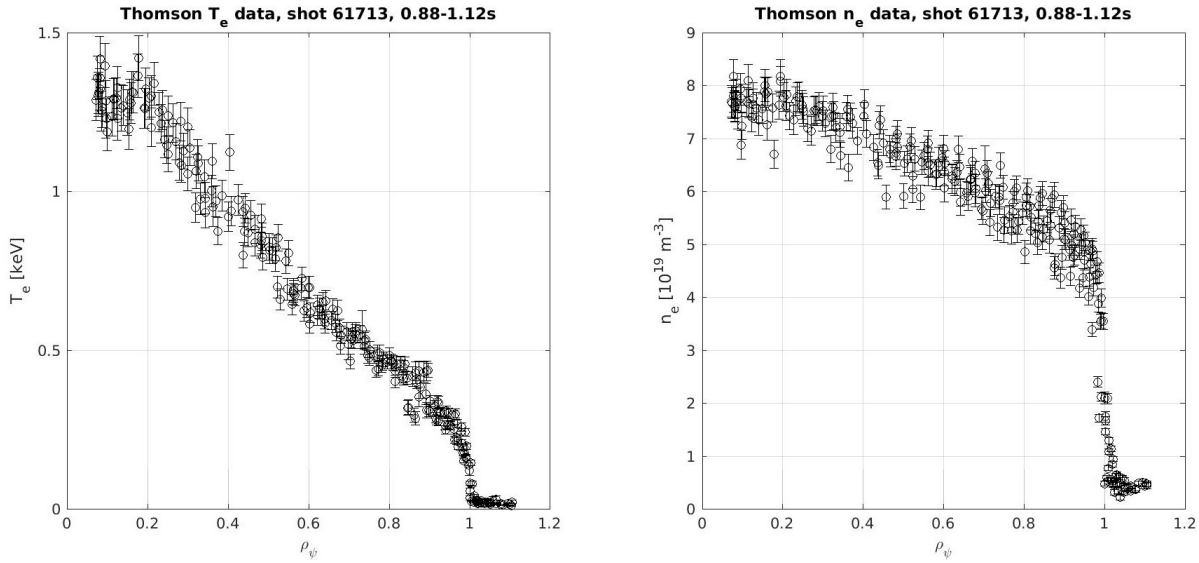


Figure 3.4: Raw Thomson scattering temperature and density profiles

This quantity, along with the quantity $\rho_\psi = \sqrt{\psi}$, are the x-axis values mainly used in this thesis. The existing tokamaks may have different magnetic configurations one from the other, caused by the poloidal magnets, which will result in a different poloidal magnetic field section per machine; in the case of TCV, which main feature is exactly the possibility to change this configuration at will, this argument is even stronger; for this reason, the normalized flux coordinate is used, since it normalizes the poloidal magnetic cross section from whatever configuration it was to a circumference, which means that profiles from different shots, or even different machines, can be directly compared by using this coordinate. All the quantities in the database are expressed as a function of $\psi$, while $\rho_\psi$, frequently used at TCV, is used for the calculations in the program in various occasions, and in several figures as well (see figures 3.2 and 3.4).
The first thing that had been done was the removal from the dataset of NaN (Not a Number) values in the raw profiles, located at the extremes of the profiles; this removes about one third of the data points from the profile. Moreover, the fits are related to the pedestal only, so, in order to have a better fit, the points in the core plasma region have been removed; the program selects the points at $\psi \geq 0.7$, but it includes the option to change the threshold value if needed. At the end of this selection, the non-null data points after $\psi = 0.7$ are $\sim 30$ out of 89 per single ELM (every time interval may contain more than one ELM).
As a first approximation, the data profiles have been fitted with a series of straight lines, all connected with each other so that they best represent the pedestal profile. This kind of fit has been called linear fit, and it is the way to give a first, rough approximation of the pedestal shape.
In order to recreate such profile, the Heaviside function has been used:

$$H(\psi - b) = \begin{cases} 1, & \text{if } \psi > b \\ 0, & \text{if } \psi < b \end{cases} \tag{3.2}$$

which, combined with the expression of a line, can give a segment of the pedestal. The complete pedestal is then the sum of three such combinations between Heaviside functions and lines.
Several boundary conditions have been enforced in the program on the fit:

- The three segments must make a continous function, hence the points at the edge between them must be the same.

- The slope of the last segment (the "tail" of the pedestal) has been imposed equal to zero, under the approximation that the plasma is not present after the LCFS, and as a way to prevent the fitted profiles to go below temperature, density and pressure values of zero.

- The slope of the first segment (the one representing the "core" plasma before the pedestal) has been imposed as $\leq 0$.

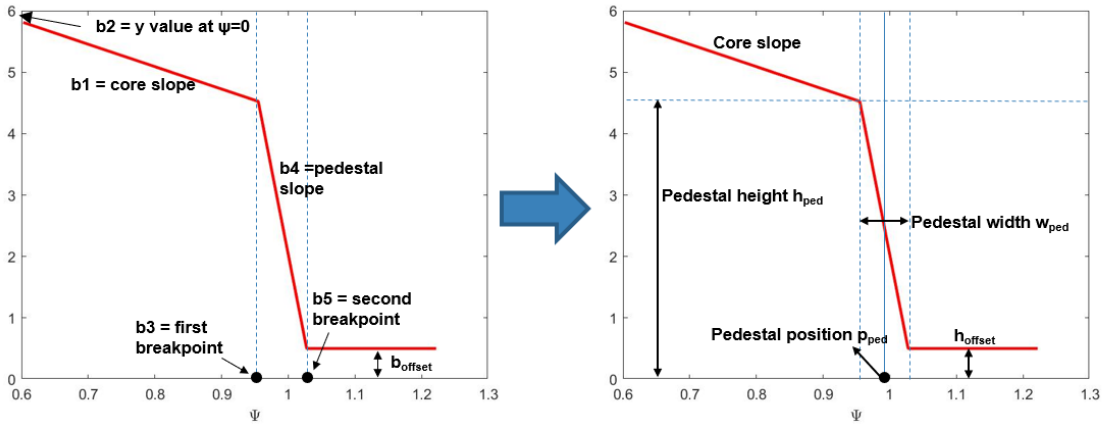


Figure 3.5: linear fit and parameters used in the fit (left); linear fit with the parameters inserted in the database (right).

By using these conditions, the equation describing the linear fit is:

$$linfit([b_1, b_2, b_3, b_4, b_5, b_6], \psi) = (b_1\psi + b_2) \times H(b_3 - \psi) + (b_4\psi + b_{01}) \times H(\psi - b_3) \times H(b_5 - \psi) + b_{offset} \times H(\psi - b_5) \tag{3.3}$$

One more boundary condition had been added:

- The vertical offset of the tail of the pedestal has been set to zero for the temperature and the pressure profiles, since after the pedestal these quantities are so low compared with the inside of the plasma that can be neglected; however, the density profile has been left with an offset, since the density in the SOL is not negligible.

The resulting equation for the temperature and pressure profiles is:

$$linfit([b_1, b_2, b_3, b_4, b_5], \psi) = (b_1\psi + b_2) \times H(b_3 - \psi) + (b_4\psi + b_{01}) \times H(\psi - b_3) \times H(b_5 - \psi) \tag{3.4}$$

Even though the approximations mentioned above have been used, the program allows the removal of the conditions about the slope of the pedestal tail being 0 and its offset being 0 as well, thus allowing some degree of flexibility; this is done by modifying the array containing the initial guesses for the parameters, at the beginning of the program, and the section of the program supervising the fits will change the fitting procedure accordingly.
The Matlab function *fit*() has been used to derive the parameters of eq. 3.4; however, due to several shots having one ELM only ($\sim$ 30 data points only) and a smooth pedestal slope, the resulting fit could have resulted in a straight line; in order to prevent that, an iterative procedure has been implemented; for each iteration, the values of the two parameters $b_3$ and $b_5$, corresponding to the two extremes of the pedestal (or break-points), have been chosen as an initial guess; after that, the fit is carried out, with the introduction of upper and lower conditions specified by empirical observations: one of these is noting that in all the shots at TCV the pedestal extremes are never below $\psi = 0.9$ or above $\psi = 1.1$; the fit results are stored into a matrix, and the next iteration, with incremented

values of $b_3$ and $b_5$, is computed. This procedure repeats itself until reaching the extremes of the domain, one of which is $\psi = 0.7$ as specified, while the other is the right-most value of $\psi$. After this iteration, the resulting matrix contains not only the fit parameters, but also the goodness-of-fit values related to them; in particular, the data are chosen according to the $R^2$ goodness-of-fit parameter, which has been used later in the program to make another selection of the profiles (see section 3.3.5); the higher the $R^2$ value is (which goes from 0 to 1), the better the fit approximates the experimental data; the final outputs of the linear fitting procedure here outlined are the fit parameters with the highest $R^2$.
The output parameters have then been used to reconstruct the linear fit by substituting them into equation 3.4. There are other outputs from the *fit*() Matlab function; in particular, the goodness-of-fit parameters have been stored, as well as some informations about the fitting iteration, such as the number of iterations before the method converged.
It should be noted that, in the database, the quantities related to the pedestal fit are more comprehensible quantities derived from the parameters in the Matlab function; the quantities introduced are the pedestal position ($p_{ped} = (b_5+b_3)/2$), height ($h_{ped} = b_1 b_3+b_2$) and width ($w_{ped} = b_5 - b_3$), the core slope ($coreslope = b_1$) and finally the offset of the tail ($h_{offset} = b_4 b_5 + b_3(b_1 - b_4) + b_2$) (fig. 3.5).

### 3.3.3 Profile fitting: mtanh fit

After the linear fit, the program fits the data by using a modified hyperbolic tangent as a fitting function. It is a special function based on the hyperbolic tangent, and it has the form:

$$mtanh(x) = \frac{e^{ax} - e^{-bx}}{e^{cx} + e^{-dx}} \tag{3.5}$$

The function has been proposed due to its similarity with the pedestal, and it does not rely on piecewise functions such as the linear fit one. The parameters used for define the mtanh fit of the pedestal are the plasma profile core slope immediately before the pedestal, the pedestal height, width and position, as well as the eventual offset the profile has at the tail of the pedestal profile, like in the linear fit case. With these parameters, the fitting function becomes: ($p_{ped} = (b_5 + b_3)/2$), height ($h_{ped} = b_1 b_3 + b_2$) and width ($w_{ped} = b_5 - b_3$), the core slope ($coreslope = b_1$) and finally the offset of the tail ($h_{offset} = b_4 b_5 + b_3(b_1 - b_4) + b_2$) (fig. 3.5) Moreover, the pedestal width and core slope are derived by:

$$w_{ped} = 4w \qquad core\ slope = \frac{h^{ped} - h^{offset}}{4w} s \tag{3.6}$$

Where the boundary condition $h_{offset}$=0 in order to keep consistency with the linear fit; similarly to the linear fit, the option to use $h_{offset} \neq 0$ has been implemented in the program by modifying the length of the initial guess values array for the mtanh fit.
The Matlab function used is the *lsqcurvefit*(), which is similar to the function *fit*() previously used; however, *lsqcurvefit*() uses the least squares optimization as the only fitting method, while in the function *fit*() this can be different.
The advantage of the mtanh fit with respect to the linear one is that the mtanh function

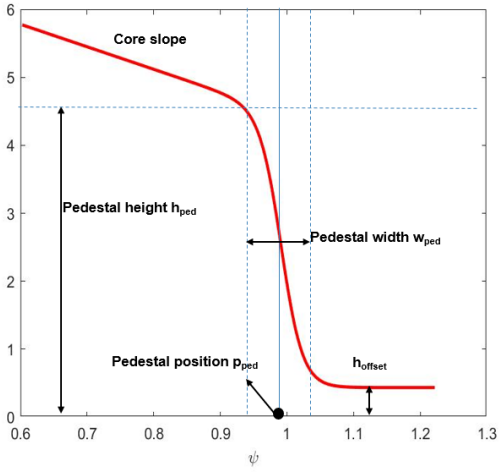


Figure 3.6: Modified hyperbolic tangent fit.

is, as mentioned before, continous and differentiable, and not a piecewise function like the linear fit; as such, the fitting procedure is simpler and faster, since it does not require the iterative procedure used in section 3.3.2. As far as the $R^2$ goodness-of-fit value is concerned, *lsqcurvefit*() does not have it as one of its output values; it has been therefore necessary to carry out the calculation by using the formula:

$$\begin{gathered} R^2 = \frac{SSR}{SST} = 1 - \frac{SSE}{SST}, \quad \text{where SST=SSE+SSR} \\ SSE = \text{Sum of Square Error} = \sum (y_i - \hat{y}_i)^2 \\ SSR = \text{Sum of Squares of the Regression} = \sum (\hat{y}_i - \overline{y})^2 \\ SST = \text{Sum of Squares about the mean} = \sum (y_i - \overline{y})^2 \end{gathered} \tag{3.7}$$

Where $y_i$ are the experimental data, $\hat{y}_i$ are the fitted data, and $\overline{y}$ is the mean value of the data points. The parameters of the mtanh fit can be seen at fig. 3.6.

### 3.3.4 Profile fitting: Pedestal shift

As explained in section 3.3.2 the normalized flux coordinate $\psi$ has been introduced in order to normalize the profiles from different shots. However, there is an additional convention that is used in order to normalize the shots, so that they can become easily comparable; this convention is to impose a fixed value of temperature in the pedestal profile at the separatrix, $\psi = 1$; the value used varies from machine to machine: at AUG and JET, this value is $T_{e,sep.}$=100eV, while at MAST and TCV is $T_{e,sep.} = 50eV$. The consequence of this convention is to shift the temperature pedestal fits so that $T_{e,sep.}(\psi = 1) = 50eV$, and apply the same shift to the density and pressure profiles; all the data related to $\psi$ in the database, such as the pedestal position $p_{ped}$, have been corrected by this shift, and then stored into the database. The program allows for this shift to be taken into consideration in the database computation or not.
The resulting profiles, by including the experimental data and the shifted profiles as well,

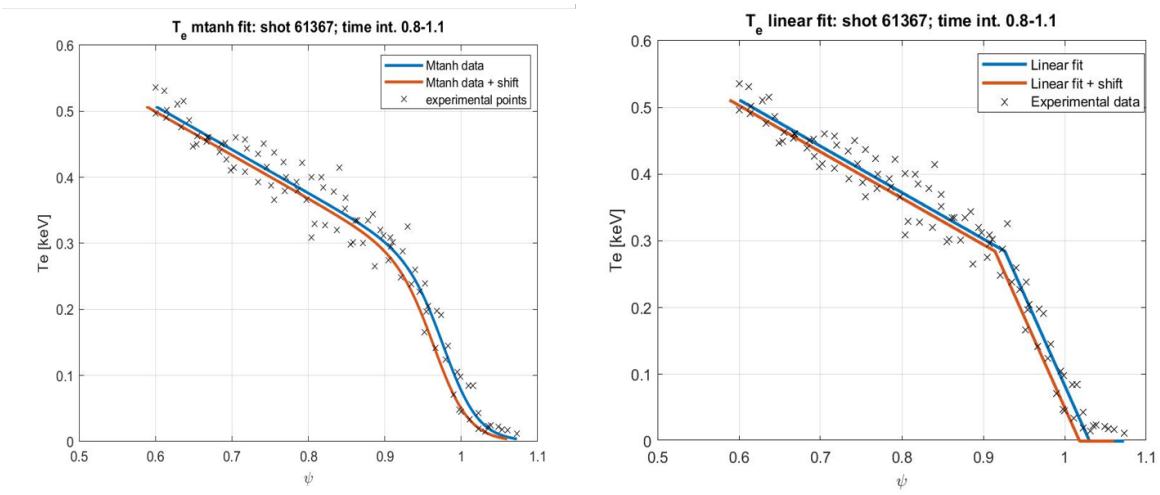


Figure 3.7: Electron temperature pedestal profiles

are shown in fig. 3.7.

### 3.3.5 Selection of the shots by using the $R^2$ goodness of fit parameter

After the data profiles have been fitted, another selection, based on how good the fit represents the data, is carried out. The goodness of fit $R^2$ is used in this selection; this is a parameter that estimates how reliable a fit is in approximating the behavior of the experimental data; the $R^2$ value ranges from o to 1, 1 meaning the fit perfectly represents the data, and viceversa for 0. As such, a value of $R^2$ as close to 1 as possible has been sought. In particular, a threshold value of $R^2$ has been established, below which the shot has been discarded by the program; this value has been set to $R^2$=0.91.
It is important to note that the temperature and density profiles of both the linear and mtanh fit are subjected to this selection, meaning that even one fit out of four being below the threshold value leads to discarding the shot. This is the most strict selection method implemented in the program building the database, cutting about 50% of the shots that have been manually selected by using jScope (see chapter 3.2). The surviving shots after this selection had been $\sim$ 140.

### 3.3.6 Core profile fit

After the pedestal data have been fitted into a profile, the program fits the core profile as well, and then connects the two into a single profile; because of the higher quality of the pedestal, as well as more reliable data, only the mtanh fit has been used to derive a complete fit of the plasma over $\rho_\psi$ (or $\psi$). This separation has been done in order to prevent the incorrect fitting of the pedestal: if the entire profile (core and pedestal) would have been fitted, the core data would have distorted the shape of the pedestal, sometimes to the point that the pedestal disappears completely.
The core fit has been approximated as a $4^{th}$ order polynomial, with the addition of some

boundary conditions:

- The core and pedestal profile must connect at the abscissa value of $\psi = 0.7$.
- The derivative of the pedestal and core profiles at $\psi = 0.7$ must be the same.
- The derivative at the abscissa $\psi = 0$, at the magnetic axis, must be zero.

After making these considerations, the fitting has been carried out by using a Matlab custom function called *mmpolyfit()*, which allows the introduction of the boundary condition in a very simple and intuitive way. After computing the fit, the pedestal and core profile have been represented as a whole, complete profile (see fig. 3.8). This operation has been done because the complete profile will be an input parameter in order to solve the self-consistent problem by using the code CHEASE.

## 3.4 Solution of the equilibrium: CHEASE code

The plasma behaves in a self-consistent way, due to the fact that a charged particle interacts with the other particles in the plasma, which in turn interact with the considered particle; this means that the complexity of the problem does not allow an analytical solution; the only way to solve the problem is to use an iterative procedure, by proposing a first guess solution, and then solve the problem; this will give as an output another solution, which will replace the previous one in the problem computation; the problem is solved again, and the iterations will go on until the difference between the solution used to solve the problem and the solution found after solving the problem coincide to a certain degree, determined by a threshold tolerance level.
At TCV a code, called *LIUQE* (EQUIL backwards) is used for the calculation of all the quantities and parameters immediately after a shot has taken place. Because of that, the main goal of LIUQE is that to be fast enough to retrieve all the data between one plasma shot and the other. However, in the program, this task is carried out by using another code, called *CHEASE* [5], which stands for **C**ubic **H**ermite **E**lement **A**xisymmetric **S**tatic **E**quilibrium. The detailed description of this code, not argument of this thesis, can be found in [5]; the main objective of CHEASE is to iteratively solve the Grad-Shafranov equation 2.22, thus deriving the state of equilibrium of the plasma; this means that the complete current profile at equilibrium, derived from F, can be computed, which means the bootstrap current can be derived as well, as well as the magnetic field and the pressure profile p.
The code CHEASE has been used with respect from LIUQE because the former uses an Hermite bicubic finite element discretization [5], while the latter uses a series of polynomials for *p'* and *TT'*, and fits those to the measurements of the magnetic probes installed at TCV by using the least-square method; as a consequence, LIUQE is faster, but less accurate, while CHEASE is more precise, but it requires more time to compute.
As said before, one of the quantities CHEASE has to compute is the bootstrap current

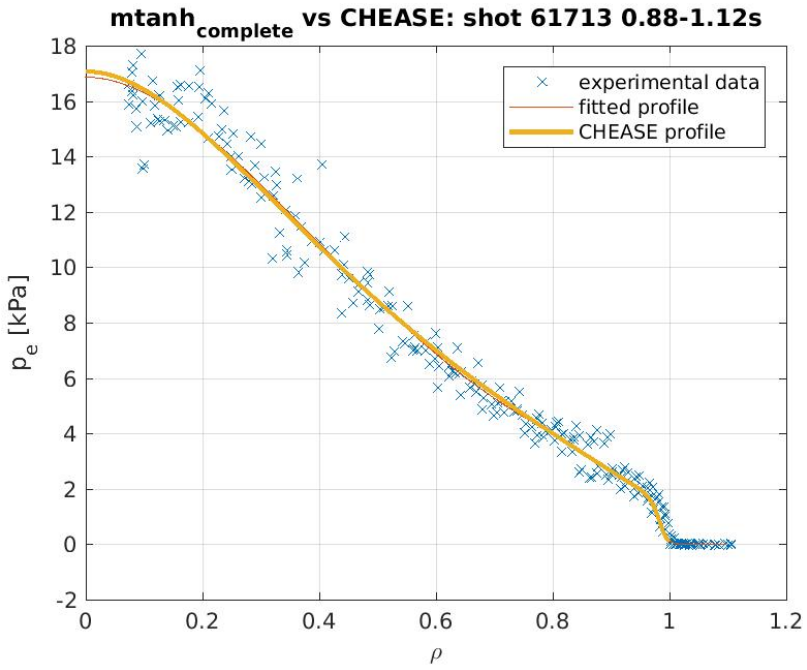


Figure 3.8: Electron pressure CHEASE profile vs fitted profile of the shot 61713, time interval 0.88-1.12s; the points are the experimental data

$J_{//,BS}$, expressed by [6], [5]:

$$\langle \vec{J} \cdot \vec{B} \rangle_{BS} = T(\psi) p \Bigg[ A_1 \frac{\partial ln(n_e)}{\partial \psi} + R_{pe}(A_1 + A_2) \frac{\partial ln(T_e)}{\partial \psi} + (1 - R_{pe}) \times \left( 1 + \frac{A_3}{A_1} \alpha \right) A_1 \frac{\partial ln(T_i)}{\partial \psi} \Bigg] \tag{3.8}$$

$$J_{//,BS} = \frac{\langle \vec{J} \cdot \vec{B} \rangle_{BS}}{\langle \vec{B} \cdot \nabla \phi \rangle}$$

Where $A_1, A_2, A_3, \alpha$ are functionals, $R_{pe} = p_e/p$ is the ratio between electron and total pressure, and $n$ and $T$ are respectively the density and temperature profiles;. The subscript refers to both electrons and ions, where the ions were assumed to be so that $T_i = 0.7T_e$; the same has been done for the density. The current density profile is represented in figure 2.4.

As far as the profiles are concerned, the code returns the density, temperature and pressure profiles after having solved the self-consistent problem; the resulting profile differ very slightly from the initial fits, in particular in the region of the pedestal. The complete electron pressure profile derived form the fit, as well as the one computed by CHEASE, can be seen in figure 3.8. The data are then saved in three different array of Matlab structures for quick access to the data; the complete output from the code is saved as well into a folder specified by the user. As a last remark, the output has been calculated by using initial guess profiles with a shift of $\psi$, so that $T_e(\psi = 1) = 50eV$, as seen in chapter 3.3.4.

### 3.4.1 Parameters derived from CHEASE

In addition to the profiles, the CHEASE code has been used to return various parameters related to the plasma stability and equilibrium.
One of the first quantities that can be retrieved from the solution of the self-consistent problem are the pedestal and total plasma volume; the pedestal volume is defined as the volume of plasma until the value of $\psi$ or $\rho_\psi$ where the pedestal top position is located, while the total volume is the one calculated until the pedestal bottom position is located, by assuming that this position is where the LCFS is; these positions have been found by interpolating the volume profile with the respective pedestal positions of both the linear and mtanh fitted profiles). After that, the pedestal stored energy for electrons has been calculated as:

$$w_{th,e,ped,lin./mtanh} = \frac{3}{2} p_{e,ped,lin./mtanh} \frac{(V_{tot,lin./mtanh} + V_{ped,lin./mtanh})}{2} \tag{3.9}$$

where the subscripts *lin./mtanh* refer to the values found by using one fitting method or the other.
Another parameter derived from CHEASE is the normalized pressure gradient, and it is connected with plasma stability (see chapter 2.2.2); it is defined as:

$$\alpha = -\frac{2}{(2\pi)^2} \frac{\partial V_{tot,mtanh}}{\partial \psi} \left( \frac{V_{tot,mtanh}}{2\pi^2 R} \right)^{1/2} \mu_0 \frac{\partial p_e}{\partial \psi} \tag{3.10}$$

This quantity is used in determining the stability region of a particular plasma regime, to see in which stability conditions ELMs will form; the advantage of the normalized pressure gradient over the pressure is that the normalization is carried out over the plasma volume and the plasma pressure, thus making possible to compare data from other experiments and tokamaks. In the database, the maximum value of alpha and its position have been registered, since it will be the value for which the ELM will be triggered or not; this value will be located close to the pedestal position, where the pedestal gradient is the highest; as such, the value of $\alpha$ will describe when the pedestal collapses into an ELM, in particular, when $\alpha$ will be higher than a critical value $\alpha_{crit}$, set by MHD calculations, an ELM will be triggered. A profile of $\alpha$ is illustrated in fig. 3.9. Several more quantities that have been produced by CHEASE have been stored; one of these is the magnetic field, poloidal, toroidal and total ones; the values stored inside the database are the ones calculated at the position of the pedestal both at the HFS (High Field Side) and LFS (Low Field Side) of the plasma cross section, as well as the average value; these values has been calculated for the linear and the mtanh fit.
Of particular note is that, in the *equilibrium* section of the database, profiles such as the *FF'* and the *p'* profiles have been saved, as well as the safety factor profile $q$ and the shear profile (given by $(1/q)(dq/d\psi)$).

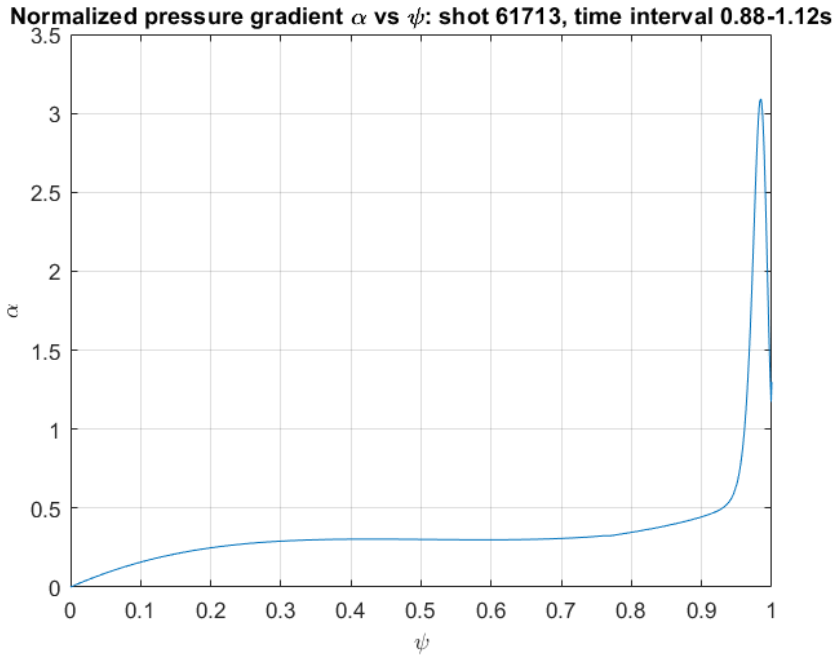


Figure 3.9: Normalized pressure gradient profile with respect to the normalized flux coordinate. The maximum value will be stored inside the database, as well as its position

## 3.5 Dimensionless parameters

After computing the fits for the experimental data, and after solving the self-consistent problem by using CHEASE, the database has been filled with fit-related informations, such as the pedestal position for all the six profiles (temperature, density and pressure for both linear and mtanh fit), and with the derived parameters discussed in section 3.4.1; in particular, at this point the sections *Parameters directly related to the fits*, *Other useful pedestal parameters*, *Derived parameters* and the part related to the magnetic fields of the section *Dimensionless parameters* of table 3.1 have been filled. After that, the other dimensionless parameters have been computed; the most important being the magnetic confinement parameter and the collisionality, as well as the normalized Larmor radius.

### 3.5.1 Magnetic confinement

As seen in chapter 2.1.4, the MHD balance equation of momentum 2.17 states that there is a balance between the plasma pressure and the magnetic field generated inside the tokamak. In particular, the pressure in the plasma in the outward direction must be balanced by the magnetic field. This is expressed by a quantity called magnetic confinement parameter $\beta$:

$$\beta = \frac{p}{B^2/2\mu_0} \tag{3.11}$$

Where p is the pressure and B is the considered magnetic field; since the values of the magnetic field and the pressure can be multiple, different values of $\beta$ can be defined. In the database, the calculated value of $\beta$ is given by choosing the value at the pedestal

of the electron pressure, and by choosing the value of the poloidal magnetic field at the pedestal position, at the HFS, at the LFS and the average between the two; moreover, these variants of $\beta$ have been calculated for both the linear and the mtanh profiles, thus resulting in 6 values of $\beta$ to insert in the database.

### 3.5.2 Collisionality

The charged particles inside the plasma will collide with each other; this collisions will have an higher probability at higher densities and, since these collisions are of electrostatic origin, they will have a lower probability at higher temperatures (hence, velocities) as well; these collisions are described by a collision frequency $\nu$, and, since this quantity is directly connected to the collision term in all plasma descriptions (see chapter 2), it plays an important role in determining the plasma equilibrium and stability, in particular in the formation of ELMs and their type. In the database, the normalized collisionality $\nu^*$ is used, and it is defined by:

$$\nu^* = \frac{connection\ length}{trapped\ particle\ mean\ free\ path} = \frac{v_{th}/\nu}{trapped\ particle\ mean\ free\ path} \tag{3.12}$$

where $v_{th}$ is the thermal velocity and $\nu$ is the collision frequency. In the database, the formula used to calculate the normalized collisionality is:

$$\nu^*_{e,ped,lin/mtanh} = 6.93 \cdot 10^{-18} ln\Lambda \frac{Rq_{95} n_e^{ped,lin/mtanh}}{\epsilon^{3/2}(T_e^{ped,lin/mtanh})^2} \tag{3.13}$$

where $ln\Lambda$ is a term appearing due to the accumulation of many small-angle collisions within the region of a a Debye sphere (region in which a particle, screened by all the other particles, lives in, of radius of the Debye length $\lambda$). In the database, the stored value is the one at the pedestal position; as such, it is expressed as:

$$ln\Lambda = 31.3 - ln\frac{\sqrt{n_e^{ped,lin/mtanh}}}{T_e^{ped,lin/mtanh}} \tag{3.14}$$

### 3.5.3 Normalized Larmor radius

The particles, when inside a magnetic field, gyrate because of the Lorentz force. The radius of this circular motion is called Larmor radius, and the gyration frequency is called cyclotron frequency $\Omega$. The normalized Larmor radius is obtained by dividing the Larmor radius by the minor radius of the tokamak ($\rho^* = \rho/a$). Like the magnetic confinement and the collisionality, the value of the normalized Larmor radius stored inside the database is the one at the pedestal position:

$$\rho^* = \frac{\sqrt{2m_e T_e^{ped}}}{eBa} \tag{3.15}$$

where B is the total magnetic field, taken at the axis, at the HFS and the LFS; since this process must be repeated for both the linear and the mtanh fit, the valuse of $\rho^*$ stored

in the database are 6, like the magnetic confinement $\beta$.

## 3.6 ELM related parameters

In this section, the part of the database directly related to ELMs, such as their frequency, are discussed. In order to finding these quantities, an auxiliary routine called *ELMfreq()*, native of TCV, has been used; this function calculates several ELM related quantities:

- The ELM frequency behavior, the average value, called $f_{ELM}$ being stored in the database under the assumption of stationariety of the shot conditions.
- The average energy an ELM loses when it takes place; this because an emission of plasma means an emission of energy out of the system (the plasma region) as well. It is indicated with $W_{ELM}$.
- The average duration for the ELM to collapse; it means the time interval in which the ELM event occurs: it is derived from calculating the full width at half maximum, or *fwhm*, of the ELM peak profile, dividing it by the total length of the ELM peak $l_{ELM}$, and thus multiplying it by the ELM duration (the inverse of $f_{ELM}$):

$$\tau_{ELM} = \frac{1}{f_{ELM}} \frac{fwhm_{ELM}}{l_{ELM}} \tag{3.16}$$

It is important to note that, due to the stochastic nature of the plasma, no ELM in the time interval of the considered shot is equal to one another. What the routine *ELMfreq()* does is to consider the $D_\alpha$ signal, and then averages all the ELM peaks in a way that a single ELM profile, representative of all the ELMs in the time interval, is derived (fig. 3.10); the ELM frequency $f_{ELM}$ will be the repetition of this representative ELM in the time interval; this can be approximated to the real situation under the assumption of stationariety, in which case the ELMs in the $D_\alpha$ signal will be very similar one to each other.
These data have been stored inside the *ELMs* section of the database.

## 3.7 Operational parameters

The operational quantities of each and every plasma shot have been stored in the database under the *Global parameters to store* section, as well as in a part of the *Equilibrium* section as well.
It must be noted that, due to the absence of diagnostics in some occasions and difficulty in calculations in other cases, some entries have not been computed; however, the database still allocates space for these entries, and the program program allows the update of existing shots' quantities; at the time of this thesis, said quantities have a value of NaN (Not a Number) as their entries. The majority of these quantities are taken from the LIUQE nodes of the main database at TCV, especially via the function *tcvget()*, while

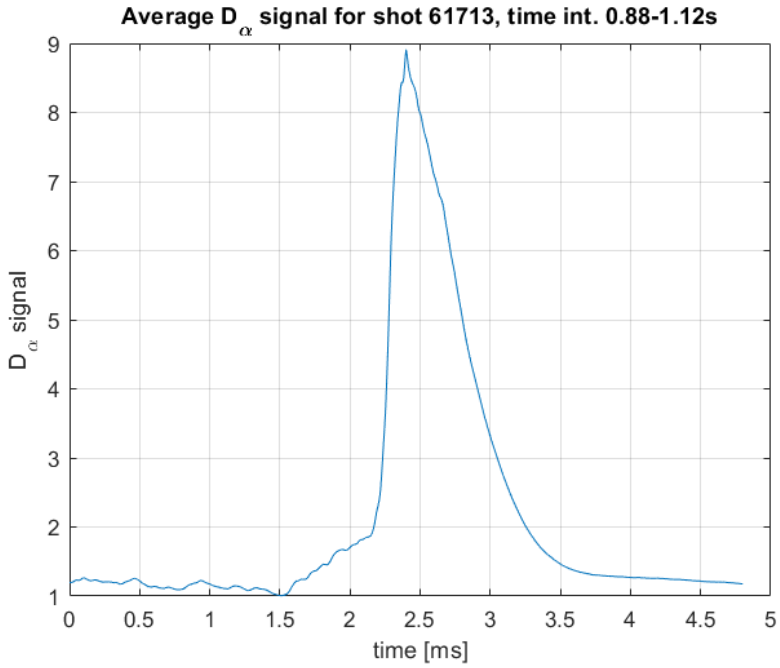


Figure 3.10: Average ELM profile in the $D_\alpha$ signal.

the others have been taken from the CHEASE data output; about the quantities taken from the LIUQE nodes, these nodes are directly related to the diagnostics and devices at TCV, so there has been the concrete possibility that the data were not available, because a particular diagnostic was not functioning for a particular set of shots: to solve this, the same *try and catch* procedure that has been implemented in the main program has been implemented in this section of the code as well; in the case the data are missing, the database entries are replaced with a NaN value, and an error will be displayed on the Matlab console; the error will be stored inside the array of structures called *error* as an output of the program.

### 3.7.1 Global parameters

The quantities stored in the database section *Global parameters to store* are mainly related to operational characteristics due to external machinery, such as power supplies and fuel and impurities injection valves; these quantities are:

- The average plasma current. This comes as a CHEASE output as a profile, so the mean value is calculated by the program.
- The NBI injected power. However, it must be noted that the quantity that should be considered in order to make calculations is the power absorbed by the plasma, which is a fraction of the injected one. However, finding the absorbed power requires a calculation for every single shot, being the conditions of the plasma of each shot different from the other. As such, it has been considered more convenient to store the value of the injected power, which is measurable.

- The ECRH injected power. What said for the NBI is valid for the ECRH as well; the absorbed power is important if calculations are to be made; however, the requirement to calculate for every single shot the fraction of ECRH power absorbed by the plasma means it is more convenient to store the injected ECRH power. There is an entry for an Ion Cyclotron Resonance Heating system, or ICRH, as well, but such a machine is not installed at TCV; however, this entry has been inserted in order to guarantee compatibility with the JET database (from where the database structure has been proposed), in the eventuality the databases from different machines would eventually be merged.

- The Ohmic power $P_\Omega$.

- The total power: it is defined as:

$$P_{tot} = P_{NBI} + P_{ECRH} + P_\Omega - P_{NBI\ shine\ through} - \frac{dW}{dt} \tag{3.17}$$

  This quantity has not been computed because of the quantity $P_{NBI\ shine\ through}$, which is too complex for this thesis to calculate.

- The radiative power $P_{rad}$

- The MHD energy $W_{MHD}$. There is an energy calculated through diamagnetic means, $W_{dia}$, but it cannot be computed at TCV.

- The normalized toroidal global confinement $\beta_{N,global,MHD}$, obtained by MHD calculations.

- The global poloidal confinement $\beta_{p,global,MHD}$, by MHD calculations as well.

- The internal inductance $L_{i,MHD}$.

- The energy confinement time $\tau_e$ discussed in chapter 1.2.

- The Greenwald density $n_{gw}$, expressed by:

$$n_{gw}[10^{19}m^{-3}] = \frac{I_p[MA]}{\pi a^2[m]} \tag{3.18}$$

  This density can be used to calculate the *Greenwald fraction fgw*, expressed by the ratio between the average electron density and $n_{gw}$, which can be used to determine where the plasma is in the stability diagrams of chapter 2.2.2; in particular, the maximum attainable stable plasma has a value of $ngw \sim 0.5$.

- Line-averaged integrated density $n_{e.l.a}$

- The $H_{98}$ parameter and the energy confinement time given by the IPB98(y,2) scaling law. These two entries have not been computed.

- The main ion and effective mass. These two entries have not been specified either.

- The H,D,He and T rates. Since only D2 is used at TCV, this is the only entry.
- Impurity seeding species. These entries have not been specified, it has been left to the operators.
- Impurity seeding rates. Even though the impurities have not been specified, the impurity rates values have been extracted from LIUQE nodes.
- The effective atomic number $Z_{eff}$, as well as the total thermal energy stored $W_{th,tot}$ and the fast particle energy $W_{fast}$. These entries have not been filled.

### 3.7.2 Equilibrium-related operational parameters

The operational quantities in the database section *Equilibrium* are related to the geometric configuration of the magnetic field of the tokamak for that particular shot, and as such they are related to the equilibrium configuration of the plasma; since TCV's main feature can adjust the generated toroidal field in order to accommodate different poloidal magnetic shapes of the cross section. As said in chapter 3.4.1, some of the quantities in this section of the database are taken from the CHEASE output data. The other quantities, taken from LIUQE are the following:

- The upper and lower triangularity, respectively $\delta_{upper}$ and $\delta_{lower}$ of the plasma poloidal cross section. They are defined as:

$$\delta_{upper/lower} = \frac{(R_{geo} - R_{upper/lower})}{a} \tag{3.19}$$

  where $R_{geo} = (R_{max} + R_{min})/2$ is the geometric major radius ($R_{max}$ and $R_{min}$ being respectively the maximum and minimum values of R along the LCFS), $a = (R_{max} - R_{min})/2$ is the minor radius, and $R_{upper}$ and $R_{lower}$ are the corresponding radii to the highest and lowest vertical points at the LCFS.
- The elongation $\kappa$ of the plasma.
- The divertor geometry; this must be specified by the operator.
- Inner and outer strike point positions, where the strike points are points where the LCFS touches the vessel. They are expressed as $r$ and $z$ coordinates.
- Coordinates of the magnetic axis $R_{mag}$ and $Z_{mag}$.
- Coordiantes of the geometrical axis $R_{geo}$ and $Z_{geo}$.

## 3.8 Conclusions

This thesis work aimed at building a database that is capable of storing a great number of significant parameters and quantities, which can then be quickly accessed. Moreover, the database is meant to run without errors that could potentially stop the database

building process. Both goals have been obtained, and the database ran over 300 shots without stopping once. The program, after compiling the database in an array of structures format, will then convert it into a more intuitive table format, allowing a quicker visualization of the needed quantities.
The whole program overview can be seen in fig. 3.11. The table is composed by 171 columns, and a number of rows specified by the operator. The whole process is started by specifying a text file in which the operator sets the shot number and the time interval of interest. The program then runs through all the shots automatically, computing all the desired quantities.
Another goal would have been to have a database as flexible as possible, which was achieved to some extent; the database routine will check if there aren't file names as the ones specified in the program; if there aren't, the routine will create all the specified quantities in the Matlab workspace (to look for which quantities will be created, see the final box of fig. 3.11), while if there are, the program will overwrite those, by adding new shot entries in the existing files (a new structure in the array of structures format, a new row in the table one). the database entries can be modified by running the shot again, by specifying a variable when calling the routine. However, the program does not allow the modification of a single quantity inside a shot, the program can be launched again for a specific shot, but it will require to run through the whole program once more, even though for a single iteration; an alternative solution would be to use MDB, a code employed at TCV that allows to build databases in a more flexible way, but this was beyond the scope of this thesis. Moreover, the database is not complete; some quantities must be calculated, while some cannot be computed (in particular, quantities like the ICRH power, since there is no such machine at TCV).
This thesis work aimed to lay the groundwork for building a database at TCV, in the hope that, in a future, may be used at ITER along the databases of several other tokamaks.

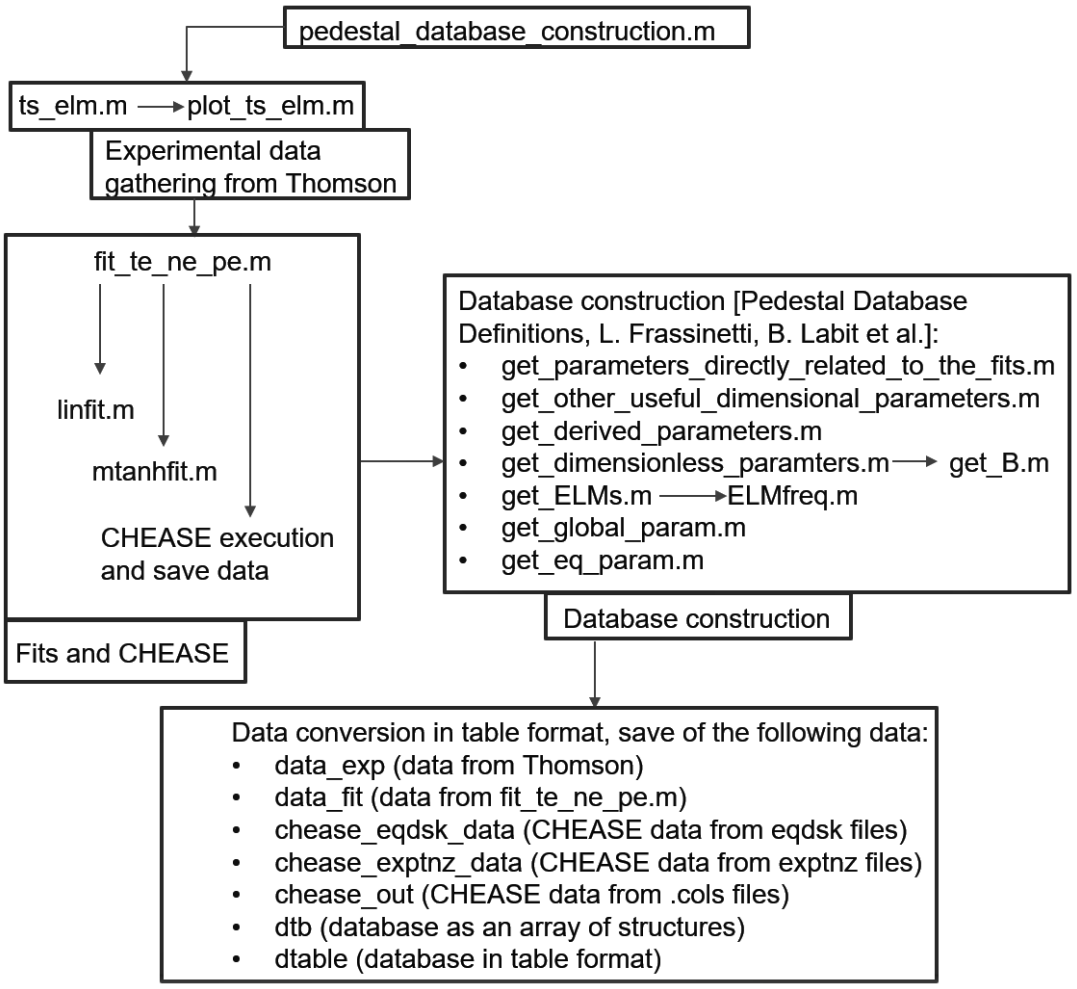


Figure 3.11: Database construction program overview

# Chapter 4

# ELMy H-Mode pedestal database results

After the construction of the database, the next step had been to try and recognize behaviors and profiles for TCV that can be common to other tokamaks as well; in particular, in this section some evaluations of said behaviors by taking a test database are carried out; this testing database has been derived from 6 mission tables, as said in chapter 3.2, which made for a total of $\sim 280$ shots to be examined. After that, the program made the selection of the fits according to the $R^2$ goodness of fit parameter, with a threshold value of $R^2 \geq 0.91$; this reduced the shots from $\sim 280$ to 140.
Moreover, additional considerations have been made, which reduced the database variables even more. In particular, the selected time interval must have been chosen no shorter than $\Delta t \geq 0.15s$; this has been made in order to have a time interval big enough with respect to the energy confinement time $\tau_e$; in particular, none of the shot has a time interval bigger than $5\tau_e$ with the above choice of $\Delta t$ ; in addition to that, some shots had to be discarded for various reasons, such as errors in the data acquisition process (e.g. in a set of shots the ELM energy loss $W_{ELM}$ was not measured), or because of errors inside the program (e.g. the ELM average duration $\tau_{ELM}$ was not computed due to an error in the calculation of the fwhm); after imposing all the conditions above, the database contained 95 entries.
These entries have been used in the following section for making qualitative considerations about the behavior of the plasma under certain conditions, as well as for trying to derive scaling laws that have been found as correct in other tokamaks.

## 4.1 Display of database entry values

Each plasma shot in a tokamak is subjected to a wide range of parameters which, directly or indirectly, are chosen by the operator; fueling and seeding rate, power input, plasma current, magnetic field, etc. are all operative quantities that are employed in a shot, conditioning the plasma behavior and the ELM generation. This section aims at making a collection of a part of the quantities taken for each shot in the database, in order to make quick comparisons between them. All the quantities presented have been put into a

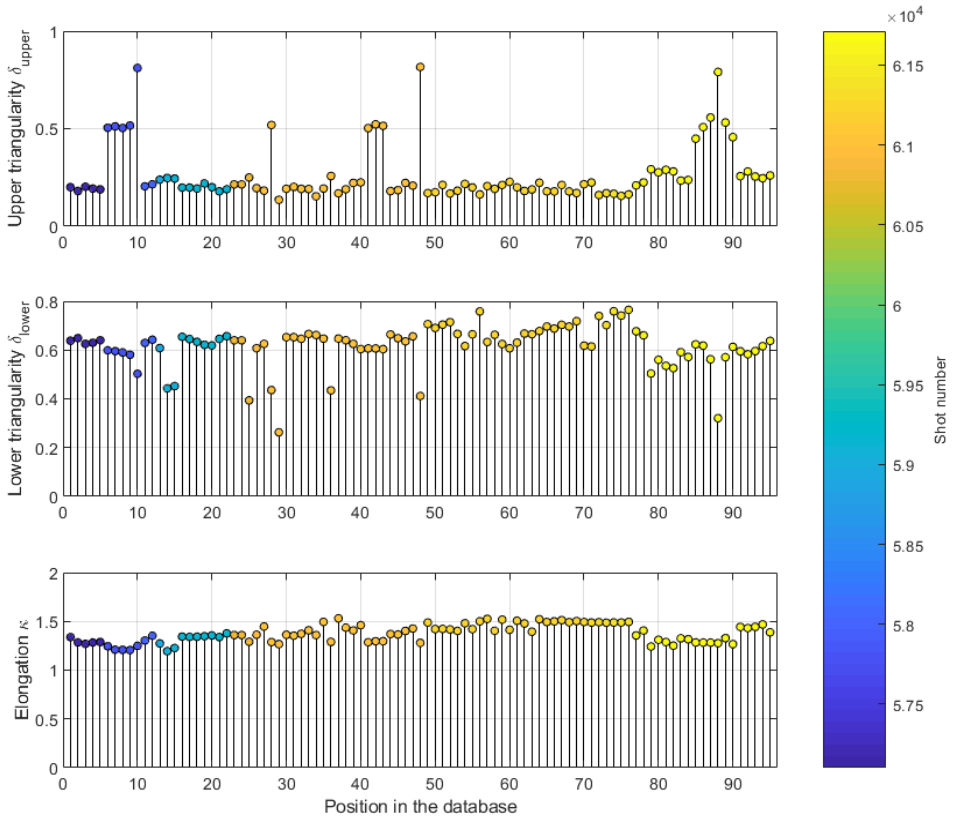


Figure 4.1: Examples of parameters related to the geometry of the poloidal cross section of the plasma for each shot in the database.

graphic where the x axis is their position in the database, and their color is the respective shot.

In fig. 4.1 the elongation and the plasma upper and lower triangularity are displayed; it can be seen that the elongation stays approximately constant for all the considered shots, ranging from about 1.2 up to 1.5, while the majority of the values for the upper triangularity $\delta_{upper}$ is around 0.2, with some shots at higher values (around 0.5 and even some around 0.8); the values of the lower triangularity $\delta_{lower}$ are between 0.5 and 0.8 for the majority of the shots, while few of them have a lower value (around 0.4 or even 0.3). In this thesis, the configuration of all the shots was the Single Null one with an upper triangularity larger than 0; in the majority of the shots the upper triangularity is less than the lower one, while for several shots (23 of them) the opposite happens.

Other important parameters include the input power injected in the system; in particular, the ohmic, NBI and ECRH power have been considered in fig. 4.2, as well as the radiative power coming from the plasma. The first consideration is that the radiative power has a set of values missing and, since they are all in the same area, these shots were plasma discharges close to each other; this means that, for a period of time, the diagnostic in charge of measuring the radiative power of the plasma was not functioning. Moreover, it can be seen that the ECRH was off for the majority of the shots, while the NBI has been employed for the vast majority of the shots. As far as the ohmic power is concerned, the

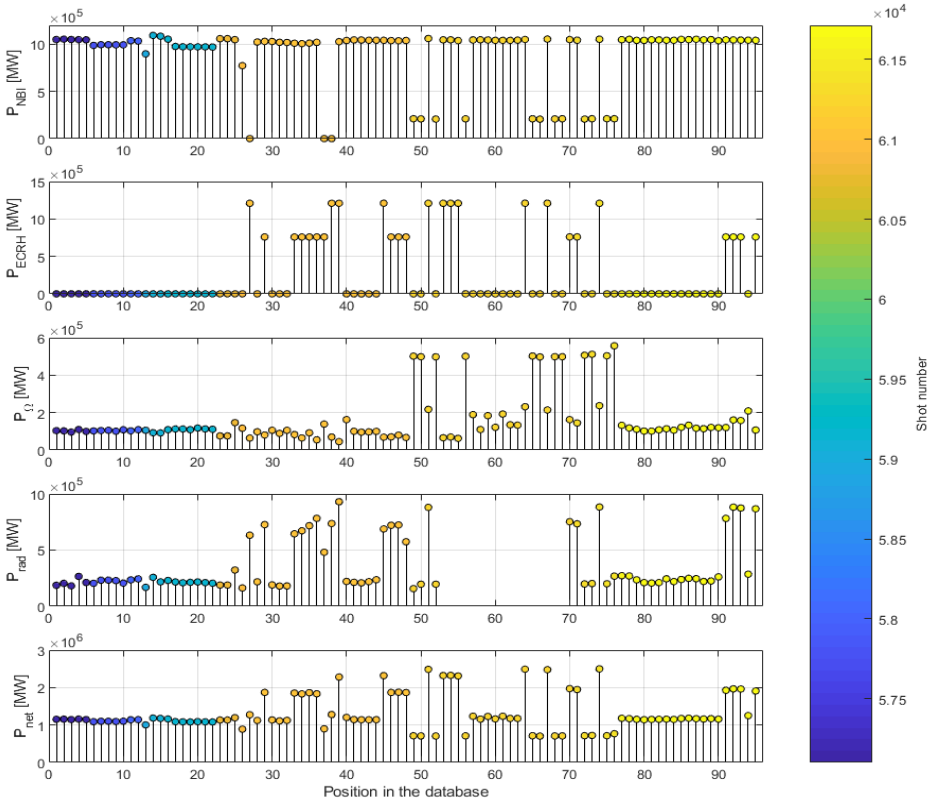


Figure 4.2: Ohmic, NBI, ECRH radiative and net power for all the plasma shots

majority of the plasma shots have a $P_\Omega$ of about 100kW, but a few of them manage reach power levels of about 500kW.
Another pair of quantities directly set by the operator are the quantities of fuel and impurities deliberately injected in the system while a shot is taking place; this is done because there seems to be a correlation between pedestal height and width with respect to the variation of these quantities [8] in the plasma. The values stored in the database are the gas fluxes in $[molecules/s]$, which can be converted in $[mbar \times L/s]$ by:

$$\left[\frac{mbarL}{s}\right] = \frac{RT_{amb}}{N_{av}}\left[\frac{molecules}{s}\right] \tag{4.1}$$

where R is the universal gas constant (=83.144 [L×mbar×K$^{-1}$×mol$^{-1}$]), $T_{amb}$ is the value at room temperature (around 300 [K]) and $N_{av}$ is the Avogadro number (=6.023×10$^{23}$ [mol$^{-1}$]). In fig. 4.3 the fueling and seeding gas flux rates are taken into consideration, the fuel being Deuterium ($D_2$). The impurity and seeding injection is realized by a series of piezoelectric valves connected with the tokamak vessel, which can release a set flux of particles by changing the applied voltage on them. The $D_2$ injection flux rate is of the order of $10^2$ bigger than seeding injection, and only in the few shots in which the valves were open. There is some degree of variability in the gas flux rate, in particular in the fueling one, and so, care must be taken when taking a particular value of both fueling

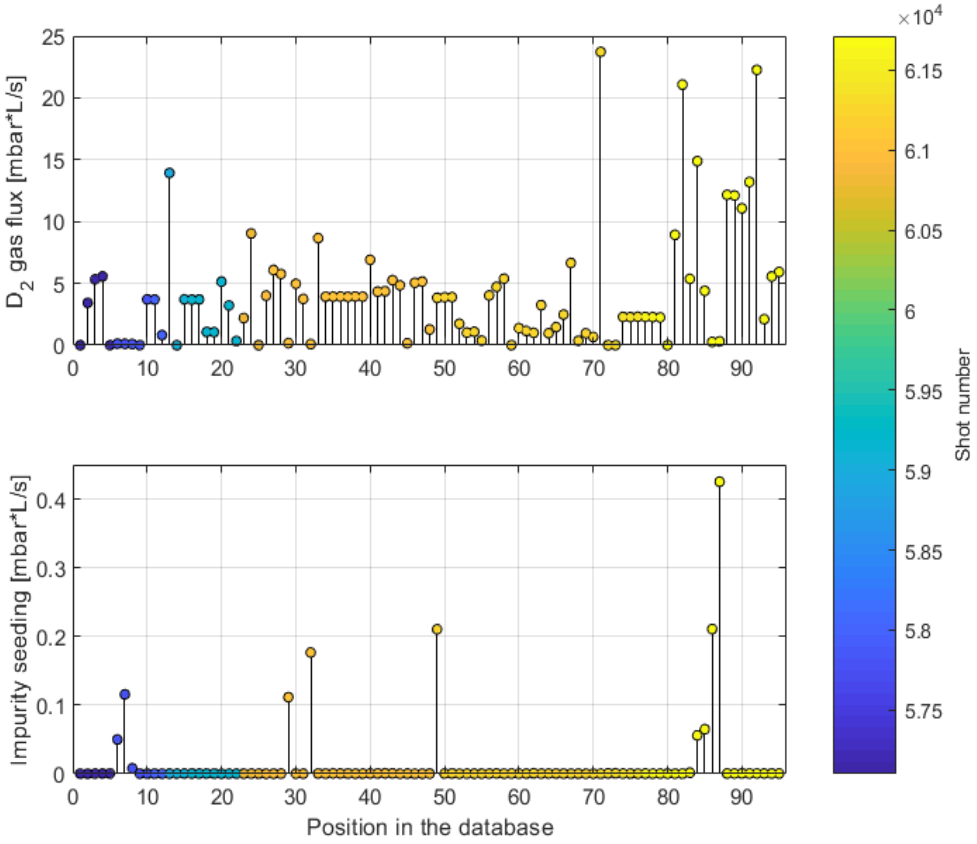


Figure 4.3: Fueling and impurity seeding in the database shots

and seeding rates.

The values of the magnetic field, as well as the plasma current, are other quantities that can be visualized (see fig. 4.4). The values of the toroidal component of the magnetic field are around 10 times bigger than the poloidal component, and they have a more constant behavior, due to the fact that plasma at equilibrium mainly changes the poloidal component; since the toroidal magnetic field is mainly unaffected, it can be considered a typical parameter of the tokamak, whose variation may imply a problem with the machine, or a deliberate decision from the operator. As expected from chapter 2.2, the plasma current influences the poloidal component of the magnetic field, since $B_{pol}$ mimics the values of $I_p$. Other values of the magnetic field at the HFS and LFS are seen in fig. 4.5. As expected, the total magnetic field has values almost identical to the toroidal magnetic field, since the values of the poloidal field are one order of magnitude less than the toroidal one.

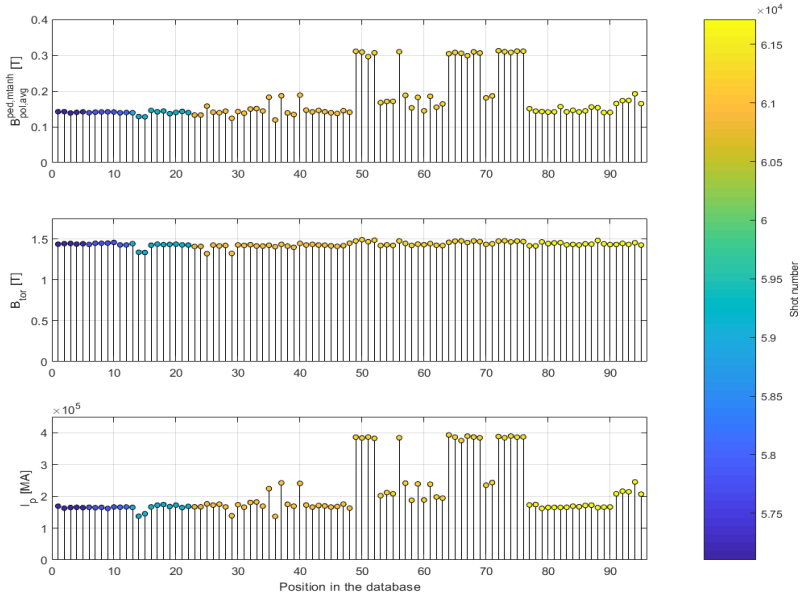


Figure 4.4: Average poloidal and toroidal magnetic field and plasma current values in the database.

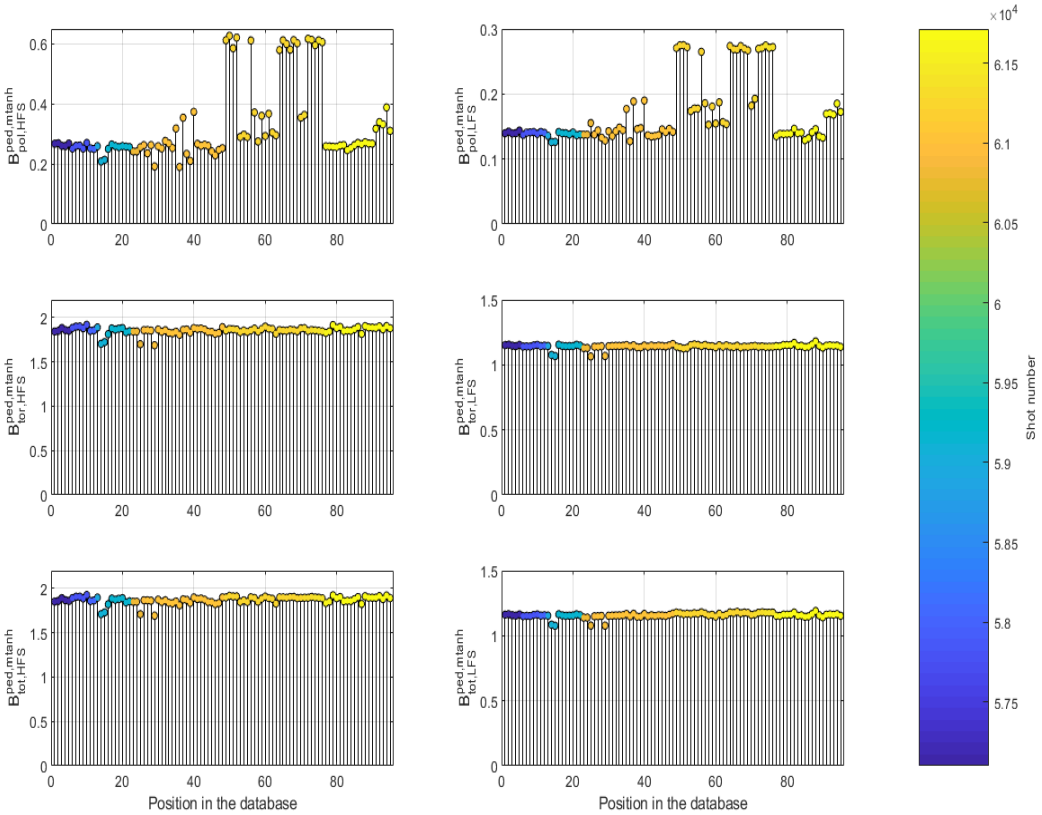


Figure 4.5: Poloidal, toroidal and total magnetic field values, calculated at the HFS and LFS positions of the tokamak vessel.

## 4.2 Input power consequences over the ELM generation in the plasma

As seen in chapter 2.4.1, the ELMs can be categorized in different types; in particular, *type-I* and *type-III* ELMs are the most recognizable, due to their higher peaks of the $D_\alpha$ signal, which corresponds to an higher emitted power per ELM; the type-I ELMs are especially dangerous for future tokamaks for this particular reason. Moreover, the two types of ELMs seem to have a distinct behavior, as far as the ELM frequency $f_{ELM}$ is concerned, when the power increases. Even though the value usually used is the power at the separatrix defined in chapter 2.4.1 [10], since there were errors in the measurement of $P_{rad}$ and the difficulty in calculating the term $dW/dt$, a simpler version of $P_{sep}$, $P_{net}$ has been adopted, which consists in the sum of the NBI, ECRH and Ohmic power:

$$P_{net} = P_{NBI} + P_{ECRH} + P_\Omega \tag{4.2}$$

This was made because the term of power loss $-dW/dt$ is difficult to calculate, while the radiative power term $P_{rad}$ has not been recorded in several shots due to an error in the diagnostic, as explained in section 4.1. Moreover, these calculations may be slightly incorrect due to the use of the injected power, whereas the absorbed power would be more correct; however, the error can be tolerated if the representations can be considered as qualitative. With these premises, an analysis of which types of ELMs were contained inside the database had been carried out. In particular, as discussed in chapter 2.4.1:

- Type-I ELMs have their $f_{ELM}$ increasing by increasing $P_{net}$, and they appear at high power levels.
- Type-III ELMs have their $f_{ELM}$ decreasing by increasing $P_{net}$; they appear at lower power levels.

The plot of the ELM frequency with respect to the net power is seen in fig. 4.6(a). It can be seen that, at net power values higher than 800kW, the ELM frequency increases; since the majority of the shots have a net power of around 1MW, the database is mainly composed by type-I ELMs.
However, there is a minority of shots below 800kW, where the ELM frequency seem to decrease with respect to the net power increasing. Moreover, the average value of the poloidal magnetic confinement parameter decreases for these particular shots with respect to all the others, which leads to infer a loss of confinement for these ELMs. All these features suggest (as seen in chapter 2.4.1, [10]) that these shots (11 in total) are type-III ELMs.
In figure 4.6(a) the normalized collisionality, in particular its negative logarithm, has been displayed for the plasma shots as well; it can be seen that $-log_{10}\nu^*$ increases for increasing net power for type-I ELMs, which is coherent with the definition of $\nu^*$, since an higher power will give an higher plasma temperature, and it will mean lower collisions of Coulomb nature (since the frequency of said collisions decrease with increasing particle velocity, and thus temperature).
For type-III ELMs, $-log_{10}\nu^*$ has higher values, even though them being at low power,

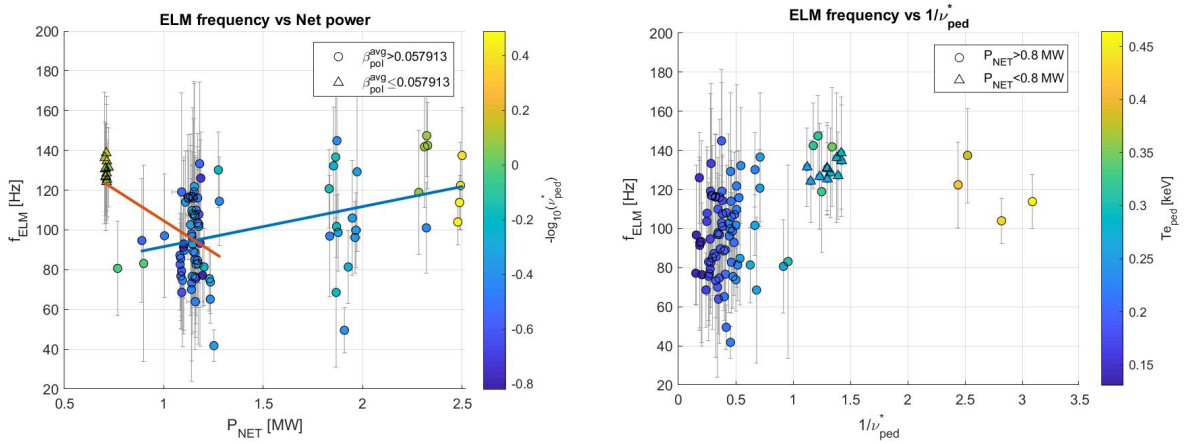


(a) (b)

Figure 4.6: ELM frequency as a function of the net power (a) and of the inverse of the logarithmic normalized collisionality (b); the legends in the left and right figure are respectively the collisionality and the pedestal temperature.

which means a lower value of $\nu^*$ (fig. 4.6(b)); this would imply that plasmas with type-III ELMs have an higher temperature at lower power.
The ELM frequency behavior with respect to the inverse of the normalized collisionality is pictured in fig. 4.6(b). It is important to note that, in fig. 4.6(a), the points are clustered in several groups. This because of the usage of the NBI and the ECRH, which have been used singularly or in combination, around certain values of power; the majority of the shots are being subjected to a power of around 1.2MW.

After a basic analysis of the ELM frequency behavior as a function of the net power and pedestal collisionality (the value derived by the mtanh fit), thus distinguishing them by types, the ELM energy has been considered. In particular, the ELM energy loss $W_{ELM}$ has been normalized with respect to the plasma energy $W_{MHD}$ obtained by the diamagnetic loop (DML) [6]; in this way, a rough estimate of the energy lost per ELM can be derived. The behavior of the energy lost per ELM, normalized to the plasma energy $W_{MHD}$, is shown in fig. 4.7; the ELM energy loss has been compared with an older set of experiments, where the ECRH was not installed [6]; in the older figure, the ■ symbol has been used to indicate Single-Null (SN) geometry with upper triangularity $\delta_{upper} > 0$, the geometry concerning the majority of experiments in this thesis, and as such they will be compared. The others are respectively the SN geometry with $\delta_{upper} < 0$ (◀), Snowflake plus (SF+, ▼) and Snowflake-like Single Null (SF-like SN, •); these other configurations are beyond the scope of this thesis, and they are investigated in further details in [6].
The main characteristics for type-I ELMs are that the ELMs are confined in a region between 25÷100 Hz in the older experiments, while in the newer ones (with NBI installed) they do appear to cover a larger area, between $25 \div 200$ Hz. Moreover, in the older dataset, their normalized energy loss is $5\% \div 20\%$, while in the newer database is lower, going around $2.5\% \div 15\%$; this would imply that an higher input power can improve the confinement of the plasma. Finally, a common characteristic in both datasets is that the pedestal collisionality behavior is the same, by increasing at higher ELM frequency and energy loss. However, the values of the two are different, since the older database

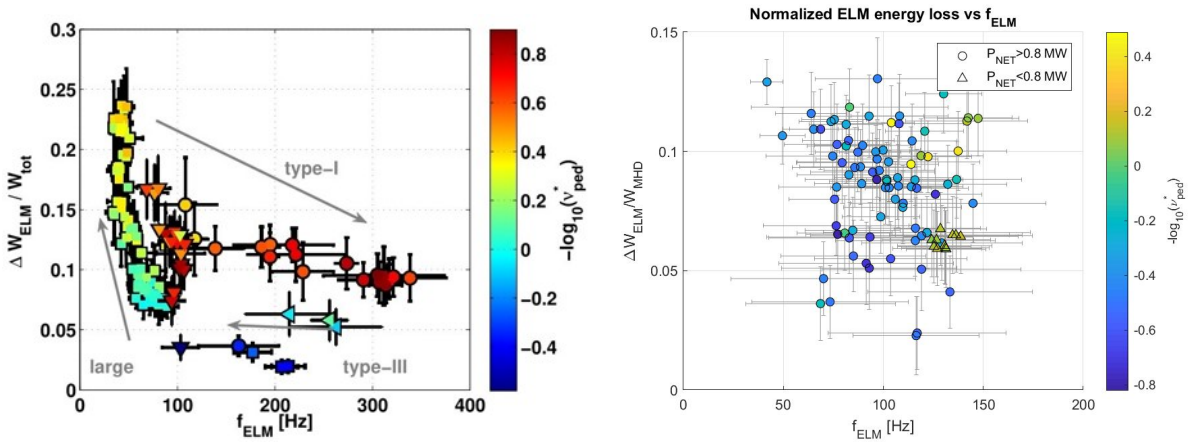


(a) (b)

Figure 4.7: Energy loss per ELM, normalized to the MHD plasma energy, with respect to the ELM frequency, before [6] (a) and after the installation of the NBI (b).

uses a definition of $\nu^* = 10^{-14} Z_{eff} R_0 n_{e,ped} T_{e,ped}^{-2}$, while in the newer one, the definition in chapter 3.5.2 is employed.
In the case of the minority of type-III ELMs in the database, they seem to belong to a narrow region between $125 \div 150$ Hz in the new dataset, with an ELM energy loss between $5\% \div 7.5\%$; the pedestal collisionality is lower than the type-I ELMs counterpart in the same region as well.
Another representation of the normalized energy loss with respect to the normalized pedestal plasma collisionality is shown in fig. 4.8.
The distinction in ELM energy loss between ELMs above 800kW and below it further implies a different type of ELMs involved, since the type-I ELMs have an higher energy loss per ELM, as expressed by the higher peaks in their $D_\alpha$ signal, while the peaks in the type-III ELMs related ones are significantly lower.

However, type-III ELMs have an higher frequency than type-I ELMs, as seen in fig. 4.7. This would mean that the fractional ELM power loss (defined by $\Delta W_{ELM} f_{ELM} / P_{net}$) should be higher than type-I ELMs, due to the higher ELM frequency. This is verified in fig. 4.9, where it can be seen that the power lost by type-I ELMs range from 2% to 20% of the total input power, while the type-III ELMs in the database range from 15% to 25% of it. The pedestal electron temperature (obtained from the mtanh fit) displayed as a legend in fig. 4.9 is coherent with the value of $\nu^*$, by increasing with diminishing collisionality (or increasing of $-log_{10}(\nu^*)$).

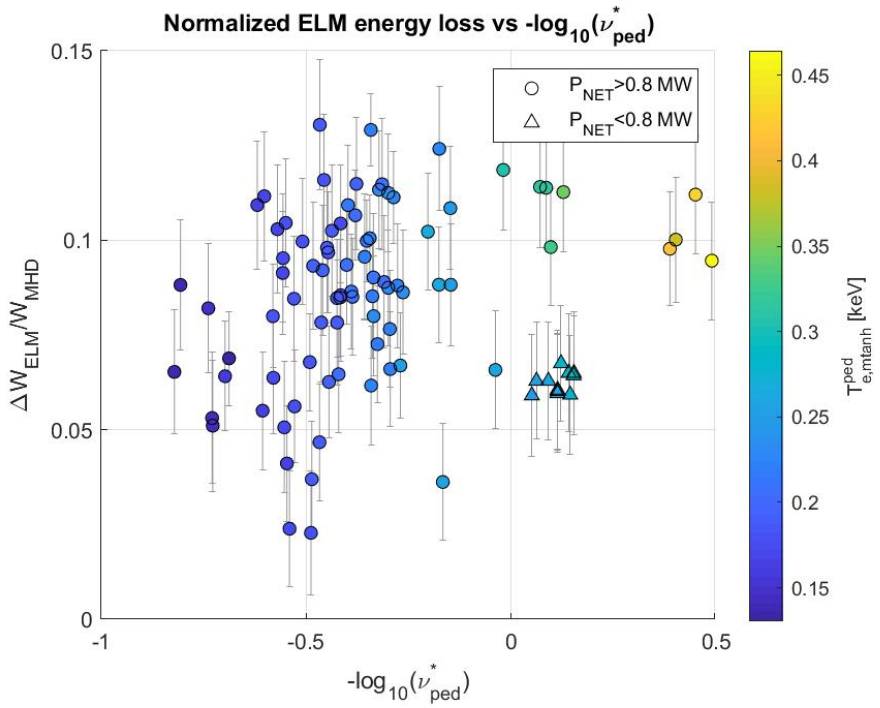


Figure 4.8: Normalized ELM energy loss with respect to the negative logarithm of the normalized pedestal plasma collisionality; the legend specifies the pedestal temperature for the different plasma shots

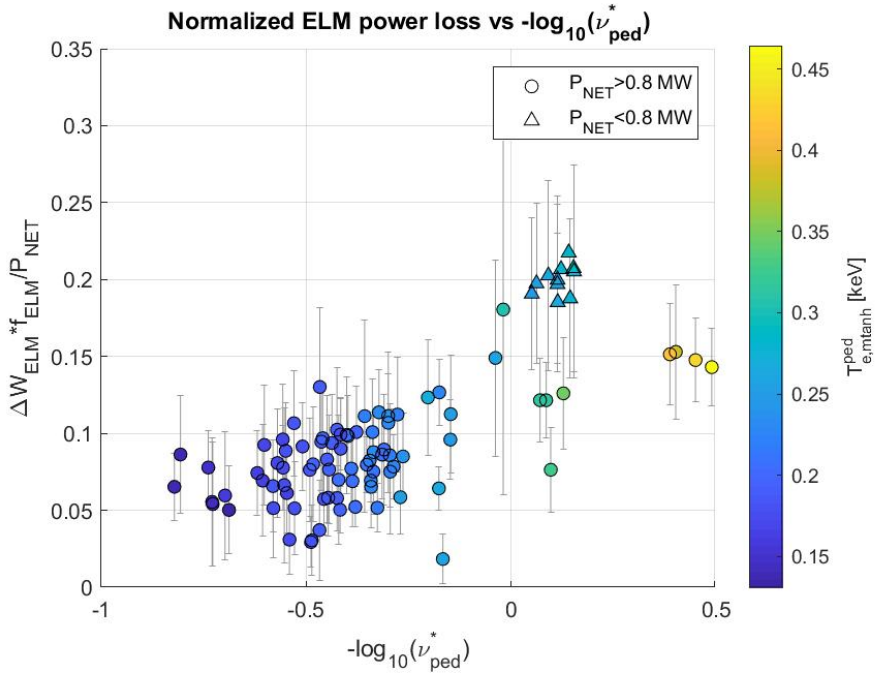


Figure 4.9: Fractional ELM power loss with respect to the logarithmic plasma collisionality at the pedestal

## 4.3 Electron pedestal temperature and density profiles behavior

The behavior of the temperature and density of the electron profile are discussed in this section. In particular, the aim would be to see whether or not the input power has some influence over these quantities, as well as the fueling and . In figure 4.10, it can be seen the representation of the electron and density values at the pedestal position; the isobars are plotted as well.
If the net input power increases, the absorbed energy from the plasma will be higher, and the plasma temperature will be higher as well; this is coherent with the figure, where the plasma pedestal temperature increases from less than 150eV at a power of about 1MW, up to less than 500eV at a power of about 2.4MW (due to the combined action of NBI and ECRH switched on together).
There are also a group of points that have a pedestal temperature of about 300eV, but with a lower power than the others around them, of about 800kW; these are the type-III ELMs discussed in the previous section.
As far as density is concerned, there seem to be no clear indication that a change in density occurs for higher values of the input power.

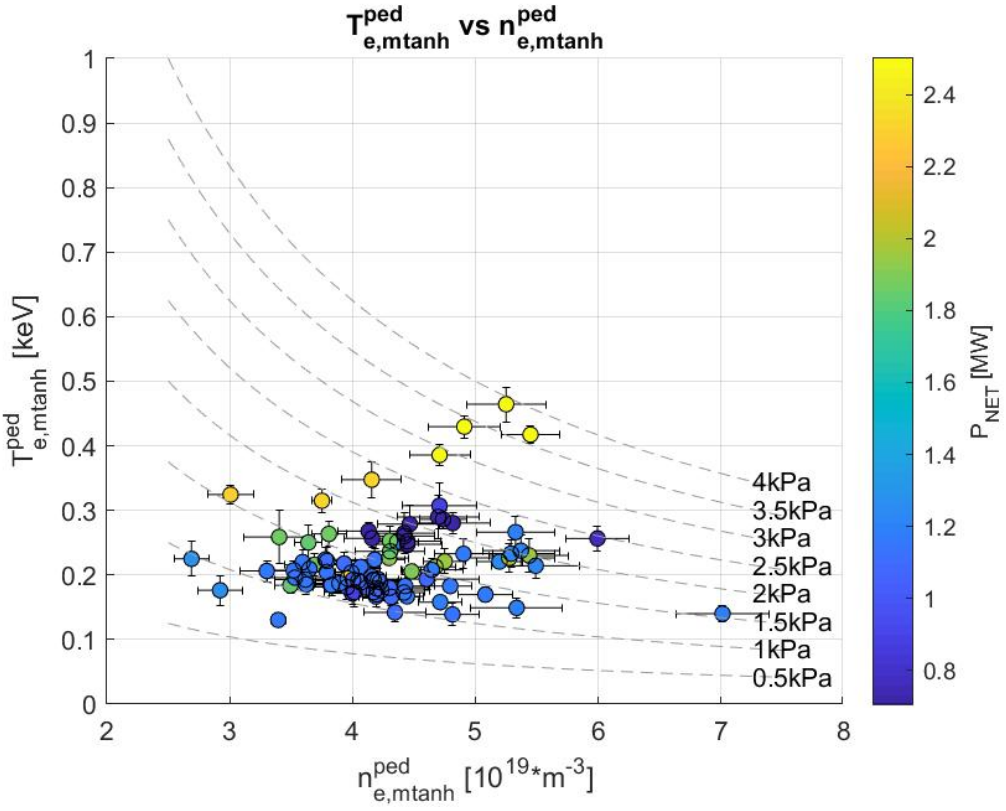


Figure 4.10: Electron pedestal temperature with respect to the pedestal density; both values are derived from the values of the database obtained with the mtanh fitting method; the legend shows the net power $P_{net}$ of each shot, and the isobars are shown as well.

### 4.3.1 Validity of using the mtanh fit values vs the linear fit ones

All the data in this section refer to the mtanh fit; however, there could have been discrepancies between the linear and mtanh fit. In order to see whether or not discrepancies between the two fits arise, a linear regression has been made. As linear regression approaches the line $y = x$, the values from the two fits have a better agreement in fitting the data. The most important of these are listed in table 4.1. All of them are very close to the origin, but some of them (namely the pedestal temperature $T_e$, the density pedestal width $w_{n,e}$, the pedestal position of the density profile $p_{n,e}$, and the max. value of the pedestal gradient of the density profile $grad_{n,e}^{max}$) are not too close, an indication that the fitting procedure can be further improved, or the selection criteria of the shots (such as the use of the $R^2$ goodness-of-fit parameter) could be more strict.

| **Quantities** | **Linear regression** |
|---|---|
| Temperature at the pedestal [keV] | y=11.1545+0.8279x [keV] |
| Density at the pedestal [$m^{-3}$] | y=-0.0320+0.9999x [$m^{-3}$] |
| Pedestal width of $T_e$ [adim.] | y=0.0001+0.9758x [adim.] |
| Pedestal width of $n_e$ [adim.] | y=-0.0043+0.8754x [adim.] |
| Pedestal position of $T_e$ [adim.] | y=0.0803+0.9196x [adim.] |
| Pedestal position of $n_e$ [adim.] | y=0.2036+0.7895x [adim.] |
| Core slope of the temperature $T_e$ [keV/adim.] | y=92.9653+1.0661x [keV/adim.] |
| Core slope of the density $n_e$ [$m^{-3}$/adim.] | y=0.2592+0.9656x [$m^{-3}$/adim.] |
| Maximum value of the gradient at the $T_e$ pedestal [keV/adim.] | y=84.3264+0.9905x [keV/adim.] |
| Maximum value of the gradient at the $n_e$ pedestal [$m^{-3}$/adim.] | y=-15.4781+1.5631x [$m^{-3}$/adim.] |

Table 4.1: Linear regression results between parameters belonging to the linear (x) and the mtanh (y) fit.

### 4.3.2 Pedestal temperature profile behaviors

In this section some behaviors from the temperature profile, obtained from the database data, are qualitatively discussed. Due to the presence of some other abnormal data (too high pedestal gradient values or too low pedestal width with respect to the value of pedestal temperature at which they were), these shots (3 of them) have been discarded.

- The first qualitative analysis has been performed on the behavior of the pedestal width of the electron temperature with respect to the value of the temperature at the pedestal position (fig. 4.11). As far as the collisionality $\nu^*$ is concerned, the pedestal temperature increases for decreasing collisionality, in agreement with what said in the previous sections. At lower values of $T_{e,ped}$ (below 350eV), the pedestal width $w_{T_e,ped}$ assumes a wide range of values, but there seem to be a trend of increase of the pedestal width by increasing the pedestal temperature. At higher values of $T_{e,ped}$, above 300 eV, the trend seem the opposite than before, with $w_{T_e,ped}$ decreasing as $T_{e,ped}$ increases; however, the small number of data prevent to make more accurate assumptions.
  The range of the pedestal width can be influenced by the fueling and impurity seeding injections inside the shots as well [8], as reported in fig. 4.11.

- The maximum value of the pedestal gradient as a function of the pedestal temperature has been investigated next (see fig. 4.12). The qualitative behavior is that $\nabla T_{e,max.}$ increases by increasing $T_{e,ped}$.

- In the case of the normalized maximum value of the pedestal temperature gradient, (fig. 4.13), the behavior seem to increase as a function of the pedestal temperature, like in the previous figure.

The fueling and seeding scan conditions for each shot are represented in figures 4.11(b), 4.12(b) and 4.13(b); the purpose of these figures is not to derive any kind of behavior, which would not be correct due to the high number of variables involved for each shot, but as a general comparison of the different fueling and seeding conditions for all the data in the database.

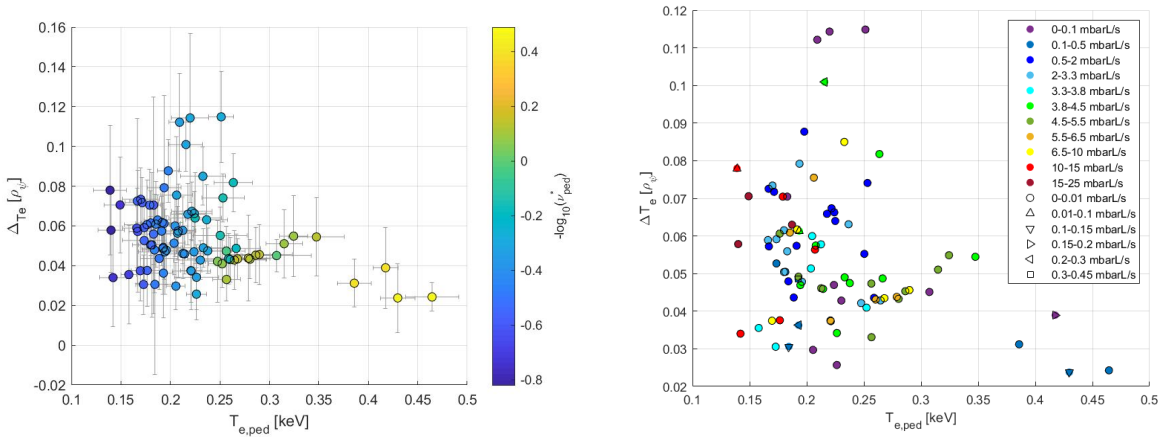


(a) (b)

Figure 4.11: Pedestal width with respect to the pedestal temperature value, with the collisionality (a) and the fueling and seeding gas fluxes displayed (b); the fueling rate value is displayed by the color of the data point, while the seeding rate value is displayed by its shape (see legend).

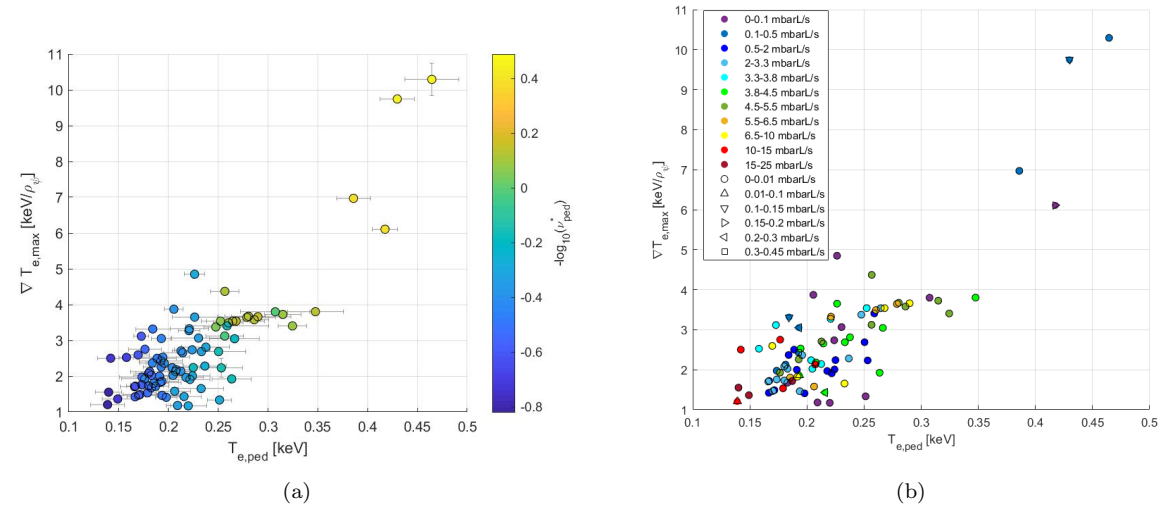


(a) (b)

Figure 4.12: Maximum value of the pedestal gradient compared with the pedestal temperature. The legend definitions are the same as in figure 4.11

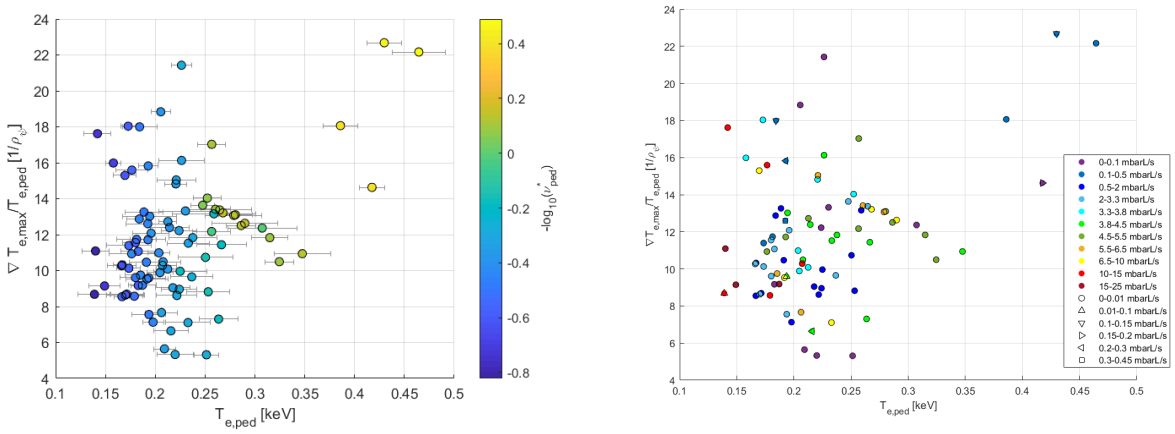


(a) (b)

Figure 4.13: Maximum value of the normalized pedestal gradient (with respect to the pedestal temperature) compared with the pedestal temperature. The legend definitions are the same as in figure 4.11

### 4.3.3 Pedestal density

Like in the previous section, the relevant quantities related to the pedestal density profile have been investigated. The same shots discarded in the previous section have been discarded here as well, in order to keep coherence with the data.

- The pedestal width of the density profile seem to slightly increase with the pedestal density; however, the data are very sparse over a wide range of values, so the trend is not clearly defined (fig. 4.14).
- The pedestal maximum gradient of the density profile increases with increasing pedestal density (fig. 4.15). There are several points that do appear to have an high value of the pedestal gradient, as well as a low value of the pedestal width; this would mean these shots have a narrower pedestal region than the others.
- As far as the pedestal gradient normalized per pedestal density, it seems to have no clear behavior as well (fig. 4.16).
- The pedestal collisionality seem to have no influence over the density values, since there is no clear dependence for any of the quantities listed.

Like in the previous section, figures 4.14(b), 4.15(b) and 4.16(b) are showed as a general comparison of the different fueling and seeding conditions for all the database shots.

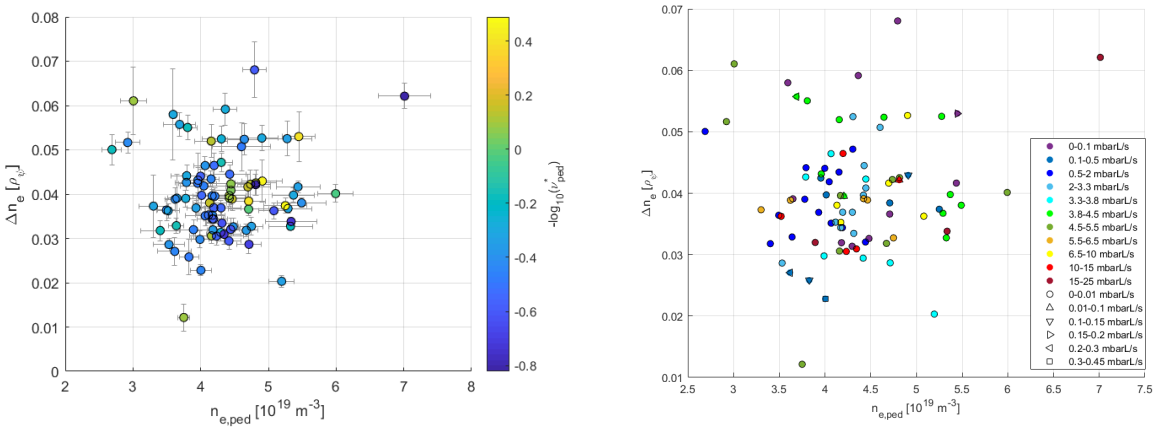


(a) (b)

Figure 4.14: Pedestal width with respect to the pedestal density value, with the collisionality (a) and the fueling and seeding gas fluxes displayed (b); the fueling rate value is displayed by the color of the data point, while the seeding rate value is displayed by its shape.

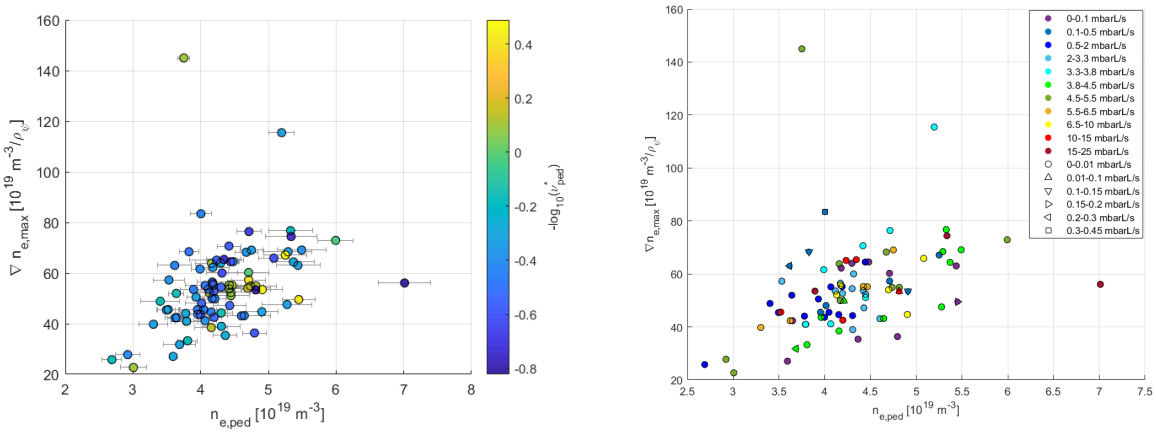


(a) (b)

Figure 4.15: Maximum value of the pedestal gradient compared with the pedestal density. The legend definitions are the same as in figure 4.14

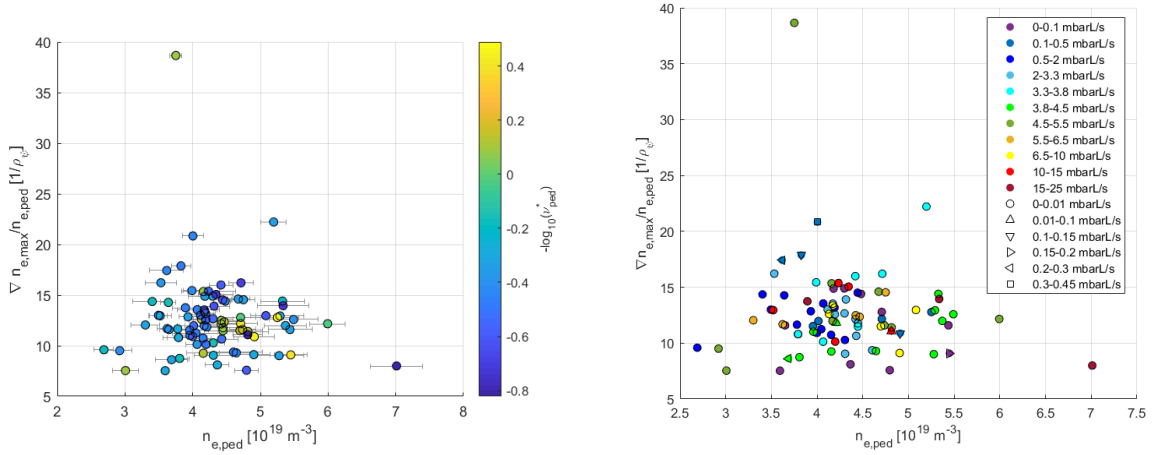


(a) (b)

Figure 4.16: Maximum value of the normalized pedestal gradient (with respect to the pedestal density) compared with the pedestal density. The legend definitions are the same as in figure 4.14

## 4.4 Analysis of scaling laws

As already said across this thesis work, the construction of a database with parameters belonging to multiple tokamaks is the first step towards managing to derive profiles from them, which can be used for extrapolating the values of the considered parameters for machines that are yet to be constructed; in particular, this is the approach being taken for analyzing the possible future ELM behavior in the H-mode plasma that will be generated in ITER.

These laws are purely empirical, and are found by inferring a model for the data, and then looking at the dependencies of the considered quantities; these laws are called *scaling laws*.

In this chapter, a couple of models for the TCV ELM behavior have been tested. It must be noted that, since type-I ELMs are the most dangerous ones that can be generated in a tokamak, the analysis has been carried out on this ELM type only.

### 4.4.1 ELM average duration scaling law

It has been implied in [7] that the average duration of an ELM depends on the values of temperature (in eV) and density (in $10^{19}m^{-3}$) at the pedestal, as well as the ELM energy loss $\Delta w_{ELM}$ in percent, thus following the scaling law:

$$\tau_{ELM,reg} = \tau_0 \times T_{e,ped}^{C_T} \times n_{e,ped}^{C_n} \times \left(\frac{\Delta W_{ELM}}{W_{MHD}}\right)^{C_{\Delta W}} \tag{4.3}$$

where $\tau_0$, $C_T$, $C_n$ and $C_{\Delta W}$ are the scaling law coefficients. According to [7], the data at JET-ILW + JET-C show that the parameters, obtained with a non-linear regression, are respectively $\tau_0 = 43.06$, $C_T = -0.69$ and $C_n = 0.61$, with an $R^2$ goodness of fit value of 0.67; the value of $C_{\Delta W}$ was 0.04, so the term has been neglected.

In fig. 4.17(a) the model has been applied to the TCV data. The parameters that have been obtained give the scaling law:

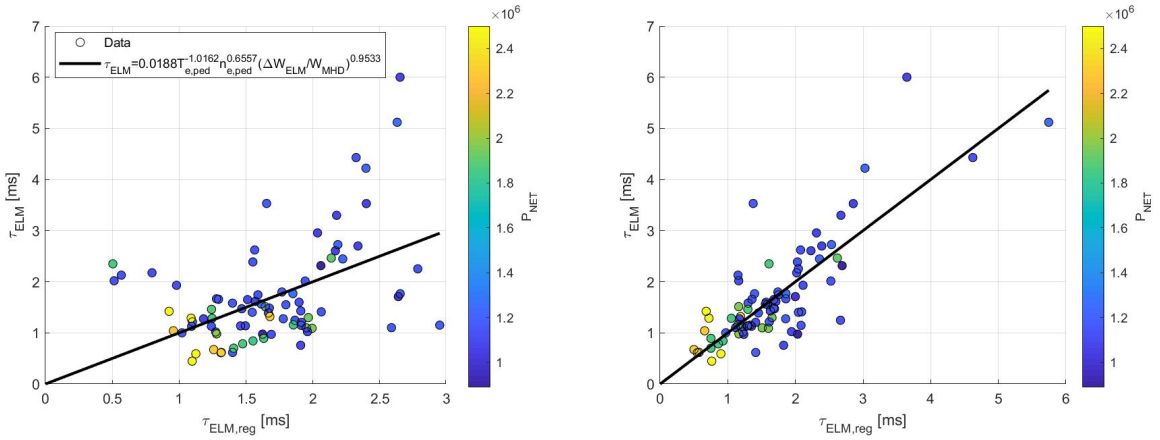


(a) (b)

Figure 4.17: (a) Scaling law for the average ELM duration as proposed in [7]. (b) Alternative model for the ELM average duration.

$$\tau_{ELM,reg} = 0.0188 \times T_{e,ped}^{-1.0162} \times n_{e,ped}^{0.6557} \times \left(\frac{\Delta W_{ELM}}{W_{MHD}}\right)^{0.9533} \tag{4.4}$$

with a value of $R^2$=0.1842, thus significantly lower than the one found in [7]. Moreover, the dependency of the fractional energy loss per ELM ($\Delta W/W$) is not negligible anymore. As a consequence, the proposed model may not be accurate. An alternative model has been devised, which depends on the ELM frequency, the global normalized confinement parameter $\beta_{N,global}$ and the total pedestal temperature, given by the electron and ion temperature, assuming that $T_{i,ped} = 0.7T_{e,ped}$; the results are:

$$\tau_{ELM,reg} = 27.4783 \times (T_{e,ped} + 0.7T_{e,ped})^{-0.5121} \times \beta_{N,global,MHD}^{-1.6646} \times f_{ELM}^{-1.3356} \tag{4.5}$$

with an $R^2$ goodness of fit value of 0.6651, significantly better than before. The behavior of equation 4.5 is shown in figure 4.17(b).

### 4.4.2 EPED1 model: pedestal width

As discussed in chapter 2.4.2, the EPED1 model predicts a scaling law for the pedestal width that depends on the poloidal magnetic confinement parameter $\beta_\theta$ as:

$$w_{ped} = D\sqrt{\beta_\theta^{Ped}} \tag{4.6}$$

where the coefficient D is a number that can differ for different tokamaks, being $D = 0.076$ for DIII-D, $D = 0.11$ for ASDEX-Upgrade, while for Alcator CMOD a slightly different scaling law, $w_{ped} = 0.084(\beta_\theta^{Ped})^{0.43}$, has been found [8]. From the comparison of the data gathered from the database and these scaling laws (fig. 4.18), it can be seen that the data do not follow the EPED1 scaling law.

The grey points in fig. 4.18(a) have very high values of $\alpha_{exp}$, too high to be possible (between $5 \div 15$; this has been attributed to an error in the fits, since in the temperature

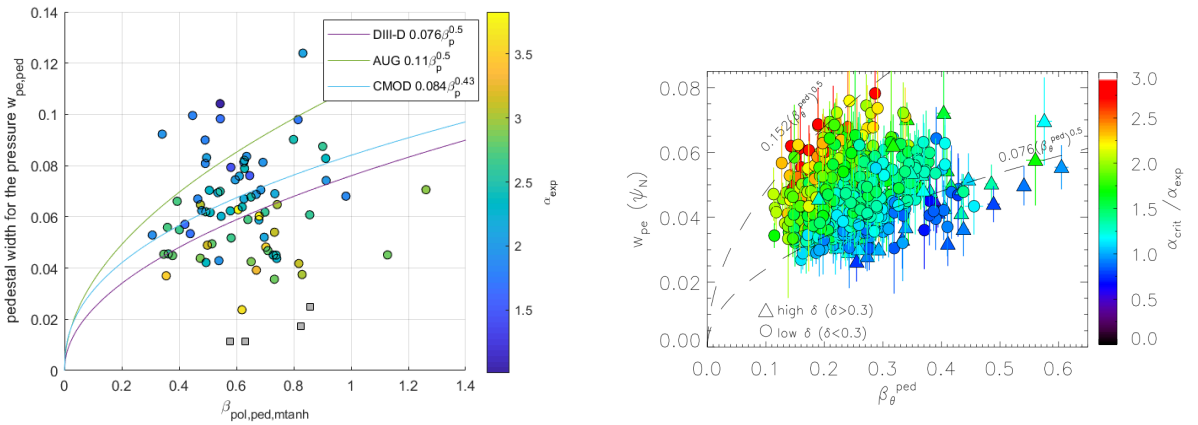


(a) (b)

Figure 4.18: Database pressure pedestal width with respect to $\beta_{pol,ped,mtanh}$, for TCV (a) and JET-ILW (b) [4]; the value $\alpha_{crit}$ in (b) is the critical value of the normalized pressure gradient for a stable plasma in the Peeling-Ballooning (PB) limit, calculated by means of stability calculations by using the ELITE code [1], [4], whose purpose and functioning are beyond the scope of this thesis.

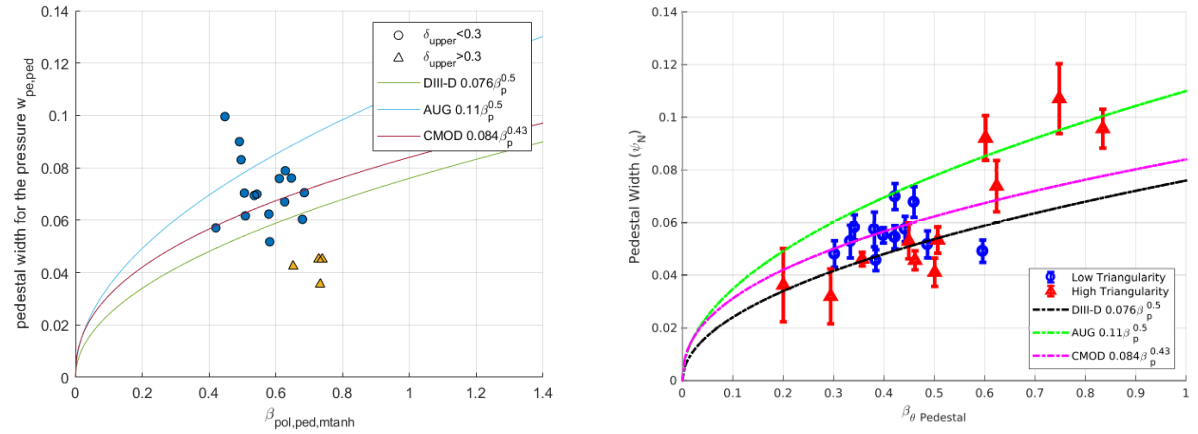


(a) (b)

Figure 4.19: Testing of the EPED1 scaling laws for (a) the test database and (b) the database used in [8]; both the datasets have been taken from the same tables on the CRPP wiki, with the same conditions.

and density profiles gathered from Thomson for these particular shots, the data points do not cover the pedestal. This anomaly is strengthened by the fact that the temperature and density gradient inside the database have values several times higher than the rest of the database. This is an issue not envisioned during the development of the database, and it must be corrected. It can be seen that the behavior of the normalized pressure gradient $\alpha_{exp}$ for the database is in agreement with the JET-ILW one (4.18(b)), which increases for increasing magnetic confinement and for decreasing pressure pedestal width.
Moreover, it has been done a comparison between the data from TCV and the ones gathered in [8]; the data have been taken in the same range of the ones in [8], which have been taken from the same data table the test database has been taken from, some of them effectively being the same; for the shots at low triangularity, the data agree with each other; however, the data at high triangularity in fig. 4.19(a) are too few in number to make a comparison.

## 4.5 Conclusion

In this chapter, the possibility of analyzing the data coming from the database has been explored.
A plasma shot can be very different from another one because of the wide range of parameters involved, ranging from parameters of geometrical nature (such as the triangularity and the elongation), power input from different machines (such as the NBI and ECRH), from the magnetic configuration (plasma current and magnetic field) and because of injection of fuel and impurities inside the plasma itself. As such, the database main function is to list all these parameters, in order to discriminate the shots according to all the conditions were put under, and possibly group them together according to the similarity of their conditions.
The data examined suggests that there are different types of ELMs inside the database, in particular type-I and type-III ELM; the different types of ELMs have several different characteristics, as introduced in chapter 2.4.1; in particular, the values of input power at which they manifest is different, the latter having a lower power than the former ones; the power level used to determine this distinction was 800kW; in addition to that, type-III ELMs have a lower value of the confinement parameter,and the values of collisionality are about the same in much lower input power conditions.
Moreover, the pedestal is an important region to be studied, since it's evolution is connected to the ELM generation itself [8]. As a consequence, the analysis of the pedestal behavior is very important. A preliminary analysis has been done, in which it can be seen that the data seem to have characteristic behaviors in some cases, while in other cases they seem not; with the expansion of the database and the collection of more data, characteristic behaviors may arise.
Finally, the derivation of scaling laws is essential in order to extrapolate, for the considered quantities, values at which there are no data, in order to predict how a machine that may no be operative yet (ITER) would perform, and which kind of plasma scenario (ELM generation, plasma configuration) has to be expected. The derivation of the average ELM duration scaling law depending on the ELM pedestal temperature, density and normalized ELM energy loss has not been successful, but a different derivation, depending on the ELM frequency, pedestal temperature and confinement parameter seem more reliable.

# Chapter 5

# Conclusion

This thesis work primary objective was to obtain a working database for TCV which had to be able to collect the desired data in order to have quick access to them, with the objective that they can be used to have a better understanding of the relaxation mechanisms, called ELMs, that happen inside a plasma when under H-mode confinement regime. In particular, a rich bibliography suggests that the region at the edge of the plasma, the pedestal, influences the ELM generation according to its evolution in time; as such, it is important to describe and analyze the pedestal characteristic quantities and the conditions in which the plasma is generated.

**ELMy H-Mode plasma**

The plasma confinement regime used in this database is the H-Mode, which differs from the ohmic regime and the L-Mode because the surpassing of a threshold value for the input power, which determines drastic changes in the plasma itself; in particular, the generation of an edge transport barrier, which allows the density, temperature and pressure values inside the plasma to increase; the profile becomes steeper towards the plasma edge, thus originating the pedestal. However, in the H-Mode confinement regime the plasma is subjected to a periodic relaxation caused by MHD instabilities; these relaxations are the Edge Localized Modes (ELMs), and their main consequence is the ejection of matter from the plasma towards the tokamak vessel, thus originating pulsed heating loads on key components which face the plasma, like the divertor. As such, the database is constructed in order to understand the ELMs and to predict their behavior in machines that are yet to e operational, such as ITER.
The database of this thesis comprehends data gathered at TCV, containing type-I and type-III ELMs. The configuration for each of the collected shots is the Single Null (SN) configuration, with an upper triangularity bigger than 0.

### Data collection and fitting

The data have been collected by using diagnostic systems, such as the Thomson Scattering System, and the most important database at TCV, LIUQE. In particular, all the data concerning the pedestal profiles come from the Thomson Scattering System, a diagnostic that employs the Thomson Scattering phenomenon to gather data on the plasma temperature and density during the plasma experiment (or "shot"). The data have then been fitted by the program written during the course of this thesis, by using both a piecewise linear function and one which used a modified hyperbolic tangent one as fitting functions; this procedure has been done for the temperature, density and pressure pedestal profiles. These profiles have then been selected according to the $R^2$ goodness of fit parameter, and being discarded if a threshold value of this parameter was not reached; this allowed to have better data profiles in the database, eliminating all the ones that could have been incorrect fits of the desired profile.

### CHEASE

After having fitted the profiles, these have been used in order to solve the equilibrium problem; this meant the self-consistent problem, in particular the Grad-Shafranov equation, had to be solved in an iterative way, and the profiles found with the previous fitting procedure became the profiles used as a guess in the first iteration. The iterative process has been done by another code, called CHEASE, which allowed the solution of the problem, and the calculation of equilibrium-related quantities, such as the magnetic field, the pressure profile and the plasma current.

### The database

After fitting the profiles and solving the self-consistent problem, the database has been constructed according to the desired quantities; the database has been thought as a process that never stops when encountering an error, since it is meant to be used to calculate a big number of shots all at once; in order to achieve that, a *try and catch* procedure has been used, by storing the error thanks to an appropriate Matlab function, but leaving the program free to pass onto the next shot should an error occur.
Several quantities have been stored: the parameters which have been directly derived from the fitting profiles, such as the pedestal height and width, as well as its maximum value of the gradient; derived parameters, like the magnetic confinement parameter and safety factor, as well as the plasma collisionality at the pedestal position; operational parameters, some of their quantities being the NBI, ECRH and ohmic power, as well as the fueling and impurity seeding gas flux rates; ELM related quantities, such as the ELM frequency, the energy loss per ELM and the average ELM duration; and finally equilibrium related parameters found by solving the self consistent problem.
All the data are then stored into a table format to quick access and visualization of the data, which is saved into the user's folder.

**Analysis of the data**

After the database construction, a basic analysis of the quantities obtained has been done. Some of the operational quantities of each database entry have been listed, in order to show that each ELM shot is subjected to a vast range of operational conditions, allowing different plasma scenarios and types of ELMs.
A qualitative analysis of relevant pedestal related quantities, such as pedestal density and temperature, width and gradient, have been carried out; however, the gathered data not always defined a clear trend, and thus the addition of new data may solve this issue.
The verification of proposed scaling laws has been investigated too, by looking at a scaling law for the ELM average duration, and trying to verify the EPED1 scaling law for the pedestal width, which allows considerations over the plasma stability and, ultimately, over the ELM generation mechanism [8].

**Considerations over the future of the ELM behavior**

This thesis work aimed at creating a first iteration for a database that will be used at TCV for collecting data, in order to use them to better understand the physics underlying the ELM instabilities that originate in the plasma when in H-Mode. This has been done with the goal to create an international database, spanning multiple tokamaks, which will be then used to study the ELM generation inside bigger machines, such as ITER and (at a later time) DEMO, the tokamak that should prove the feasibility of fusion for commercial purposes. A remark that must be said is that this database is far from being perfect; different errors still arise, and they are stored inside an array taking into account all the errors, or even by displaying on console the error itself; these can range from errors in calculating the ELM average duration to fits that failed to correctly represent the data, and thus they had to be removed. However, hopefully, this database has been able to give a small contribution on the research field of plasma instabilities and ELM generation, whose work is very important for the future of the plasma fusion for the production of electric power.

# Appendices

# Appendix A

# Introduction on Thomson Scattering

When the photons in a beam have frequency $w_i$, if the electric field they produce influences particles such as free electrons, these will start oscillating, thus emitting their own photons by dipole oscillation. If the energy the photon beam carries is smaller than the rest energy of the electron, then the phenomenon is called Thomson scattering. Energies below 1keV ($\sim 1\%$ of the electron rest energy) can mostly be described by non-relativistic physics [6], [3].
The scattered electrical field is determined from the Maxwell's equations, by considering the electric and magnetic field as composed by the scalar $\phi$ and vector $\vec{A}$ potentials, and by using the Lorentz gauge:

$$\vec{E} = -\nabla\phi - \frac{\partial \vec{A}}{\partial t} \qquad \vec{B} = \nabla \times \vec{A} \tag{A.1}$$

$$\textbf{Lorentz gauge:} \quad \nabla \cdot \vec{A} + \frac{1}{c^2}\frac{\partial \phi}{\partial t} = 0 \tag{A.2}$$

from the Liénard-Wiechert retarded potentials of a moving electron with velocity $\vec{v}_e$, we obtain the potentials $\vec{A}$ and $\phi$:

$$\phi = \frac{e}{4\pi\epsilon_0}\frac{1}{R(1-\vec{\beta}(t')\vec{e}_s(t'))} \qquad \vec{A} = \frac{e\mu_0}{4\pi}\frac{\vec{v}_e}{R(1-\vec{\beta}(t')\vec{e}_s(t'))} \tag{A.3}$$

Where $R = \|\vec{R}\| = \|\vec{x} - \vec{r}\|$ is the distance between the scattered electron and the observation point, and t$'$ is the retarded time; by introducing the far-field approximation ($R \gg r$) and the non-relativistic condition ($\vec{\beta} = \vec{v}_e/c \ll 1$), we then obtain the electric field of the scattered electron:

$$\vec{E}_s = \frac{r_e}{R}[\vec{e}_s \times \vec{e}_s \times \vec{E}_i] \tag{A.4}$$

where $r_e$ is the classical electron radius:

$$r_e = \frac{e^2}{4\pi\epsilon_0 m_0 c^2} = 2.82 \times 10^{-15} m \tag{A.5}$$

If the wave is linearly polarized, the power radiated by an electron in an infinitesimal solid angle $d\Omega$ is:

$$\frac{dP_s}{d\Omega} = R^2 c\epsilon_0 \|E_s\|^2 = r_e^2 sin^2(\alpha) c\epsilon_0 \|E_i^2\| \tag{A.6}$$

where $\alpha$ is the angle between the scattered direction $\vec{e}_s$ and the incident electric field $\vec{E}_i$. Thus, the differential cross section of scattering can be found as:

$$(\frac{d\sigma}{d\Omega})_s = r_e^2 sin^2(\phi) \tag{A.7}$$

If we integrate the expression over dΩ, we obtain the total Thomson scattering cross section:

$$\frac{8\pi}{3} r_e^2 = 6.65 \times 10^{-29} m^2 \tag{A.8}$$

In the case of many electrons, the superposition principle can be applied, adding the scattered electrical fields of the single electrons; this requires information for each electron, in particular regarding the amplitude of the field and its phase relatively to the observation point. In the case of a plasma, a charged particle will be surrounded by other charged particles of opposite sign; this leads to a screening effect of the considered particle by the other particles. However, since the system is a plasma, each and every charged particle inside it will be subjected to the same effect; the typical distance of this screening cloud is of a characteristic length, called the Debye length:

$$\lambda_D = \sqrt{\frac{\epsilon_0 e T_e}{n_e e^2}} \tag{A.9}$$

where $T_e$ is in eV. While ions are screened by electrons, the electrons will be screened by electron holes, since the ions are much slower.
A phase correlation parameter can be written, assuming that the difference in wavelength is very slight, $\|\vec{k}_s\| \simeq \|\vec{k}_i\|$:

$$\alpha = \frac{\lambda_i}{2\pi\lambda_D 2sin(\Theta/2)} \tag{A.10}$$

Where $\Theta = \pi - \phi$ is the angle between the scattered wave vector $\vec{k}_s$ and the axis of observation.
This scattering is incoherent, since the distribution of electron and the carriers of positive charge, which are not the too slow ions, but the holes, are randomly distributed. As such, this phenomenon, called Thomson incoherent scattering, has the total scattered power equal the sum of the individual electron scattered powers, which means that the superposition principle can be applied. Since $\alpha \ll 1$ in order to have motions of the charged particles of the order of the Debye length, by having at TCV a Thomson scattering system where the scattering angle $\Theta$ is between 60 and 120 degrees, a temperature of the order of tens of eV (pretty low) and density of $n_e \sim 10^{20} m^{-3}$, and by choosing a laser wavelength of $\lambda_i = 1064$ nm, we obtain that $1/14 \leq \alpha \leq 1/27$, which satisfies the condition above.
In order to calculate the total incoherent scattered power from many electrons, one needs to know their position and velocity for each time. In order to do so, the scattered electric

field for a single electron, given by equation $A.4$ can be Fourier transformed by using the far field approximation. As a result, the scattered field of this electron has a single frequency:

$$w_s = w_i + \vec{k} \cdot \vec{v} = w_i + (\vec{k_s} - \vec{k_i}) \cdot \vec{v} \tag{A.11}$$

which is the double Doppler-shifted frequency of the input wave; this arises from the electron motion with respect to the source of the incident wave and from the motion with respect to the observation point; this is the electric field gathered by the diagnostics, and by analyzing them, one can derive the average temperature and density of the system.
The total incoherent scattered power spectrum is equal to the integral in phase space of the distribution function f, where f is the Maxwellian distribution if the electrons are in thermal equilibrium. We can then write:

$$\frac{d^2P}{d\Omega_s dw_s} = r_e^2 \int_V \langle S_i \rangle \int |\Pi \cdot \vec{e}|^2 \kappa f(\vec{x}, \vec{v}) \kappa \delta(\vec{k} \cdot \vec{v} - w) d\vec{v} d\vec{x} \tag{A.12}$$

where $\langle S_i \rangle$ is the mean incident Poynting vector $P_i/A$, V is the scattering volume for which the scattered radiation is observed and $\Pi = \vec{e_s} \times \vec{e_s} \times$ is the polarization operator. However, in the case of TCV, the temperature electron reach is 1eV$\leq T_e \leq$15keV; as such, the operator $\Pi$ becomes dependent on $\beta$. As a consequence, a small fraction of the scattered light, of the order of $\beta^2 = eT_e/mc^2$ will be polarized orthogonally to the incident polarization, because the electron will see the incident light with a slightly different orientation. In the case of TCV, where the $T_e$ $\sim$10 keV, this depolarization is of the order of $\sim 2\%$. Moreover, the scattered spectrum is modified because of this relativistic aberration, making preferentially observe a greater intensity from particles that move towards the observation point. Even more, the relativistic correction to the scattering will modify the Doppler shift, which goes towards the blue of the visible spectrum.
A simple derivation of the Thomson scattering spectrum was derived [6]; the scattered spectral power can then be written, for 100eV$\leq T_e \leq$100keV as:

$$\frac{d^2P_s}{d\lambda_s d\Omega} = P_i n_e L r_e^2 S(T_e, \epsilon, \Theta) \tag{A.13}$$

Where $\vec{k}$ and w are replaced by $\theta$ and $\lambda_s$, and S is a function characteristic of this method (see [6], chapter 3).

# Bibliography


[1] A.W.Leonard. Edge localized modes in tokamaks. *Physics of Plasmas*, 21(090501), 2014.

[2] Y.R.Martin et al. H-mode threshold power in TCV Ohmic plasmas. *Plasma Physics and Controlled Fusion*, 44(A143), 2002.

[3] Stefan Franke. *Application of Thomson scattering at 1.06 μm as a diagnostic for spatial profile measurements of electron temperature and density on the TCV tokamak*. École Polytechnique Fédérale de Lausanne, 1997. Ph.D. Th. N.1654.

[4] L. Frassinetti and B. Labit et al. The EUROfusion JET-ILW pedestal database. *Plasma Physics and Controlled Fusion*, 60(1), 2017.

[5] H.Lutjens, A.Bondeson, and O.Sauter. The CHEASE code for toroidal MHD equilibria. *Computer Physics Communications*, 97(3), 1996.

[6] Andreas Pitzschke. *Pedestal Characteristics and MHD Stability of H-Mode Plasmas in TCV*. École Polytechnique Fédérale de Lausanne, 2011. Ph.D. Th. N.4917.

[7] Bernhard Sieglin. *Experimental Investigation of Heat Transport and Divertor Loads of Fusion Plasma in All Metal ASDEX Upgrade and JET*. Max-Planck-Institut fūr Plasmaphysik, 2014.

[8] U.A.Sheikh, M.Dunne, L.Frassinetti, P.Blanchard, B.P.Duval, B.Labit, A.Merle, O.Sauter, C.Theiler, and C.Tsui et al. Pedestal structure and energy confinement studies on TCV. *Plasma Physics and Controlled Fusion*, 61(1), 2018.

[9] John Wesson. *Tokamaks, $3^{rd}$ edition*. Clarendon Press - Oxford, 2004.

[10] H Zohm. Edge localized modes (ELMs). *Plasma Physics and Controlled Fusion*, 38(105), 1996.

# Acknowledgements

I want primarily to thank my parents, Ivano and Emanuela, without whose support I would not have been writing this thesis right now; they made great sacrifices for me and I would not be here at all without them.
On the economic side, I would like to thank Fusenet as well for partially funding my experience at Lausanne thanks to their scholarship programme.
I would like to thank the Professor Matteo Passoni, whose courses and passion for what he teaches drove me to choose this Master course in Nuclear Engineering when I was at the third year of my Bachelor, and inspired me to choose nuclear fusion as my primary interest during my Master.
Moreover, I would like to thank all the personnel at TCV in helping me with the development of my thesis; it was a great, exciting and friendly environment to work within. In particular, I would like to thank Dr. Benoit Labit for coordinating the thesis work and helping me a great deal when problems and issues arose during the development of the database program, and TCV Director and Professor Ambrogio Fasoli, as well as Professor Christian Theiler, for giving me the opportunity of developing this thesis in the first place.
I would like to thank Dr. Umar Sheikh and Dr. Antoine Merle as well for helping me during the writing of the code, in particular in understanding the CHEASE code and calculating the normalized pressure gradient after several failed attempts and headaches, as well as Dr. Lorenzo Frassinetti from the MST-1 group for giving me suggestions for the database (since he was the one who wrote it).
Finally, I would like to thank all the Ph.Ds at the department, some of which are Filippo Bagnato, Matteo Fontana, Federico Pesamosca, and my fellow Master Internship Jean Cazabonne for listening to all my incoherent ramblings.